Synthesis of high purity zirconium tetrafluoride for nuclear applications

Dissertation submitted in fulfilment of the requirements for the degree

Master of Science

in the

Department of Chemistry
Faculty of Agricultural and Natural Science

at the
University of the Free State
Bloemfontein

by

ODUETSE SYDNEY MONNAHELA

Supervisor: Prof. A. Roodt
Co-Supervisors: Dr. J.B. Wagener and Dr. P.A.B. Carstens

November 2008

Synthesis of high purity zirconium tetrafluoride for nuclear applications

ABSTRACT

The RSA has a great abundance of the potentially valuable zircon ($Zr(Hf)SiO_4$) mineral, which is mostly exported in unexploited form, leading to huge losses in potential revenue. The purpose of this project was to attempt to purify Zr of Hf as well as 3d metals for nuclear applications. The fluoride route was used to exploit the difference in sublimation temperatures as a selective separation method for ZrF_4 from HfF_4, or vice versa, depending on the volatility of these species.

The fluorination of ZrO_2, HfO_2 and plasma dissociated zircon (PDZ) samples and the identification of viable conditions for separation of ZrF_4 and HfF_4 in an anhydrous hydrogen fluoride and fluorine atmosphere were primarily investigated.

The fluorination of these species was performed to understand the chemical behaviour of the tetrafluoride species prior to separation and whether this behaviour could not be manipulated to effect separation.

Thermogravimetric analyses indicated that the formation of ZrF_4 is possibly via the oxyfluoride. X-ray powder diffraction was used to confirm the results.

The theoretical equilibrium composition calculations for separation of ZrF_4 and HfF_4 were simulated. The separation was further studied by theoretically calculating the separation coefficients of ZrF_4 and the metal fluoride impurities.

To my son Atlegang

whom I want to inspire by example

Acknowledgements

I would like to express my sincere gratitude and appreciation to God who has given me the talent to perform this research, my supervisors, Professor A. Roodt, University of the Free State, Dr. J.B. Wagener and Dr. P.A.B. Carstens, South African Nuclear Energy Corporation Limited (Necsa) for their support, suggestions, mentorship and guidance.

I would also like to thank the following people:

1. My family for their support, encouragement and understanding.
2. Mr. B.M. Vilakazi for generating the thermogravimetric data and assistance with regard to the operation of a thermobalance. Thank you very much.
3. Mr. D. Moolman for the insightful discussions of the thermogravimetric results.
4. Mr. W.L. Retief for assistance with the literature survey and linguistic editing of the dissertation.
5. Mr J.P. le Roux for assistance with part of Chapter 3.
6. Dr. D. de Waal for assistance with Raman analyses and discussions.
7. Necsa and the University of the Free State for financial assistance.
8. Pelindaba Analytical Laboratories and the University of Pretoria for XRF and XRD analyses, respectively.

LIST OF ABBREVIATIONS AND SYMBOLS

Abbreviation	Description
ASTM	American Society for Testing and Materials
Á	Angstrom
AMI	Advanced Metals Initiative
B_p	Boiling point
ca.	Approximately
DST	Department of Science and Technology
F_2	Fluorine gas
FG	Fluoride glass
GPa	Gigapascal
HSC	Enthalpy, Entropy and Heat Capacity
HF	Hydrogen fluoride
IR	Infrared
K	Kelvin
MIBK	Metylisobutylketone
M_p	Melting point
M	Molecular weight
N	Mole fraction
PDZ	Plasma Dissociated Zircon
PMC	Palaborwa Mining Company
PWR	Pressure Water Reactor
PBMR	Pebble Bed Modular Reactor
PAL	Pelindaba Analytical Laboratories
p^o	Equilibrium vapour pressure
ppb	Parts per billion
ppm	Parts per million
RSA	Republic of South Africa
REE	Rare earth element
SEM	Scanning Electron Microscope
TGA	Thermogravimetric Analyzer
T_s	Sublimation Temperature
TBP	Tributylphosphate
US	United States
$	United States Dollar
UV	Ultraviolet
%	Percent

°C	Degree Celsius
kg	Kilogram
MW	Megawatt
nm	Nanometer
cm^{-1}	Wavenumber
mg	Milligram
g	Gram
ℓ	Litre
min	Minute
wt	Weight
t_p	Triple point
s_p	Sublimation point

Table of Contents

List of Figures

Chapter 1

Chapter 3

Chapter 4

Chapter 5

Chapter 6

List of Tables

Chapter 1

Chapter 2

Chapter 3

Chapter 4

Chapter 5

CHAPTER 1

INTRODUCTION

1.1 THE ROLE OF THE AMI IN THE NECSA ZrF_4 MANUFACTURING PROJECT

The RSA has a great abundance of potentially valuable minerals like zircon ($ZrSiO_4$), rutile (TiO_2), ilmenite ($FeTiO_3$) and fluorite or fluorspar (CaF_2). Most of this is exported in unbeneficiated form, leading to huge losses in potential revenue. The Department of Science and Technology (DST) has recognized the need for a national mineral beneficiation initiative, especially with regard to **zircon** and fluorite. With the escalation of global warming caused by emission of CO_2 and CH_4 from conventional fossil-fuel-burning power stations, the generation of electricity via nuclear means is gaining popularity by the day. The metals zirconium and hafnium play an important role in nuclear energy generation and they can both be manufactured from **zircon**.

The DST established the Advanced Metals Initiative (AMI), with the aim to promote the manufacturing of three groups of metals, namely:

1. Ti, Al and Mg (so-called Light Metals),
2. Au, Ag and Pt (so-called Precious Metals) and
3. Zr, Hf, Ta and Nb (so-called “New” Metals).

Necsa has been tasked with the development of the “New” metals. Any developed route should be novel, economic and environmentally-friendly. The feedstock for Zr and Hf production is to be zircon and for Ta and Nb, ores like tantalite. The founding principle of the initiative is based on collaborative research, involving a network of key institutions and researchers. These networks are schematically presented in Fig. 1.1.

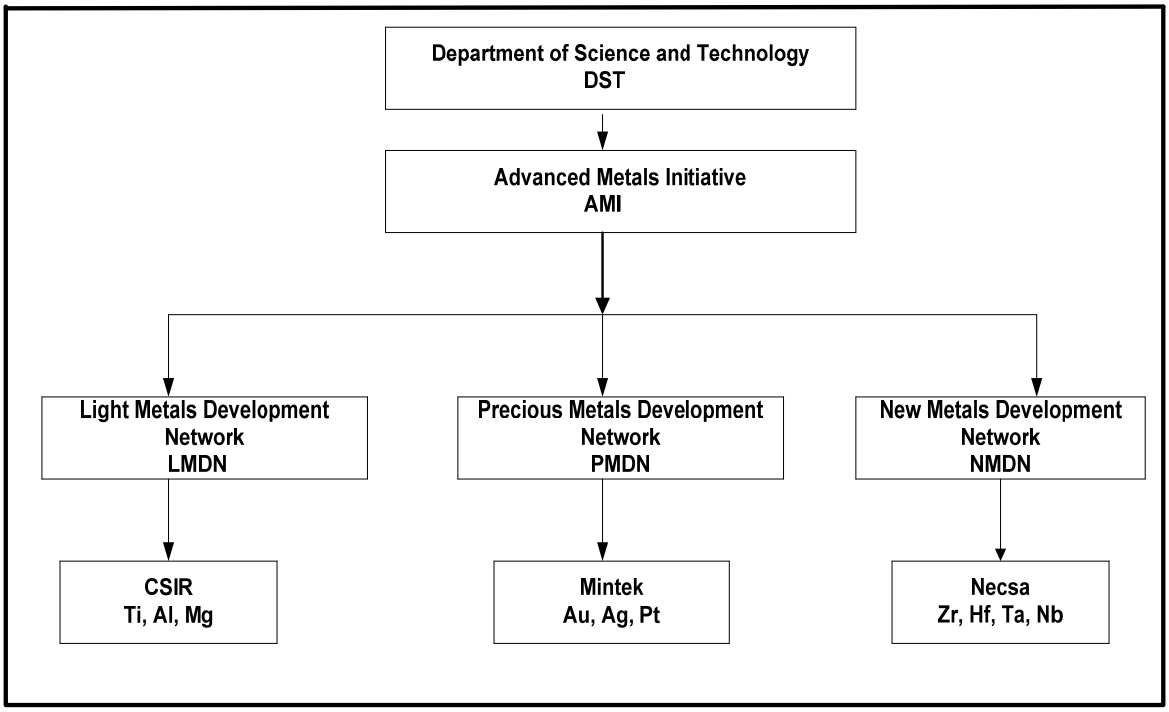

Figure 1.1: Schematic representation of the three Networks of the AMI.

The Zr/Hf separation project has already been "kick-started" due to the availability of the feedstock material and this forms the basis of this dissertation. The manufacturing of Ta and Nb will receive due attention at a later stage due to the relative unavailability of the feedstock material.

Necsa was entrusted with this task because it possesses very valuable plasma and fluorochemical expertise and infrastructure. A **prerequisite** for manufacturing nuclear-grade zirconium metal is to manufacture a **nuclear-grade Zr-containing precursor**, hence this study.

1.2 BACKGROUND AND HISTORY

Zircon has been known as a gem mineral since biblical times and was known as zargun in Sri Lanka (Ceylon) and as hyacinth or jacinth in France[1, 2]. Zircon is not mined on its own but as a byproduct of Ti-containing ores such as rutile (TiO_2) or ilmenite ($FeTiO_3$). The name zircon possibly comes from the Arabic zargun for the gold or dark amber colour of the more common gemstone. Zircons may be colourless, amber, red, reddish brown, blue,

green or black. The German chemist Martin Heinrich Klaproth[3, 4] found it was an oxide in 1789, which he later called “Zirkonerde”.

In 1797, Vauqelin studied this new earth, to which the name zirconia was given. In 1824 the Swedish chemist Jöns Jacob Berzelius prepared the first crude zirconium metal, an impure black powder, by heating potassium and potassium hexafluorozirconate in a closed container[5, 6]. In 1914 Lely and Hamburger[7] prepared the first relatively pure zirconium by the reduction of zirconium tetrachloride with sodium in a bomb reactor by producing malleable, corrosion-resistant zirconium pellets. The earliest method of purifying useable quantities of the metal was developed in 1925 by Dutch chemists Anton E. van Arkel and J.H. de Boer[8], who developed the iodide process, which produced the first massive zirconium metal that could be cold-worked and which exhibited good ductility at room temperature.

The chemistry of fluorine compounds of zirconium is different from that of the Cl/Br/I halogen compounds, primarily because of the greater strength of the Zr-F bond and because of the smaller size of the fluorine atom. However, it is imperative to emphasis the prominent role that the halides play in the production of zirconium metal.

In 1938 William Justin Kroll[9, 10, 11] carried out the first inert-atmosphere magnesium reduction of zirconium tetrachloride. In 1944 the U.S. Bureau of Mines started a project to manufacture ductile zirconium economically. By 1947, a pilot plant was producing 30 kg of zirconium sponge per week. Concurrently, researchers evaluated the physical and atomic properties of metals as potential uranium fuel cladding materials for nuclear power stations. In 1948 hafnium-free zirconium was selected as most promising. By 1949 zirconium had been chosen as the structural material for the fuel core of the submarine thermal reactor and during 1949 to 1950 a satisfactory hafnium separation process was developed at Oak Ridge.

1.3 ZIRCONIUM ORES

Zirconium has been identified in S-type stars, the sun and meteorites. Samples taken from the surface of the moon have also been found to contain high levels of zirconium compared to terrestrial rock[12]. Zirconium in chemically combined form is widely distributed in nature as a component of the lithosphere. There are many minerals, but only a few are of commercial value, e.g.

1. Baddeleyite (Natural zirconium dioxide or ZrO_2);
2. Zircon ($ZrSiO_4$ which occurs widely in so-called beach sand deposits and is commercially the most abundant zirconium-containing mineral);
3. Columbite (Contains up to 11 % ZrO_2);
4. Zirkelite ($(Ca, Fe)_{0.2}(Zr, Ti, Th)O_2$), containing up to 53 % ZrO_2;
5. Catapleiite ($Na_2ZrSi_6O_{15}.3H_2O$), containing up to 40 % ZrO_2;
6. More than 35 other less significant minerals are also known.

Baddeleyite would have been the prime choice as feedstock mineral but due to insufficient ore supplies, globally it accounts for a very insignificant portion of zirconium demand.

The chief mineral source for zirconium is zircon of which the RSA possesses 60 % of global reserves and currently supplies 40 % of global demand. Zircon ($ZrSiO_4$) occurs as an “accessory” mineral in silica-rich igneous rocks particularly granite, nepheline, syenite and pegmatite as well as in metamorphic and sedimentary rocks[13]. Zircon is rarely found in rocks in economically mineable concentrations. Weathering and erosion of rocks free the zircon grains and the combined action of rivers, seas and wind concentrate the heavier minerals by natural gravitation processes in placer deposits, deltas and ocean beaches. As an ore, zircon is recovered from unconsolidated sands in beach deposits.

Until 1922 it was not recognized that all the zirconium occurring in the lithosphere contains a small proportion of the element of atomic number 72. This initially unrecognized element had been following zirconium in all the processing of its ores and its subsequent handling as though it were a huge isotope of zirconium. In 1923 it was identified as hafnium (Hf), from Hafnia an ancient name for Copenhagen, where it was first identified by George von Hevesy et al.[14]. Hafnium does not exist as a free element in nature, but is normally derived from minerals such as zircon sand. The hafnium content of which is normally approximately 2 % by weight of the combined metals.

1.4 CHEMISTRY OF ZIRCONIUM

For non-nuclear applications the hafnium content of Zr metal poses no problems but nuclear-grade zirconium alloys must be hafnium-free to a level of at least <100 $mg.kg^{-1}$ (ppm). The separation of Zr and Hf is however very problematic due to their very similar chemical behaviour. This is ascribed to the following:

1. The similarities in valence electron configurations of Zr and Hf

   Zr (40): $4d^2\ 5s^2$

   Hf (72): $5d^2\ 6s^2$

2. The lanthanide contraction of Hf, which causes the two elements to have very similar atomic radii of 1.45 Å and 1.44 Å, for Zr and Hf respectively. Thus the expected size increases of elements of the third transition series relative to those of the second transition series, due to an increased number of electrons and higher principal quantum numbers of the outer ones, are almost exactly offset, and there is in general much less difference in atomic and ionic sizes between the two heavy atoms of a group, whereas the corresponding atom and ions of the first transition series are significantly smaller[15].

Zirconium and hafnium are classified in subgroup IVb of the Periodic Table with their sister metallic element titanium, as illustrated in Table 1.1.

Table 1.1: Periodic Table showing elements adjacent to zirconium.

3	4	5
IIIb	IVb	Vb
Sc	Ti	V
Y	**Zr**$^{91.224}$	Nb
La	Hf$^{178.49}$	Ta

It is pertinent to note that both elements exclusively have the most common oxidation number of 4 in their compounds, and are covalently bound to the maximum extent that is sterically possible. The chemistry of zirconium is characterized by the difficulty of reduction to oxidation states less than four. Zirconium is a hard shiny ductile metal which is similar to stainless steel in appearance. It can spontaneously ignite in air in a fine powder form, especially at high temperatures.

These two elements (zirconium and hafnium) are chemically and physically so identical that they are extremely difficult to separate from one another. When separated, they must be to qualify as nuclear grade because of a quirk of nature which boils down to the fact that Zr has such a low cross-section for thermal neutrons that they can pass virtually unimpeded through zirconium metal which possesses a cross-section of only 0.18 barn and as such the zirconium metal is said to be “transparent” to the neutrons. The hafnium metal however has a cross-section value of 108 barn and therefore acts as a “poison” to thermal neutrons and is utilized as fuel control rods to moderate the nuclear fission reaction. The difference in the neutron absorption cross-section of the two metals is the only commercial factor that necessitates separation of the two metals.

Globally, the separation of Zr of Hf has been effected by major nuclear entities by means of expensive, relatively inefficient, difficult to implement and

environmentally-unfriendly processes such as extractive distillation in molten $KCl/AlCl_3$ in the most modern present purification process (CEZUS process)[16], or by older less favourable processes like liquid-liquid extraction (MIBK process)[17, 18] or by the even older TBP[19, 20] process in which Zr is extracted in a solution of concentrated nitric acid and tributylphosphate in kerosene. The TBP and MIBK processes have all been abandoned, with the CEZUS process being favoured. Some of these processes will be described in the following chapter.

A small fledgling nuclear player like the RSA cannot hope to compete with the established major players in the field and will have to search for a competitive edge based on novelty as well as economic and ecological factors. In order to accomplish this, a radical new approach is necessary. Such an approach would be to abandon aqueous routes altogether and opt for an anhydrous purification/separation route. This would typically employ processes like sublimation. Unfortunately, the driving force in a successful sublimation process is a large enough difference in sublimation temperature between the mother specie and the contaminant of which the difference does not exist between gaseous Zr and Hf species. Special techniques to enhance the effectiveness of the sublimation process will therefore have to be employed. It is the main purpose of this study to identify/accomplish this in order to be able to manufacture a nuclear-grade zirconium compound and specifically zirconium tetrafluoride (ZrF_4) from which to manufacture nuclear-grade Zr metal.

While it is a well-established fact that Hf is probably the most deleterious contaminant in Zr alloys, this has been discussed solely from the viewpoint of efficiency of the fission reaction. In the Table 1.2 below the maximum permissible contaminant levels as specified by ASTM[21] International are listed:

Table 1.2: Nuclear-grade zirconium sponge, maximum permissible contaminant levels according to ASTM number B350.

Element	**Permissible impurities max. ppm**
Aluminum	75
Boron	0.5
Cadmium	0.5
Carbon	250
Chlorine	1300
Chromium	200
Cobalt	20
Copper	30
Hafnium	100
Iron	1500
Manganese	50
Molybdenum	50
Nickel	70
Nitrogen	50
Oxygen	1400
Silicon	120
Titanium	50
Tungsten	50
Uranium (total)	3.0

Detrimental influences of a selected number of the contaminants are the following:

Boron, Cadmium, Hafnium → Neutron capture poisons

Uranium, Thorium → Fissioning in the Zircaloys can cause defaults

Nitrogen, Oxygen → Can influence the metallurgical properties of the Zircaloy.

As can be seen from the above Table 1.2, certain contaminants are obviously less detrimental than others, therefore they have higher permissible levels specified. It is important that these maximum permissible contaminant levels

be taken into account when developing manufacturing, purification or reduction routes.

When manufacturing the chosen ZrF_4, all precautions must be taken to prevent incorporation of these contaminants, since it is extremely difficult to purify the Zr metal.

1.5 APPLICATIONS OF ZIRCON

The major end-uses of zircon other than for the manufacturing of zirconium metal, are in refractories, foundry sands and ceramic opacificers. Zircon is also marketed as a natural gemstone used in jewellery and the oxide of pure zirconium is processed to produce cubic zirconia, a brilliant clear crystal which is used as a low-cost substitute for diamonds.

1.6 APPLICATIONS OF Zr METAL AND COMPOUNDS IN THE NUCLEAR INDUSTRY

With the current global and the RSA upswing in demand for energy generation which will not negatively impact on the environment (generation of energy via the burning of fossil fuels like coal in conventional generation systems leads to effects like global warming) nuclear energy generation has been put into the spotlight again. At present the RSA has been operating the “Koeberg" Nuclear Power Station (a conventional pressurized water reactor (PWR) system) and plans are on the table to build and commission another Koeberg.

In the future the RSA will most probably also invest in advanced high-temperature gas-cooled reactors, of which the PBMR (Pebble Bed Modular Reactor) is an example. The fuel particles of the PBMR is coated with SiC but in the future it is envisaged that higher operating temperatures will be at the order of the day and SiC will no longer be suitable as coating. The most likely candidate for coating purposes is a transition metal carbide, ZrC[22, 23], which is characterized by:

1. High hardness;
2. High melting point;

3. High strength;
4. Electrical conductivity;
5. Oxidation resistance.

These properties give it the potential to be a useful engineering ceramic. The manufacturing of nuclear-grade ZrF_4 will no doubt also feature prominently in this regard. New generation PBMR reactors will eventually be using alternative cladding layers like zirconium carbide (ZrC), etc. However the use of ZrC in engineering applications has been limited by the lack of a fully developed, commercially viable sintering process.

The development of water-cooled nuclear power reactors brought about the use of zirconium for uranium fuel cladding and for structural components. Materials for fuel cladding and structural components in nuclear reactors are restricted because of the following crucial requirements:

1. Low absorption cross-section for thermal neutrons;
2. Adequate strength, creep resistance and ductility after prolonged irradiation in reactor coolant;
3. Excellent corrosion and oxidation resistance;
4. Absence of interactions with the fuel material and fission products.

The properties of zirconium make it particularly suitable for use in thermal reactors[24]. The requirements of such reactors in addition to a low neutron absorption cross section are:

1. Mechanical strength and stability under severe stresses resulting from high thermal gradients;
2. Leakage reliability in high-temperature, high-pressure, corrosive, dynamic and radioactive systems;
3. Resistance to mechanical damage by radiation;
4. Limited formation of high-activity products by nuclear reactions;
5. Adaptability to simple remote maintenance and repair.

Zirconium alloys such as the Zircaloys and Zr-2.5Nb, have been developed to meet these requirements. These zirconium metal alloys play an important role in nuclear fuel rods. In water-cooled reactors, zirconium alloys have found extensive use for fuel cladding and as pressure tubes.

1.7 NON-NUCLEAR APPLICATIONS OF Zr METAL AND THEIR COMPOUNDS

Zirconium metal has a low absorption cross-section for thermal neutrons, which makes it ideal for nuclear energy uses, such as cladding for fuel elements[25]. Zirconium metal has strong corrosion-resistance properties as well as the ability to confine fission fragments and neutrons so that thermal or slow neutrons are not absorbed and wasted, thus improving the efficiency of the nuclear reactor. More than 90 % of zirconium metal production is consumed by commercial nuclear power generation. Modern commercial-scale reactors can use as much as 150,000 meters of zirconium alloy (Zircaloy) tubing.

Zirconium is used in the steel industry to remove nitrogen and sulfur from iron, thereby enhancing the metallurgical quality of the steel. When alloyed into iron it improves iron's machinability, toughness and ductility. Zirconium metal, when alloyed with niobium, is intentionally oxidized to produce an abrasion-resistant, high-integrity zirconium oxide ceramic surface for total hip or total knee replacement devices and it also becomes superconductive at low temperatures and is therefore used to make superconductive magnets with possible large-scale electric power uses.

Zirconium metal is pyrophoric (flammable) and has been used in military incendiaries such as Dragon's Breath. Its carbonate was used in poison-ivy lotions until it became evident that many people are allergic to it. Impure zirconium oxide, zirconia, is used to make laboratory crucibles that can withstand heat shock, for linings of metallurgical furnaces and by the ceramic and glass industries as a refractory material. Zirconium refractories such as ZrC can be used as an abrasive on sandpaper and flap discs etc.

Bicycle manufacturers incorporate zirconium-aluminum alloys in their top-of-the-range bicycle frames. This combination provides the frame with tougher durability; likewise, the frame becomes lighter and much stronger. Zirconium metal is also applied in the molecule aluminum zirconium octachlorohydrex GLY, which is an anti-perspirant. In 2007, zirconium cost approximately $150/kg. Zirconium has a large variety of applications which cannot be covered in full detail in this dissertation.

1.8 EXTRACTION OF ZIRCONIUM VALUES FROM ZIRCON

Zircon is a refractory mineral with a rigid and stable crystal structure whose decomposition requires the use of high temperature and aggressive chemicals[26, 27]. The following procedures are conventionally used to crack/overcome the inertness or the crystal structure of the ore:

1. Caustic Fusion
2. Carbochlorination
3. Carbiding
4. Fluorosilicate Fusion
5. Lime Fusion

The above processes are all relatively expensive and on many occasions environmentally-unfriendly, and an alternative process was developed at Necsa, namely non-transfer-arc plasma conversion technology. With this technology, so-called **P**lasma **D**issociated **Z**ircon [PDZ ($ZrO_2.SiO_2$)] is formed, which is very amenable to subsequent chemical processing. The ZrO_2 used in this study was obtained from PDZ.

1.9 AIM OF THE STUDY

The purpose of this study was to develop a competitive process to manufacture nuclear-grade ZrF_4, which can serve as precursor for the subsequent manufacturing of nuclear-grade zirconium metal. The manufacturing route must be novel, economic and ecologically-friendly. This preferred precursor, zirconium tetrafluoride, must be purified of contaminants

like hafnium tetrafluoride (HfF_4) and 3d metals, in order to be able to manufacture nuclear-grade zirconium metal.

This study is broken down into the following chronological order:

1. The premise of this study is that Plasma Dissociated Zircon (PDZ) will eventually be the precursor for the synthesis of ZrF_4 but the initial focus however, will be on commercially available ZrO_2;
2. A literature survey regarding conventional non-aqueous purification routes to obtain nuclear-grade ZrF_4 precursor material;
3. Thermodynamic evaluation of proposed purification methods;
4. Theoretical calculation of separation coefficients;
5. Synthesis of ZrF_4;
6. Experimental verification of proposed purification methods;
7. Suggestions and recommendations on separation/purification methods.

The experimental studies were performed by means of thermogravimetric analysis (TGA), supported by X-ray powder diffraction (XRD), Raman, X-ray fluorescence (XRF), scanning electron microscopy (SEM) and thermodynamic equilibrium studies.

CHAPTER 2

LITERATURE SURVEY

2.1 INTRODUCTION

As South Africa is moving from a third to a first world country the need for high purity materials is increasing. The responsibility lies with the emerging first world country to enhance its economy by the beneficiation of a substantial percentage of its natural resources. South Africa is a major producer of zircon but the technology for beneficiation is not recognized or available.

The focus of this dissertation is the production of nuclear-grade zirconium tetrafluoride (ZrF_4). Zirconium metal plays a vital role in the nuclear energy generation industry, because of factors like excellent corrosion resistance, low cross-section capture for thermal neutrons, very good mechanical strength and so forth which have been elaborated on in Chapter 1. Unfortunately Zr is always associated with Hf, with which it co-exists in nature.

Therefore, during the manufacturing of the precursor from which the Zr metal will eventually be manufactured, or during the process of manufacturing the Zr metal, the unwanted Hf should be removed to satisfy nuclear requirements. Conventionally these purification procedures involved intricate, expensive and often environmentally-unfriendly aqueous extraction processes like MIBK, TBP and also anhydrous processes like CEZUS, which will be discussed at a later stage.

It is the purpose of this study to develop novel alternative processes, preferably anhydrous. The present literature survey was done based mainly on patents, to decide which alternative beneficiation processes of the mineral are possibly viable. The study was done with emphasis and focus on providing information regarding effective and commercially adaptable and viable processes for separation of the preferred zirconium and hafnium halides, using the anhydrous route.

This study also comprises a literature survey on the applicability of Raman spectroscopy with respect to the interaction of ZrO_2 with HF (and/or F_2) and whether there is varying adsorption at different temperatures. In the present study Raman has been used to identify the starting materials, intermediates and products formed, and to better understand the reaction mechanism.

2.2 ZIRCONIUM METAL MINERAL FEEDSTOCK

Historically there have been only two feedstock materials for zirconium and hafnium metals in the world. The first one is natural baddeleyite (ZrO_2) of which the RSA was the leading global supplier up until two decades ago. At that time Palaborwa Mining Company (PMC) was mining baddeleyite together with copper ores. However, declining ore grades in conjunction with limitations coupled to the open-cast type of mining operation employed by PMC, culminated in the cessation of baddeleyite mining operations at Phalaborwa. The second and only other viable ore in the RSA is the mineral zircon ($ZrSiO_4$). However, most of this potentially lucrative mineral is exported in unbeneficiated form, leading to substantial potential forex losses every year.

Zircon, the primary ore for nuclear-grade zirconium, contains about 66 % ZrO_2, 33 % SiO_2 and 1 % HfO_2. It is however a very chemically inert mineral, and requires considerable thermal and chemical manipulation to transform it to a chemically desirable precursor. These conventional processes are outlined in Chapter 1. Two such technologies, which were developed at Necsa during the abandoned nuclear fuel cycle programme, were plasma and fluorochemical technologies. The zircon can namely be converted by free-falling it through a non-transfer-arc plasma, to **P**lasma **D**issociated **Z**ircon (PDZ, ($ZrO_2.SiO_2$))[28].

$$ZrSiO_4 \xrightarrow{>1800°C/Plasma} ZrO_2.SiO_2 \quad \text{.....2.1}$$

This PDZ now consists of submicron (crystalline, monoclinic) ZrO_2 particles, cemented together by amorphous silica (SiO_2). Thus the dissociation of zircon results in a marked increase in chemical reaction susceptibility of the zircon. Whereas zircon ($ZrSiO_4$) was impervious to attack even by anhydrous HF, this PDZ ($ZrO_2.SiO_2$) now dissolves exothermally in 40 % HF (provision has to be made for cooling) or can be desilicated at temperatures below 130 °C by anhydrous HF to afford ZrO_2. The reactions can be depicted as below:

$$ZrO_2.SiO_2 + 12HF(aq) \rightarrow H_2ZrF_6 + H_2SiF_6 + 4H_2O \quad .....2.2$$

$$ZrO_2.SiO_2 + 4HF(anhy) \rightarrow ZrO_2 + SiF_4 + 2H_2O \quad .....2.3$$

The ZrO_2 produced by reaction 2.3 can be transformed to ZrF_4.

$$ZrO_2 + 4HF \rightarrow ZrF_4 + 2H_2O \quad .....2.4$$

The H_2ZrF_6 produced by reaction 2.2 can be transformed to K_2ZrF_6 by KOH or KF addition.

$$H_2ZrF_6 + 2KOH \rightarrow K_2ZrF_6 + 2H_2O \quad .....2.5$$

then

$$K_2ZrF_6 \xrightarrow{>800\,^\circ C/\Delta} ZrF_4 \uparrow + 2KF \quad .....2.6$$

From the above it is obvious that ZrF_4 can quite readily be manufactured from zircon, utilizing plasma and fluorochemical technology. It has also already been pointed out that nuclear-grade zirconium metal needs to be purified of Hf to levels not exceeding 100 ppm. Furthermore, it has been pointed out that this purification should already be effected at the ZrF_4 precursor level. Since this purification is the actual focus of this thesis, a purification strategy should now be conceived. The following is important in this regard:

1. To be able to competitively purify ZrF_4 of unwanted contaminants, an alternative purification procedure to those based on aqueous routes, will have to be developed. This implies an anhydrous route. The first anhydrous route that springs to mind is that of sublimation.

2.3 INDUSTRIAL PROCESSES FOR SEPARATION OF ZIRCONIIUM FROM HAFNIUM

Experience from literature has taught that it is extremely problematic to purify the Zr metal of Hf, therefore purification must be carried out at the precursor level in this study the precursor material is ZrF_4. Up until present day, purification of the precursor up to nuclear-grade specification had predominantly been carried out in aqueous phase. Early attempts to purify Zr of Hf utilized classical fractional crystallization or fractional precipitation methods which are unfortunately slow and particularly tedious to perform, even in aqueous solution at room temperature.

The need to separate zirconium from hafnium is solely based on the requirements of the nuclear industry. It is probable that, in the absence of this need, hafnium metal would have been just an exotic material up to present time, perhaps zirconium metal too. Fig. 2.1 illustrates some of the different industrial processes for zirconium beneficiation, which are also briefly summarized thereafter[29].

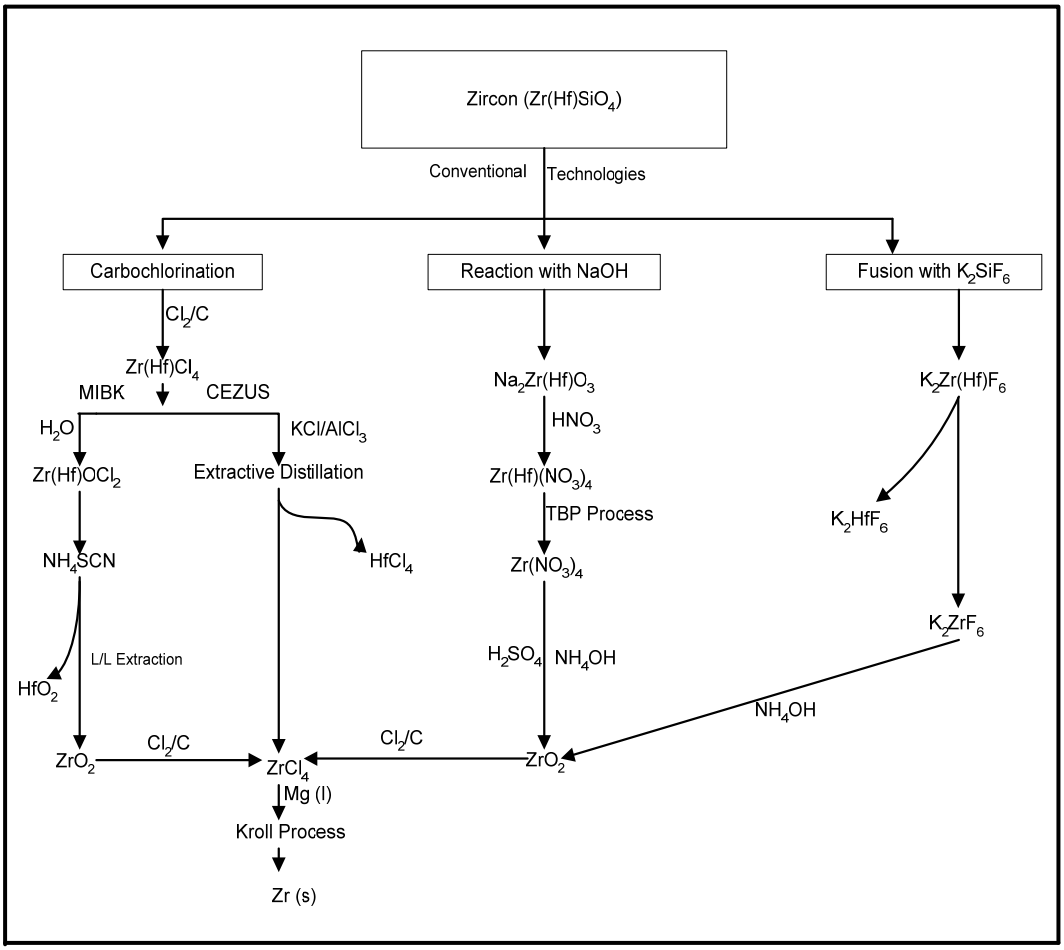

Figure 2.1: Various routes for zirconium beneficiation.

2.3.1 The TBP process

In this process an organic phase (tributylphosphate (TBP) diluted in kerosene) is contacted with a nitric acid solution (3N), and $NaNO_3$ is added as a salting-out agent[30, 20]. The maximum metal content (Zr + Hf) of the liquor is kept low (30 g/l) to avoid third phase formation. Under these conditions, the distribution factor for zirconium is approximately 1.5, favoring the organic phase, and that of hafnium is around 0.15.

This process was abandoned by the US at the end of the 1950's, France did the same in 1978 and presently it is used in India. The main disadvantages of the process are the low metal concentration in the aqueous and organic phases, the large consumption of chemicals and the inability to produce

hafnium of nuclear quality. The TBP process produced nuclear-grade $ZrCl_4$ at twice the cost of that of the MIBK process.

2.3.2 The MIBK process

In this process the thiocyanic complexes of zirconium and hafnium formed in 2.0M HCl exhibit a significantly different solubility in methylisobutylketone (MIBK)[17, 31]. This process produces a separation factor around seven. In the MIBK process, it is hafnium, the minor component that is concentrated in the organic phase. This fact makes it possible for both elements to be produced conforming to nuclear specifications.

However this process is falling more and more into disfavour because of ecological factors, tediousness and cost. The solvent is volatile and highly flammable and is soluble up to 2 % in water. Waste streams contain high concentrations of ammonium, cyanides and organic products.

2.3.3 Aliquat 336 process

In this process aqueous phases are prepared by dissolving $ZrCl_4/HfCl_4$ mixtures in a solution containing 0 to 12M HCl[32]. Aliquat 336 is introduced and saturated with hydrochloric acid solution. The aqueous and organic phases are shaken mechanically and mixed to reach extraction equilibrium. However, the extraction of Zr and Hf increase with increasing acidity up to 8M for Zr and up to 11M for Hf. Hafnium has a lower tendency to form anionic complexes than zirconium. Thus at 7M HCl hafnium is not extracted by Aliquat 336, although zirconium is extracted (50 %) in the organic phase by the liquid anion exchanger. At high chloride concentration (>10M), both Zr and Hf form anionic complexes that are extracted by Aliquat 336. This process proved that zirconium could be extracted with Aliquat 336 in toluene by an anion exchange reaction.

2.3.4 The CEZUS process

In 1978 the French state company, CEZUS, started a new industrial plant producing zirconium and hafnium using the Besson process[16], involving distillation in molten salts. The success of this process was based on the

replacement of several processing steps by a single distillation step. Sehra and Mallikarjuanan[33] recommended adopting the CEZUS process in India to replace the TBP process in 1989.

In the CEZUS process the distillation of zirconium and hafnium chlorides in a molten salt bath is carried out at one atmosphere and at ca. 540 °C. It exhibits a separation factor of approximately two, which means that about 90 stages are required to achieve the desired separation. It produces both zirconium and hafnium according to nuclear specifications.

The disadvantages are the requirement of highly corrosion resistant alloys and sophisticated technologies to pump and handle the vapour streams, avoiding any air moisture contamination. However the cost for the CEZUS process is reported as being even lower than that of the MIBK route. At the present time about two thirds of global zirconium production still comes from the MIBK process[34]. Nevertheless, increasing environmental concerns and an eventual growth in energy demand could push the nuclear industry to devote attention to improvement of zirconium and hafnium separation technology in the future.

2.4 Zr PRECURSOR FOR PURIFICATION STUDIES

Necsa is steeped in technology pertaining to the beneficiation of zircon, especially via plasma and fluorochemical routes. Since these two routes inevitably produce ZrF_4 as product, this was historically the precursor of choice. Of course ZrF_4 can also be manufactured by routes other than from $ZrSiO_4$, but these invariably involve converting pre-precursors. These are well described in literature.

From literature, which was mainly based on patents, the main emphasis was on ZrF_4 not for nuclear applications, but rather with the manufacturing of ZrF_4 optical fibers in mind, whereby the above processes were used. In these fluoride glasses (FG) hafnium plays no detrimental role at all but rather the 3d transition metal cations[35, 36, 37].

The term fluoride glasses refers to particular vitreous materials belonging to the general family of halide glasses in which the anion are from elements in group VII of the Periodic Table, namely fluorine, chlorine, bromine and iodine[38]. Crystalline fluorides play a significant role in material science, e.g. as lenses in infrared (IR), optics (CaF_2), laser hosts (LaF_3, CaF_2), fast ion conductors (β-PbF_2) and fluoride-ion-sensitive electrodes (LaF_3)[39]. Their melts however, are very fluid, largely ionic and unlikely candidates for glass formation. Nevertheless, many fluoride glass-forming systems have been identified with useful properties such as extended IR transmission and the added advantage of ease of fabrication.

The metal fluoride for IR application must have very low levels of impurities with respect for example to: transition elements, rare earths and hydroxide ions in order to minimize absorption in the 2 to 4 micron range of the IR region of the spectrum. Furthermore, particulate materials such as the metal oxide, carbide, carbon, coke, phosphides and the like must be essentially absent since they serve as scattering centres for the electromagnetic radiation and thus produce undesirable attenuation[40]. The other major impurities that are important are Fe, Ni, Co and Cu, which should be present in less than parts per billion (ppb) amounts for fluoride glass applications[41].

It was found that the primary method of producing metal fluorides at a purity level of ppb is via ion exchange. This method is capable of producing high-purity material in large quantities, but cannot achieve ultra-purification without encountering significant increased cost and time and decreased efficiency.

For nuclear purposes however, the ZrF_4 must be purified of contaminants that are detrimental to the nuclear industry, especially Hf and the 3d metal impurities. To affect this, with whatever precursor, entails totally different technological routes. Up till the present, the global nuclear players have utilized mainly aqueous purification routes.

2.5 PURIFICATION PROCESSES FOR THE PRECURSOR TO NUCLEAR GRADE

A number of techniques are known for producing high-purity metal fluorides such as zirconium tetrafluorides. These processes can be divided into two categories:

1. Conventional aqueous routes and
2. Novel anhydrous routes

2.5.1 Conventional aqueous routes

There are different techniques that can be used when employing the conventional aqueous routes, which are based on ion exchange[42], solvent extraction processes, etc. All of the conventional aqueous routes produce hydrated metal fluorides such as zirconium tetrafluoride monohydrate, which makes it difficult to minimize the oxide and hydroxide content of the formed ZrF_4.

These conventional aqueous routes can provide very low transition element concentrations in the hydrated metal fluorides such as $ZrF_4.H_2O$, but the low levels are not maintained during the dehydration step. Thus, removal of hafnium from zirconium by solvent extraction is a costly and energy-inefficient process.

When using the conventional aqueous purification techniques, the purification normally involves dissolution followed directly by purification, whereas with the anhydrous route the removal of the impurities is effected via additional subprocesses. The aqueous chemistry of Zr has been more extensively studied than that of Hf. However, due to their similarity, the expected behaviour of dissolved Hf can often be deducted from the knowledge of analogous Zr solutions.

In a previous project[43] the zirconia and silica in the Plasma Dissociated Zircon (PDZ) was dissolved in a HF solution, with the reaction products such as H_2ZrF_6 and H_2SiF_6 also being soluble in the aqueous hydrogen fluoride, so

that only zircon that was not dissociated in the plasma, as well as poorly soluble or insoluble fluoride impurities or trace elements such as U, Th, Fe, Ti, Al and Ca remained as more or less undissolved solids. The undissolved solids ('**white fraction**') can thus be removed as a solid fraction by suitable means, such as filtration, decantation or settling. Since this project was terminated, the optimization of this purification by selective precipitation was not persued to eventual success. However, these contaminants can be removed according to the process of the invention, but a more effective process will have to be developed.

It is therefore quite plausible to expect that efforts to enhance this preferred separation process, could lead to an H_2ZrF_6 product that is much purer than can be conventionally obtained.

Pin et al.[44] combined cation exchange and extraction chromatography for the concomitant separation of Zr, Hf, Th and the lanthanides. These authors reported that "during HF dissolution of silicate rocks and minerals, negatively charged fluoride ions such as ZrF_6^{2-} are formed during the initial decomposition step. In addition, sparingly soluble complex fluorides are also formed. Major amounts of REE and Th can be trapped by these fluoride precipitates". This finding is in accordance with that cited in the reference by Johannes Theodorus Nel[43].

However, these aqueous routes all have disadvantages and limitations with respect to the degree of purification because of recontamination from the background levels of contaminants present in the processing chemicals[36], therefore for the purpose of this dissertation the use of an anhydrous route will rather be investigated.

2.5.2 Novel anhydrous routes

The anhydrous route solves some of the problems associated with oxide and hydroxide formation. It also creates other problems due to the complex engineering design to accomplish the high-temperature vapour-phase reaction in the presence of corrosive hydrogen fluoride and of elemental

fluorine. The disadvantage of the anhydrous route is that a low or non-existent thermodynamic driving force for removal of the contaminants limits the vapour separation techniques. Any anhydrous Zr-Hf separation scheme will entail the use of additional purification procedures to achieve trace element removal.

One method of producing anhydrous zirconium tetrafluoride is via ZrO_2 and HF. According to an invention[45] anhydrous zirconium fluoride was produced by a three-step method:

1. Subjecting ZrO_2 to the action of hydrofluoric acid until an essentially complete reaction is effected between zirconium oxide and HF.
2. Heating the resulting products to dryness.
3. Calcining the dried products to produce anhydrous zirconium fluoride.

However, it is preferred that the hydrogen fluoride be provided as aqueous hydrofluoric acid (30 – 70 % HF). It is further essential that step 1 be carried out in such a way that fluorination of the zirconium compound is substantially complete, in order to avoid side reactions during steps two and three.

Zirconium tetrachloride was also used as a precursor whereby a process for removing hafnium tetrachloride from zirconium tetrachloride was outlined[46]. Heating the compound in vacuo or inert atmosphere with finely divided metallic zirconium, magnesium, aluminum, zinc or another reducing agent of sufficient oxidation-reduction potential, effects the reduction. The zirconium tetrachloride may be reduced to the trichloride or dichloride with zirconium metal at a preferred temperature of 300 to 350 °C. The hafnium tetrachloride remains substantially unchanged during the reduction, and it may be recovered readily from the zirconium subhalides or metal because of its comparatively greater volatility.

Even though hafnium tetrachloride can be recovered from the zirconium halides, it is quite difficult to handle the lower valence halides e.g. $ZrCl_3$ and $ZrCl_2$.

$$ZrCl_4 + Zr \rightarrow ZrCl_{4-x} + HfCl_4 \uparrow \text{.....2.7}$$

The unvolatilized residue consisting of reduced zirconium compounds may be converted into zirconium tetrachloride and metallic zirconium by heating in vacuo at 600 °C until disproportionation of zirconium dichloride is substantially effected.

$$2ZrCl_3 \Leftrightarrow ZrCl_4 + ZrCl_2\,(> 300\,°C)\text{.....2.8}$$
$$2ZrCl_2 \Leftrightarrow ZrCl_4 + Zr\,(> 600\,°C)\text{.....2.9}$$

The resultant zirconium tetrachloride can be pumped off and condensed, containing less than 0.1 percent of hafnium tetrachloride.

For a subsequent dry purification route zirconium tetrachloride will preferably have to be converted to ZrF_4[47].

$$ZrCl_4 + HF \rightarrow ZrF_4\,(90\%) + HF \rightarrow ZrF_4\text{.....2.10}$$

There are numerous patents regarding these processes[48, 49].

Newnham extended the original concept of this patent by effecting the reduction in a molten-salt medium, such as $AlCl_3$-NaCl, LiCl-KCl, or other mixtures, containing at least one alkali chloride salt. The molten-salt medium was said to keep the temperature close to the optimum required for selective reduction. The patent claims that the separation can be carried out through decantation or filtration, as $ZrCl_3$ is a solid in a liquid medium.

Dehydrated $ZrOCl_2$ was also regarded as a precursor material, and can affordably be obtained from China[50].
Furthermore, during the synthesis of $ZrOCl_2$ from e.g. zircon, some degree of purification might already have taken place.

$$ZrOCl_2 + HF \rightarrow ZrF_4.xH_2O \xrightarrow{110\,°C} ZrF_4.H_2O \xrightarrow{575\,°C} ZrF_4\text{...2.11}$$

Regrettably the researchers cite that during the dehydration of the oxychloride (at a temperature of 200 to 300 °C while fluorinating the dehydrated product with gaseous hydrofluoric acid at between 200 and 400 °C) certain difficulties were experienced:

1. During the dehydration step of the oxychloride, part of the oxychloride was converted to the zirconium oxide, which was not as easily convertible to the fluoride as is the chloride; consequently the yield of zirconium tetrafluoride from $ZrOCl_2$ was not as satisfactory as from $ZrCl_4$.
2. Furthermore, the zirconium tetrafluoride obtained by hydration process, being contaminated with zirconium oxide, had to be purified by sublimation.
3. Zirconium tetrafluoride obtained by sublimation is very hard and rather difficult to grind.

Sublimating $HfCl_4$ from $Zr(Hf)Cl_4$ is not a recommended technology since there is only a small difference between the vapour pressures of $ZrCl_4$ (331 °C) and $HfCl_4$ (317 °C) and therefore it is imperative to convert the $ZrCl_4$ to ZrF_4 for sublimation purposes.

Zirconium tetrafluoride has been prepared by numerous methods, which is summarized by Blumenthal[51] as follows:

1. Synthesis from the elements[52]

$$Zr + F_2 \xrightarrow{>190^\circ} ZrF_4 \quad \text{.....2.12}$$

2. Displacement of oxygen[52]

$$ZrO_2 + F_2 \xrightarrow{525^\circ} ZrF_4 + O_2 \quad \text{.....2.13}$$

3. Thermal decomposition of fluozirconates[64]

$$(NH_4)_2ZrF_6 \xrightarrow{<300^\circ} ZrF_4 + 2NH_4F \quad \text{.....2.14}$$

4. Metathesis from the oxide[53]

$$ZrO_2 + 4HF \xrightarrow{550^\circ} ZrF_4 + 2H_2O \quad \text{..... 2.15}$$

5. Metathesis from zircon[54, 55]

$$ZrO_2.SiO_2 + 8HF \xrightarrow{\text{white heat}} ZrF_4 + SiF_4 + H_2O \quad ....2.16$$

6. Metathesis from the tetrachloride[49]

$$ZrCl_4 + 4HF \rightarrow ZrF_4 + 4HCl \quad .....2.17$$

7. Hydrofluorination of oxyfluozirconic acids[56]

$$H_2ZrO_2F_2 + 2HF \xrightarrow{550^\circ} ZrF_4 + 2H_2O \quad .....2.18$$

Conventionally ZrF_4 is synthesized from either ZrO_2 or $ZrCl_4$ by interaction with HF or F_2. The purpose of this study is however to develop a purification procedure for purifying Zr of Hf, and the eventual ZrF_4 might be prepared via another, preferably inherent anhydrous route.

2.6 PREFERRED Zr PRECURSOR

A distinction has to be made whether $ZrCl_4$ or ZrF_4 should be the preferred reduction precursor for manufacturing of nuclear-grade zirconium metal. The following is pertinent:

2.6.1 $ZrCl_4$ as precursor

From the literature it is evident that $ZrCl_4$ has played a very prominent role in the last decades of the previous century due to the fact that:

1. Carbochlorination processes to manufacture $ZrCl_4$ was easier to carry out than processes to manufacture ZrF_4 from e.g. zircon or baddeleyite;
2. The purification of Zr of Hf was effected mainly via chloride-based processes.

The most logical product ensuing from the above processes would probably be $ZrCl_4$. Without going into any detail, $ZrCl_4$ was almost certainly the preferred precursor for any subsequent reduction process to render zirconium metal. The preference for $ZrCl_4$ for plasma reduction processes by either H_2

or Mg metal was also borne out by Stander[57, 58], during chemical thermodynamic equilibrium studies.

The question of the hygroscopic nature of the Zr halide precursor must now be examined. The fact that $ZrCl_4$ is certainly very hygroscopic[59] "(Zirconium tetrachloride is instantly hydrolysed in water)" seems to be a foregone conclusion[60]. The effect of a precursor for reduction to nuclear-grade zirconium metal being very hygroscopic on the nuclear-grade integrity of the produced Zr metal, is a very important aspect. Becker[61] sums up the deleterious effect of the gaseous contaminants on the mechanical properties of zirconium: "Oxygen and nitrogen affect the mechanical properties of zirconium. The metal is strengthened by oxygen, thereby decreasing its ductility and formability as a metal".

Miller[62] also cites that "the Kroll process via $ZrCl_4$ as precursor was prone to failure because the oxygen introduced by hydrolysis of the extremely hygroscopic tetrachloride was ultimately transmitted to the reduced metal, as the chloride could contain as much as one percent oxygen and the resultant metal was brittle". For zirconium production, the compound to be reduced and the reducing agent should be as free of oxygen (and nitrogen and carbon) as possible to produce ductile zirconium metal. The conclusion to be drawn is that, seen in the light of the **inherent** hygroscopic nature of $ZrCl_4$, it might **not** be the preferred precursor for the manufacturing of nuclear-grade zirconium metal.

2.6.2 ZrF_4 as precursor

In contrast to $ZrCl_4$, ZrF_4 can be rendered anhydrous without much effort. The pertinent aspects can be summarized as follows:

1. Several researchers reported as to the viability of the thermal decomposition of $(NH_4)_3ZrF_7$ to afford ZrF_4[63, 64, 65, 66, 67];
2. McFarlane[63] in particular claimed that this route leads to the formation of anhydrous ZrF_4. The mechanism of thermal

decomposition (continuous evolvement of HF while the ZrF_4 is formed), greatly aids the formation of the anhydrous ZrF_4;

3. Wilhelm et al.[68] states that: “Zirconium tetrafluoride is widely used for the production of zirconium metal, either by electrolysis or by reduction with alkaline earth metals. For the production of a pure zirconium metal, it is desirable to use a zirconium tetrafluoride of high purity”;
4. Craigen et al.[69] reported that “This salt (ZrF_4) is used primarily because of its much greater stability in air against moisture pick-up, and much lower volatility”, and “The process described has proved to be feasible for the production of a high-purity anhydrous, relatively stable ZrF_4, which can be used for the production of nuclear-grade zirconium”. Craigen states further that: “Criteria for the ZrF_4 to be nuclear-grade was:
    a. Absence of $ZrF_4.H_2O$;
    b. A stability factor of ca. 0.01 %/h moisture pick-up at 50 % relative humidity”.
5. Rivas[70, 71] mentions that the most stable form of zirconium tetrafluoride is anhydrous ZrF_4 (β-ZrF_4). Isomorphs (alpha and gamma) will transform to the β-form upon heating. It was further mentioned that continuous exposure to wet air seems to have no effect on the hyperfine interaction pattern at room temperature, therefore no hydrolysis takes place.

From the above-cited references it can now be concluded that there exist well-described manufacturing routes for anhydrous ZrF_4. Anhydrous ZrF_4 can of course also be manufactured from ZrO_2, $ZrOCl_2$, or $ZrCl_4$, by successive treatment with aqueous and anhydrous HF, with subsequent heating. However, after careful evaluation of the above literature evidence, and backed up by Necsa thermodynamic chemical equilibrium data, the preferred anhydrous ZrF_4 can also be prepared via the thermal decomposition of $(NH_4)_3ZrF_7$, which can be manufactured directly from ZrO_2, ex PDZ.

$$ZrO_2 + 3NH_4F.HF + HF \xrightarrow{140\,^{\circ}C/\Delta} (NH_4)_3ZrF_7 + 2H_2O \text{.....} 2.19$$

$$(NH_4)_3ZrF_7 \xrightarrow{<300\,^{\circ}C/\Delta} 3NH_4F + ZrF_4 \text{.....} 2.20$$

According to all available evidence, this ZrF_4 is produced as β-ZrF_4 and remains anhydrous for extended periods of time, even in moist air.

The next question to be addressed is whether this ZrF_4 will be a good precursor for reduction to Zr metal. The following are pertinent from literature, and thermodynamic chemical equilibrium studies:

1. From literature evidence ZrF_4, and especially anhydrous ZrF_4 is described as a perfect precursor to be purified to nuclear quality, and then reduced to nuclear-grade Zr metal;
2. However, thermodynamic chemical studies under equilibrium conditions do not support the ZrF_4 as being the preferred precursor. In this regard the work done by Stander[57] clearly illustrates that ZrF_4 is not nearly an ideal precursor for plasma reduction by either H_2 or Mg metal;
3. $ZrCl_4$ is a much better choice as far as the reduction process is concerned;
4. The $ZrCl_4$, because of its **inherent** hygroscopic nature, may however not be a perfect precursor for the manufacturing of nuclear-grade Zr metal and its alloys.

$ZrCl_4$ is commonly used, although, according to Watanabe[72], fluorine-containing compounds of the metals are better starting materials and relatively easily reduced to the pure metal. This may mean that it may be more beneficial to utilize the tetrafluoride (Zr) instead of the more hygroscopic tetrachloride to manufacture the metal[73].

In the case of the present study, the ZrF_4 precursor was preferred to $ZrCl_4$ (more conventional option) for the following reasons:

a. Superior resistance to hydration;
b. Lower volatility;
c. Necsa's fluorochemical conversion expertise.

This of course leads to the next issue. Can anhydrous ZrF_4 be converted to anhydrous $ZrCl_4$? In this regard Blumenthal[67] proposed a very elegant solution. He patented a process whereby anhydrous ZrF_4 manufactured via the ammonium double salt route and is converted with $MgCl_2$ to $ZrCl_4$ (anhydrous?).

$$ZrF_4 + 2MgCl_2 \xrightarrow{>750\,^{\circ}C/\Delta} ZrCl_4 + 2MgF_2 \quad \text{.....2.21}$$

This $ZrCl_4$ was then described as the perfect precursor to reduce by convenient means to nuclear-grade Zr metal.

One of the unresolved issues however, is whether this $ZrCl_4$ will be anhydrous in order to ensure optimum quality Zr metal. This will have to be validated experimentally.

In conclusion the following manufacturing route for the nuclear-grade zirconium metal from zircon feedstock was recommended:

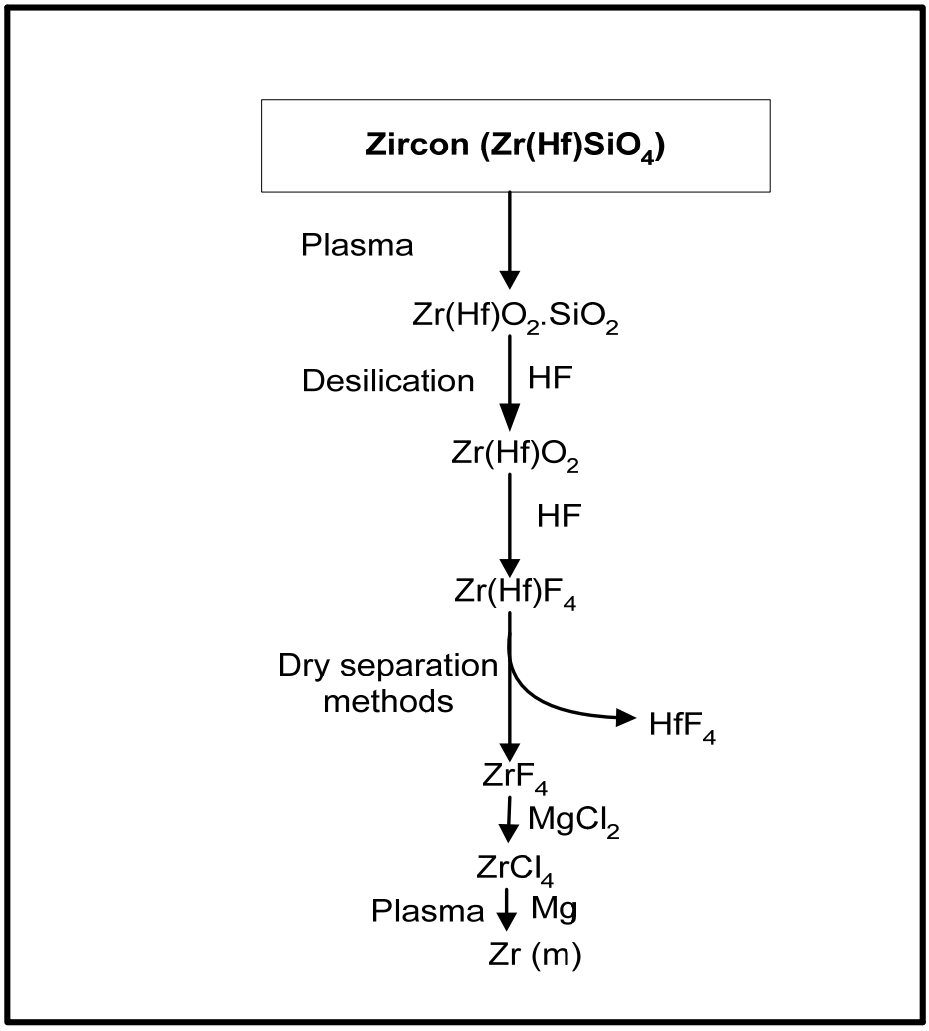

Figure 2.2: Schematic representation of the dry separation route.

1. Manufacture PDZ from zircon by plasma dissociation.
2. Desilicate the PDZ with anhydrous HF to afford $Zr(Hf)O_2$.
3. Convert the $Zr(Hf)O_2$ with HF to $Zr(Hf)F_4$.
4. Purify $Zr(Hf)F_4$ of HfF_4.
5. Convert the purified anhydrous ZrF_4 with $MgCl_2$ to $ZrCl_4$.
6. Plasma reduce the $ZrCl_4$ with Mg metal to afford nuclear-grade Zr metal.

2.7 SUBLIMATION TEMPERATURES OF ZrF_4 AND CONTAMINANT FLUORIDES

As has been stated, the choice for primary precursor to be purified is ZrF_4. All the contaminants present in the feedstock zircon, as well as the materials of construction up until the end of the manufacturing of the precursor will then most probably also be present similar to the fluorides. A list of these fluorides as well as their boiling and melting points is summarized in Table 2.1[74].

Table 2.1: List of boiling and melting points of the possible impurity fluorides present in ZrF_4, as well as their different oxidation states.

	Formula	Mp/^{o}C	Bp/^{o}C
1	AlF_3	~2250 tp	1276 sp
2	BF_3	-126.8	-101
3	CdF_2	1110	1748
4	CoF_2	1127	~1400
5	CoF_3	927	
6	CuF_2	836	1676
7	CrF_2	894	
8	CrF_3	1400	
9	CrF_4	277	
10	CrF_5	34	117
11	CrF_6	-100	
12	FeF_2	1100	
13	FeF_3	>1000	-
14	HfF_4	>970	
15	MnF_2	930	
16	MnF_3	>600	
17	MoF_3	>600	
18	MoF_5	67	213.6
19	MoF_6	17.5	34.0
20	NiF_2	1474	
21	SiF_4	-90.2	-86
22	ThF_4	1110	1680
23	TiF_3	1200	Subl.
24	TiF_4	284	1400
25	UF_4	1036	1417
26	UF_5	348	
27	UF_6	64.0 tp	56.5 sp
28	WF_4	>800	
29	WF_5	>80	
30	WF_6	2.3	17.1

A problem was encountered because very limited data was available with regard to the physical constants associated with the sublimation process. Unfortunately, there is a too small difference in the sublimation temperatures of ZrF_4 and HfF_4 to provide an adequate driving force for a successful

straightforward purification by sublimation, and as far as can be ascertained, no global player in the nuclear field up to date has successfully purified ZrF_4 of HfF_4 by straightforward sublimation. Even if data were available, it was often contradictory, with some sources reporting HfF_4 to have a higher volatility than ZrF_4, and vice versa. An example of this is presented in Table 2.2.

Table 2.2: Sublimation data obtained from literature.

Author	Year	Reference	Sublimation Temperature (°C)	
			ZrF_4	HfF_4
Tumanov	1972	[75]	~600	~400
Matweb	2006	[76]	-	970
CRC	2003	[74]	932	>970
Cantor et al.	1957	[77]	710 - 808	-
Sense et al.	1954	[78]	616 - 880	-
Sidorov et al.	1965	[79]	626 – 705	-
Galkin et al.	1963	[80]	440 - 600	-

Sublimation is normally used when the material to be purified is unstable i.e., temperature- or oxidation-sensitive at temperatures near to or below the triple point, or when the more conventional separation methods of distillation, solvent extraction, adsorption etc., are either impossible or highly expensive[81]. As a general rule, it is understood that a substance may be considered for sublimation purification if it is normally solid and has a reasonably high vapour pressure at moderate temperatures. Sublimation is a phase transition that occurs at temperatures and pressures below the triple point. The sublimation temperature T_s, is the temperature at which the sublimation pressure of the solid reaches atmospheric pressure.

From the literature it is evident that there does not exist an accurate definition of the sublimation conditions for which sublimation temperatures are quoted. Therefore, sublimation temperatures will have to be determined and their conditions clearly stated.

During the reaction of ZrO_2 with e.g. HF to form ZrF_4 there are intermediates that can possibly form, some of these can be ascribed to the formation of the oxyfluorides. The literature survey was undertaken to identify the entire stable intermediate product spectrum. The following table outlines the identified zirconium and hafnium compounds (as obtained from the ICDD database).

Table 2.3: Zr and Hf compounds with known X-ray powder diffraction patterns.

	Zr-compounds	Hf-compounds
1	ZrF_2	-
2	ZrF_4	HfF_4
3	$ZrOF_2$	-
4	Zr_2OF_6	Hf_2OF_6
5	$Zr_3O_2F_8$	$Hf_3O_2F_8$
6	$Zr_7O_9F_{10}$	-

2.8 TECHNIQUES FOR ENHANCING THE EFFICIENCY OF THE ANHYDROUS SUBLIMATION PROCESS

Most of the problems encountered with respect to the poor performance of straightforward purification by sublimation are centred around insufficient driving force for the sublimation reaction. To put it more simply, the difference in sublimation temperature between ZrF_4 and the contaminant fluorides must be increased. From literature, four so-called sublimation-enhancing techniques have been identified, and are listed below:

1. Improving the contaminant fluoride volatility by increasing the contaminant oxidation state;
2. Improving the separation by selective reduction of ZrF_4 to non-volatile species like ZrF_3;
3. Improving the separation by gettering;
4. Decreasing HfF_4 concentration by metal fluoride selective sorption.

Each of the four enhancing techniques will subsequently be discussed in more detail.

2.8.1 Improving the contaminant fluoride volatility by increasing the contaminant oxidation state

In general the vapour pressure of the contaminant fluorides will increase with an increase in the oxidation state of the contaminants. The extent to which sublimation temperatures decrease with increasing oxidation state of a contaminant is depicted in Table 2.4:

Table 2. 4: The vapour pressures of the impurity fluorides at different oxidation state.

Formula	Mp/°C	Bp/°C
CrF_2	894	
CrF_3	1400	
CrF_4	277	
CrF_5	34	117
CrF_6	-100	

The fluorides of the contaminant Cr for instance, illustrate the tendency very well. With the exception of CrF_3, the above data clearly illustrate the increase in volatility with the increasing oxidation state of the fluorides of chromium.

2.8.2 Improving the separation by selective reduction of ZrF_4 to non-volatile species such as ZrF_3

Newnham[46] is cited as reporting that separation of $ZrCl_4$ and $HfCl_4$ could be effected by selective reduction of $ZrCl_4$ by metals such as Zr (to be preferred from a contamination point of view). The reaction can be represented as follows, and is based on the reduction of $ZrCl_4$ to $ZrCl_3$:

$$Zr(Hf)Cl_4 + Zr \rightarrow ZrCl_3 + HfCl_4 \quad \text{.....2.22}$$

The $HfCl_4$ is not reduced, while the $ZrCl_3$ is not volatile, thus enabling separation.

2.8.3 Improving the separation by gettering

Withers[82] is cited as reporting that the purification of ZrF_4 containing the full spectrum of impurities can be effected by employing the so-called **gettering**

effect. ZrO_2 is added to the tetrafluoride mixture, and at the sublimation temperature of ZrF_4, zirconium oxide will react with impurity fluorides, including HfF_4, and convert them to non-volatile oxides. Thus the contaminants will stay behind as the oxides, with ZrF_4 subliming off.

The simplest way to produce anhydrous ZrF_4 is via ZrO_2 and fluorine gas.

$$ZrO_2 + 2F_2 \rightarrow ZrO_2/ZrF_4 \rightarrow ZrF_4 \quad \text{.....2.23}$$

During the process it is essential to have a small residual amount of ZrO_2 present to act as getter. The getter converts the impurity fluorides to non-volatile oxides, while zirconium dioxide is converted to zirconium tetrafluoride. By limiting the conversion during the initial reaction to less than 100 %, thus leaving a small residual amount of ZrO_2, the conversion of non-volatile impurity fluorides in the precursor zirconium dioxide to non-volatile impurity oxides is facilitated. Limiting the conversion process results in the formation of an intimate mixture between the zirconium dioxide and zirconium tetrafluoride and thus eliminates the need to separately prepare zirconium tetrafluoride and then mechanically mix it with zirconium oxide. The process is continuous, whereby zirconium tetrafluoride can be sublimed from hafnium oxide.

This process is capable of lowering the iron concentration from 7500 (average) parts per billion in the zirconium dioxide to less than 20 parts per billion in the zirconium tetrafluoride.

The technique of using zirconium dioxide as a “getter” in the zirconium tetrafluoride production phase is vastly superior to the subsequent mixing of zirconium dioxide with previously formed zirconium tetrafluoride during purification post-processing.

This technique is very important for the production of high-grade ZrF_4 to be used as a precursor for metal fluoride glasses. This ZrF_4 can be further purified of hafnium for nuclear applications.

$$Zr(Hf)F_4 \xrightarrow{ZrO_2/\Delta} HfO_2 + ZrF_4 \uparrow \text{.....2.24}$$

A further emphasis for using ZrO_2 as a getter during the purification of ZrF_4 is applied by Tatsuno[83]. This researcher cites "zirconium oxide is physically mixed with zirconium tetrafluoride prior to sublimation of zirconium tetrafluoride. The resulting sublimed zirconium tetrafluoride has a higher purity than sublimed zirconium tetrafluoride that has not been mixed with zirconium oxide".

This technique for using ZrO_2 as a getter is also described by Chandler[84] and Newnham[85]. The process is obtained by the passage of vapours containing both zirconium tetrachloride and hafnium tetrachloride over a bed containing zirconium dioxide and hafnium dioxide at elevated temperature.

$$ZrO_{2(s)} + HfCl_{4(g)} \rightarrow HfO_{2(s)} + ZrCl_{4(g)} \text{.....2.25}$$

In the above reaction, the hafnium tetrachloride reacts with the zirconium dioxide to form volatile zirconium tetrachloride, which mixes with the zirconium tetrachloride previously in the vapour phase. The hafnium tetrachloride probably accumulates in the bed by being converted to hafnium dioxide. The exact mechanism of this process is not known.

2.8.4 Decreasing HfF_4 concentration by metal fluoride selective sorption

Solov'ev and Malyutina[86] describe purification of ZrF_4 of HfF_4 by multiple sublimation of ZrF_4 out of a ZrF_4/HfF_4 mixture, in the presence of a suitable metal difluoride. The mechanism is apparently via preferential sorption of HfF_4 on the difluoride, and they reported that after eight cycles of sublimation in the presence of sorbent (specifically NiF_2), ZrF_4 with a hafnium content of

0.05 wt % was obtained. The metal difluoride should conform to the following criteria:

1. The sorbent must have a boiling point (sublimation temperature) higher than that of ZrF_4;
2. The sorbent must not melt at temperatures close to the sublimation temperature of ZrF_4;
3. The sorbent must not form non-dissociable compounds with ZrF_4 or HfF_4;
4. The sorbent must be easily available and cheap;
5. The sorbent should be easily recoverable following use.

From all the metal difluoride candidate materials, the researchers chose NiF_2. From a contaminant point of view, FeF_2 would be a better material, since the maximum impurity levels allowed in nuclear-grade zirconium alloys are:

For Ni – 70 ppm

For Fe – 1500 ppm

The sublimation purification was carried out at 700-850 °C.

Note: The researcher claims that a content of 0.05 % (500 ppm) Hf is allowed for nuclear applications, while the conventional norm is <0.01 % (100 ppm).

It is recommended that an enhanced sublimation procedure employing both gettering and selective sorption be used for optimum purification.

2.9 RAMAN SPECTROSCOPY

Raman spectral features are directly related to the vibrational motions of the structural units. It is a molecular spectroscopic technique that allows identification of the molecular structure of the catalytically active species as well as their interaction with the surrounding reactive molecules. Due to its non-destructive characteristic, Raman spectroscopy is ideally suited for *in-situ* analysis of macro and micro samples ranging from materials research to quality control. The Raman spectrum reveals valuable information about crystallinity, polymorphism and phase transitions. Raman spectroscopy

combines high information content, no sample preparation and the use of fiber optic probes for remote sensing. These features make Raman spectroscopy attractive for process applications.

Raman spectroscopy has been limited in its applications by one major problem, namely fluorescence[87]. As a phenomenon, fluorescence is approximately 10^6-10^8 times stronger than Raman scattering. Often when one tries to excite a Raman spectrum, fluorescence is the only phenomenon observed. Trace impurities, coatings on polymers, additives, etc., may influence fluoresce so strongly that it is impossible to observe the Raman spectrum of a major component. The use of UV or near-IR excitation has proved to be effective in reducing this problem.

Minimal literature regarding Raman analyses with respect to the interaction of ZrO_2 with HF (and/or F_2) is available. However vast information on Raman spectroscopic studies of ZrO_2, HfO_2 and ZrO_2-HfO_2 solid solutions is readily available. In this particular study the emphasis was placed on the understanding of the phase transformations of these samples at different temperatures and pressures.

Zirconia (ZrO_2) and hafnia (HfO_2) are similar in many respects. At room temperature, they are both monoclinic, with four formula units per unit cell[88]. They both transform to a tetragonal phase, the former between 1250 and 1450 K, the latter at approximately 873 K higher. However, zirconia exists as three well-defined polymorphs, i.e. monoclinic baddeleyite (natural ZrO_2) and the tetragonal and cubic structures[89].

Jayaraman et al.[90] carried out high-pressure Raman studies at room temperature on HfO_2, up to 50 GPa. They established that at higher temperatures (> 1700 °C) and under ambient conditions, zirconia and hafnia crystallize in the so-called monoclinic structure, which transforms to a tetragonal and then to a cubic structure.

A *in-situ* high-pressure Raman and X-ray-diffraction study[91] on pure ZrO_2 showed that when a ZrO_2 single-crystal is pressurized at room temperature, the following transformations occur consistently. With increasing pressure: (1) monoclinic to orthorhombic near 3.5 GPa, (2) orthorhombic to another unidentified structure (probably also another orthorhombic phase) near 13 GPa, and then (3) another transition at about 35 GPa, for which a tetragonal lattice different from that of the high-temperature tetragonal phase has been suggested.

The Raman spectra of ZrO_2 were also measured with respect to temperature in the range 300 to 1600 K. Ishigame et al.[89] found that "when measuring Raman spectra at increasing temperatures, the lines show red shift and an increase in line width as the temperature increases".

In view of the strong similarities that should exist between ZrO_2 and HfO_2, pressure-induced transition sequences of the same type for HfO_2 was expected. Arashi et al.[91] revealed such similarities for the first pressure-induced phase transition that occurs in HfO_2 near 4.3 GPa, and also found that the Raman spectral features of the high-pressure phase following this transition is very similar to that of the orthorhombic phase of ZrO_2. Arashi therefore concluded that this high-pressure phase of HfO_2 is orthorhombic with the space group symmetry *Pbmc*, as in the case of ZrO_2.

Kerbs et al.[92] studied the vibration spectra of HfO_2-ZrO_2 solid solutions. They found that all the observed band maxima for solid solutions of the system HfO_2-ZrO_2 do not split, but gradually shift in wave number between those observed for the pure end-members. Correlation of Raman bands of HfO_2-ZrO_2 composition is shown in their Table I.

Goldstein et al.[93] conducted a study on the vibrational spectra of ZrF_4, HfF_4 and CeF_4. They experienced some difficulty in obtaining reliable Raman data. They measured the vibrational data for the tetrafluorides of U, Zr, Hf and Ce, which are depicted in their Table 1. HfF_4 was reported to be strongly fluorescent, but a number of Raman bands could be discerned separate to

those of ZrF_4. There were considerably more bands in the Raman spectra of ZrF_4 and HfF_4 than the four reported for UF_4. Zachariasen[94] cited that only unit-cell dimensions and space grouping have been reported for ZrF_4 and HfF_4 and that these compounds are monoclinic with twelve stoichiometric molecules per unit cell. This was found to be isostructural to UF_4.

2.10 CONCLUSIONS

In conclusion of the discussion surrounding the concept of enhanced sublimation the following can be highlighted:

1. No global and viable sublimation-based purification process for the removal of Hf from Zr compounds to nuclear-grade standards has yet been identified. The only viable processes are based on aqueous routes.
2. Collation of experience at Necsa with that gleaned from world literature has lead to the conclusion that only a self-named “enhanced” sublimation purification process would be capable of purifying Zr compounds of Hf to a level complying with nuclear standards.
3. Four sublimation-enhanced processes have been identified and described in some detail.
4. Although for obvious reasons and supported by a number of literature references, the initial choice for precursor was ZrF_4, subsequent equilibrium thermodynamic studies have strongly suggested that $ZrCl_4$ is the preferred precursor for the final reduction process to render the metal.
5. It has in principle been decided upon that any purification would be done on ZrF_4 and the ZrF_4 be subsequently converted to $ZrCl_4$ by an appropriate process.

CHAPTER 3

THERMODYNAMIC EQUILIBRIUM CALCULATIONS

3.1 INTRODUCTION

This chapter deals with the calculation of the equilibrium composition and theoretical separation coefficients of ZrF_4 and metal fluoride impurities. A range of metal fluoride impurities were investigated for calculation of theoretical separation coefficients. The HSC Chemistry 6.1 program was used throughout this study. This program was designed to simulate various kinds of chemical reactions and equilibrium calculations.

Thermodynamic equilibrium calculations were done to investigate the feasibility of fluorinating ZrO_2 with anhydrous hydrogen fluoride and fluorine and the reduction of zirconium tetrafluoride by CH_4 and H_2. A thermodynamic study was also done to simulate purification mechanisms to transform ZrF_4 to nuclear grade using an open or closed system, e.g. by means of a getter principle, and furthermore to calculate the separation coefficients of impurity metals. This was to ascertain the separation mechanism and the advantages of exploiting differences in the physical properties of ZrF_4 and metal impurities.

The efficiency of removing impurities from ZrF_4 by sublimation in a system can be characterized by means of a separation coefficient. For applications in nuclear industry, zirconium has to be purified of certain contaminants to adhere to nuclear specifications, as outlined in Chapter 1. This study was undertaken to theoretically calculate the separation coefficients between ZrF_4 and metal fluoride impurities. However, one challenging aspect about these calculations is that vapour pressure data for these metal fluoride impurities are not readily available. The theoretical calculations of separation coefficients were done to provide understanding with respect to the difficulty of separation of impurity fluorides.

3.2 EQUILIBRIUM COMPOSITION CALCULATIONS

A system is said to be in thermodynamic equilibrium when it is in thermal, mechanical and chemical equilibrium. A thermodynamic equilibrium is characterised by the minimum of a thermodynamic potential. For systems at constant temperature and volume this is the Helmholtz free energy:

$$A = U - TS \quad \text{.....3.1}$$

For systems at constant pressure and temperature it is the Gibbs free energy:

$$G = H - TS \quad \text{.....3.2}$$

A thermodynamic system at constant pressure and temperature will therefore reach equilibrium when the Gibbs free energy is at a minimum value. Thus, for chemical systems at a specific temperature and pressure, the composition at equilibrium can be calculated by minimising the Gibbs free energy of the system.

The Gibbs free energy of a multi-component chemical system is equal to the sum of the Gibbs free energies of the individual components. To determine the equilibrium composition it is thus necessary to calculate the Gibbs free energies for all components of all possible combinations of chemical elements in a system, and to minimise the total Gibbs free energy. This will be valid for a closed system, i.e. a system that can exchange energy with its surroundings, but not matter.

A thermodynamic program known as *HSC Chemistry™ 6.1* was used in this study to evaluate different species for various kinds of chemical reactions and equilibrium compositions by minimising the Gibbs free energy of a system[(95)]. From this point onward this model will be referred to as HSC. The current version contains fourteen calculation modules displayed as fourteen options in the HSC main menu, which are as follows:

1. Reaction Equations
2. Heat and Material Balances
3. Heat Loss Calculations
4. Equilibrium Composition
5. Electrochemical Equilibria
6. Formula Weights
7. Eh – pH – Diagrams
8. H, S, C and G Diagrams
9. Phase Stability Diagrams
10. Mineralogy Iterations
11. Composition Conversions
12. Elements
13. Water/Steam Tables
14. Units

In this study the Gibbs free energy is calculated as a function of variables like the composition, temperature, pressure etc. The thermochemical database contains enthalpy (H), entropy (S) and heat capacity (C_p) data for more than 20,000 chemical compounds. HSC makes it possible to simulate chemical equilibria between pure substances and in ideal solutions, and to some extent, non-ideal solutions. The HSC Chemistry program is also used to develop new chemical processes and to improve current or old ones. It enables the user to simulate chemical reactions and processes on a thermochemical basis. These simulation studies were done to model separation of zirconium from hafnium compounds.

The HSC contains several calculation modules; however for the purpose of this study the *Equilibrium Module of HSC Chemistry™ version 6.1* will be primarily used. This module easily calculates multi-component equilibrium compositions in heterogeneous systems. The user must specify the substances and potentially stable phases to be taken into account in the calculations, as well as the amounts of raw materials and the temperature. The program calculates the amounts of products at equilibrium in isothermal and isobaric conditions. A range of temperatures, pressures or raw material quantities can be specified and the program will calculate an appropriate range of equilibrium compositions, which can then be plotted as a function of temperature, pressure or starting material. The equilibrium composition is calculated using the Gibbs solvers, which use the Gibbs energy minimisation method. A detailed background on the chemical thermodynamics is outlined by I.J. van der Walt[(96)].

The limitation of this method should be noted. The program can only do the calculations for pure substances and ideal solutions in a closed system. It does not take into account factors such as reaction kinetics, mass and heat transfer. Experimental work is therefore needed to verify results, but the advantage of the software is that it gives direction to experimental planning and avoids expensive trial-and-error experimentation. A detailed procedural discussion of the *HSC Chemistry™ 6.1* computer program is given in Appendix 1.

3.3 EQUILIBRIUM COMPOSITION FOR THE REACTION BETWEEN ZrO_2 AND HF

The equilibrium composition resulting from the reaction of ZrO_2 with HF from 0 to 1000 °C at standard atmospheric pressure was calculated. This was to predict the feasibility of HF as a fluorinating agent in open and closed systems.

3.3.1 The Zr-O-H-F system

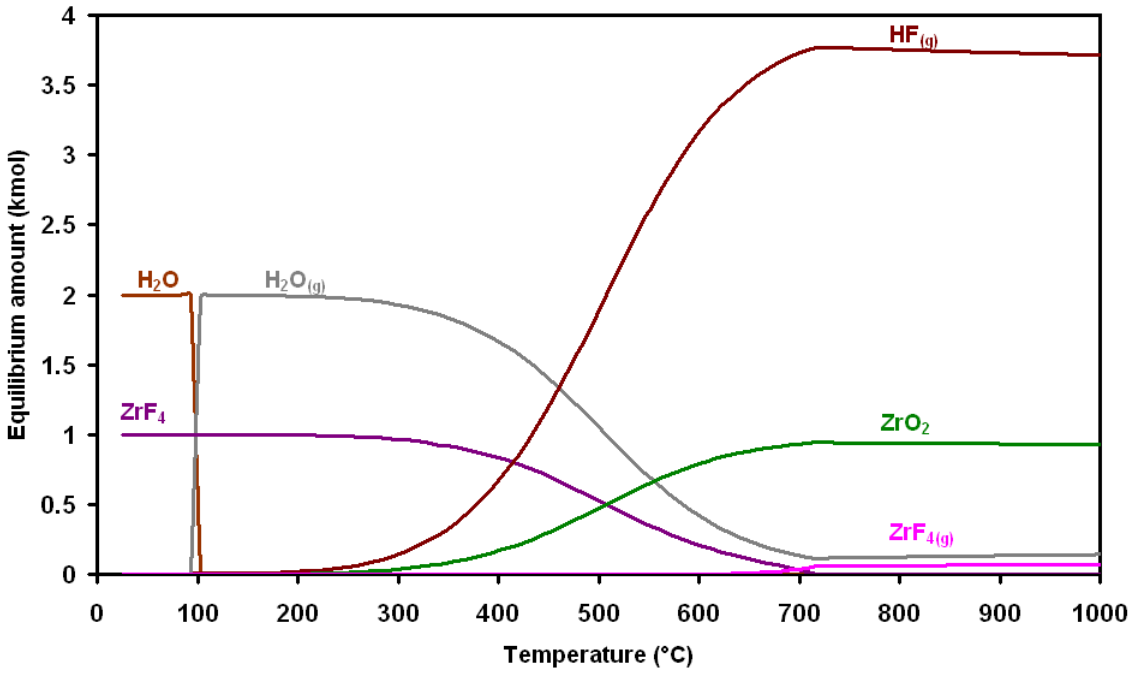

Figure 3.1: The equilibrium composition originating from the ZrO_2 + HF system.

Fig. 3.1 outlines a temperature dependence simulation for the fluorination of ZrO_2 (1 kmol) with HF (4 kmol). Nitrogen was not included in order to simulate a closed system. The simulation predicts the following reaction:

$$ZrO_{2(s)} + 4HF_{(g)} \rightarrow ZrF_{4(g)} + 2H_2O_{(g)} \text{.....3.3}$$

From Fig. 3.1 it can be seen that the formation of ZrF_4 and H_2O is predicted to occur from room temperature at an interaction of ZrO_2 with HF. At approximately 50 °C, H_2O starts to evaporate until it is completely in the vapour phase at ca. 100 °C. At ca. 200 °C the formed ZrF_4 is predicted to react with the H_2O vapour, forming ZrO_2 and HF until ca. 700 °C, where no further interaction was observed. Thus, the backwards reaction is favoured above 200 °C. A small quantity of ZrF_4 was observed at ca. 700 °C up to the maximum simulation temperature of 1000 °C.

3.3.2 The Zr-O-H-F-N system

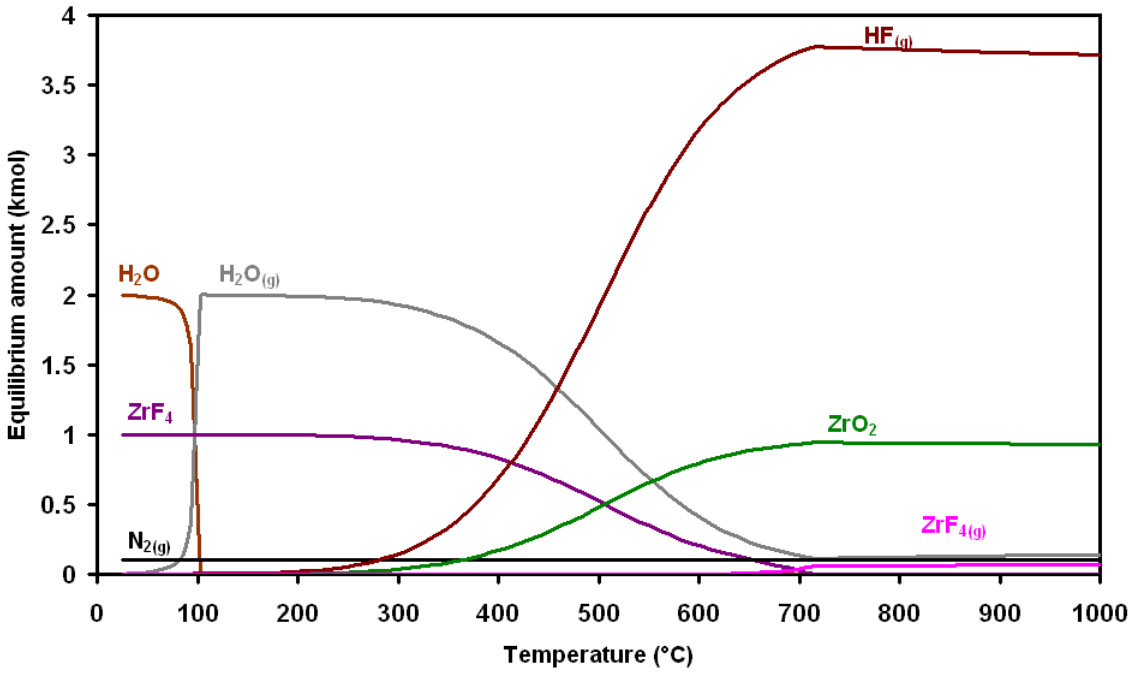

Figure 3.2: The equilibrium composition originating from the ZrO_2 + HF + N_2 system.

Fig. 3.2 depicts a temperature dependence simulation for the fluorination of ZrO_2 (1 kmol) with HF (4 kmol). Nitrogen gas was added to simulate an open system. The result is almost identical to the simulated closed system case. In general, the conclusion can be drawn that reaction 3.3 will only proceed to completion at temperatures below approximately 250 °C for both open and closed systems. Above this temperature the equilibrium starts to shift to the left. The implication is that the water that forms will have to be removed as quickly as possible to force the reaction to the right. It is concluded that thermodynamically HF can be used as a fluorinating agent.

The software predicts no oxyfluorides, but this is because there is no data for oxyfluorides in the database. Therefore the conclusion cannot be drawn that oxyfluorides will not form, but simply that the program is unable to predict this due to a lack of data.

3.4 EQUILIBRIUM COMPOSITION FOR THE REACTION BETWEEN ZrO_2 AND F_2

This paragraph simulates the equilibrium composition of the reaction of ZrO_2 with F_2 from 0 to 1000 °C at standard atmospheric pressure. This was to simulate the feasibility of F_2 as a fluorinating agent in open and closed systems.

3.4.1 The Zr-O-F system

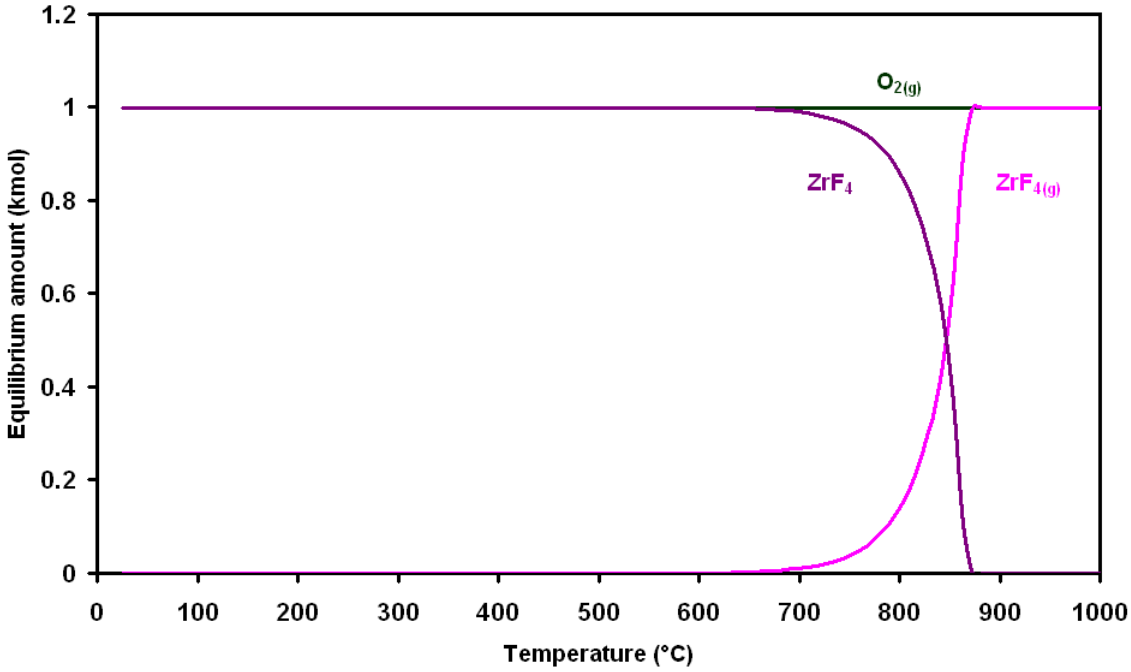

Figure 3.3: Equilibrium composition originating from the ZrO_2 + F_2 system.

Fig. 3.3 depicts a temperature dependence simulation of the fluorination of ZrO_2 (1 kmol) with F_2 (2 kmol), in a closed system. The simulation shows that the following reaction does take place

$$ZrO_{2(s)} + 2F_{2(g)} \rightarrow ZrF_{4(g)} + O_{2(g)} \text{.....3.4}$$

In general, the conclusion can be drawn that the reaction in equation 3.4 will proceed to completion at all temperatures up to 1000 °C, with sublimation estimated to commence at approximately 650 °C. From Fig. 3.3 it can be seen that the formation of ZrF_4 and O_2 is predicted to occur from room temperature at contact of ZrO_2 with F_2. At ca. 650 °C, ZrF_4 starts to sublime until it is completely in the vapour phase at ca. 870 °C.

3.4.2 The Zr-O-F-N system

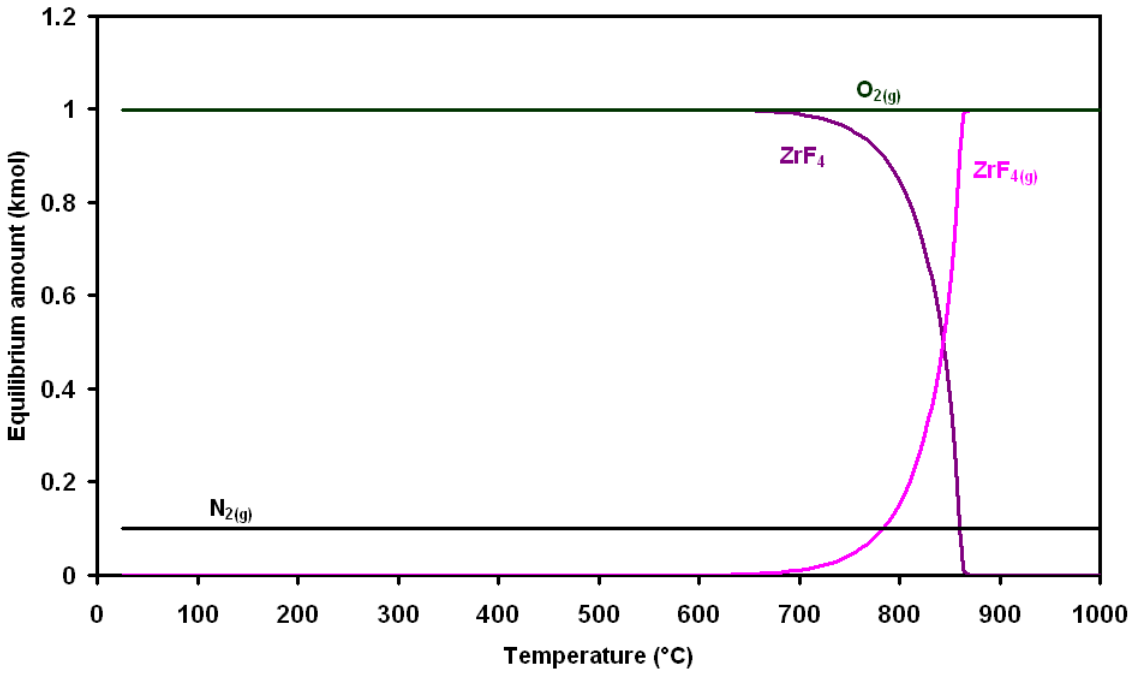

Figure 3.4: Equilibrium composition originating from the ZrO_2 + F_2 + N_2 system.

Fig. 3.4 depicts a temperature dependence simulation for the fluorination of ZrO_2 (1 kmol) with F_2 (2 kmol). Nitrogen gas was added to simulate an open system. It is concluded that the simulations of ZrO_2 with F_2 will render identical results irrespective of the open (Fig. 3.3) or closed (Fig. 3.4) systems. It is further concluded that thermodynamically F_2 is a better fluorinating agent than HF as there is no reversible reactions predicted.

The software predicts no oxyfluorides, but this is because there is no data for oxyfluorides in the database. Therefore the conclusion cannot be made that oxyfluorides will not form, but simply that the program is unable to predict this due to a lack of data.

3.5 EQUILIBRIUM COMPOSITION FOR SEPARATION OF ZrF_4 AND HfF_4

The main focus of this study is the separation of ZrF_4 from impurities, most importantly HfF_4. A sublimation-based separation was estimated using open and closed systems at different conditions. This was to render more concise and indicative information as to which system is practically viable.

3.5.1 The Zr-Hf-F system

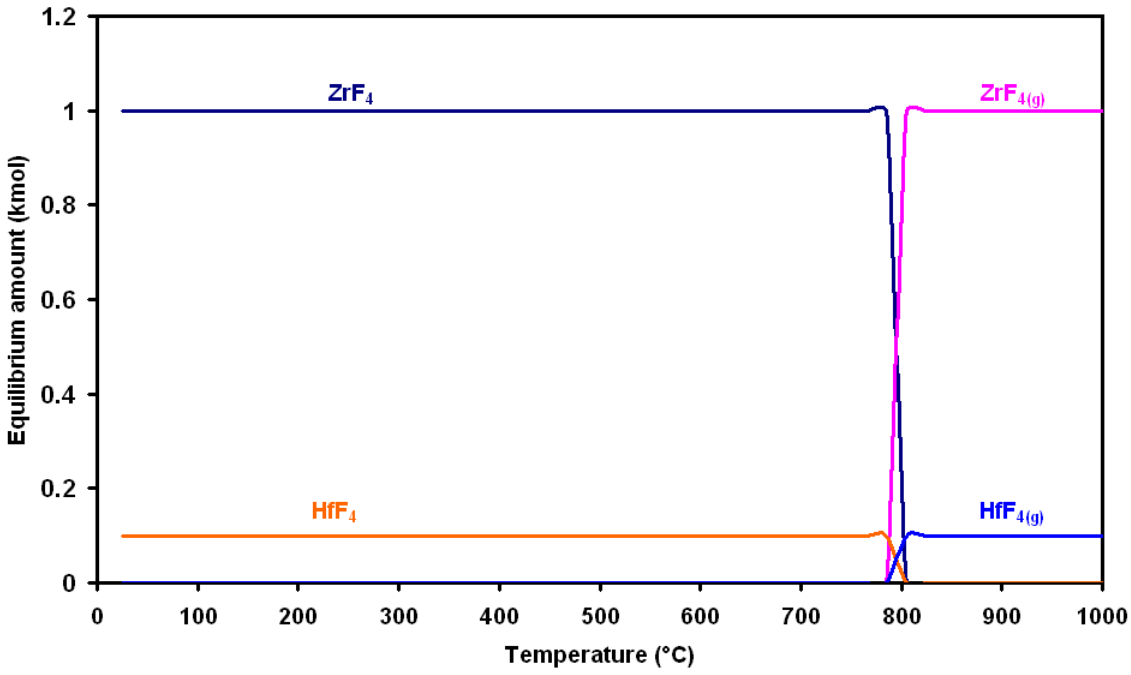

Figure 3.5: The equilibrium compositions originating from the ZrF_4 + HfF_4 system as a function of temperature at 0.1 bar.

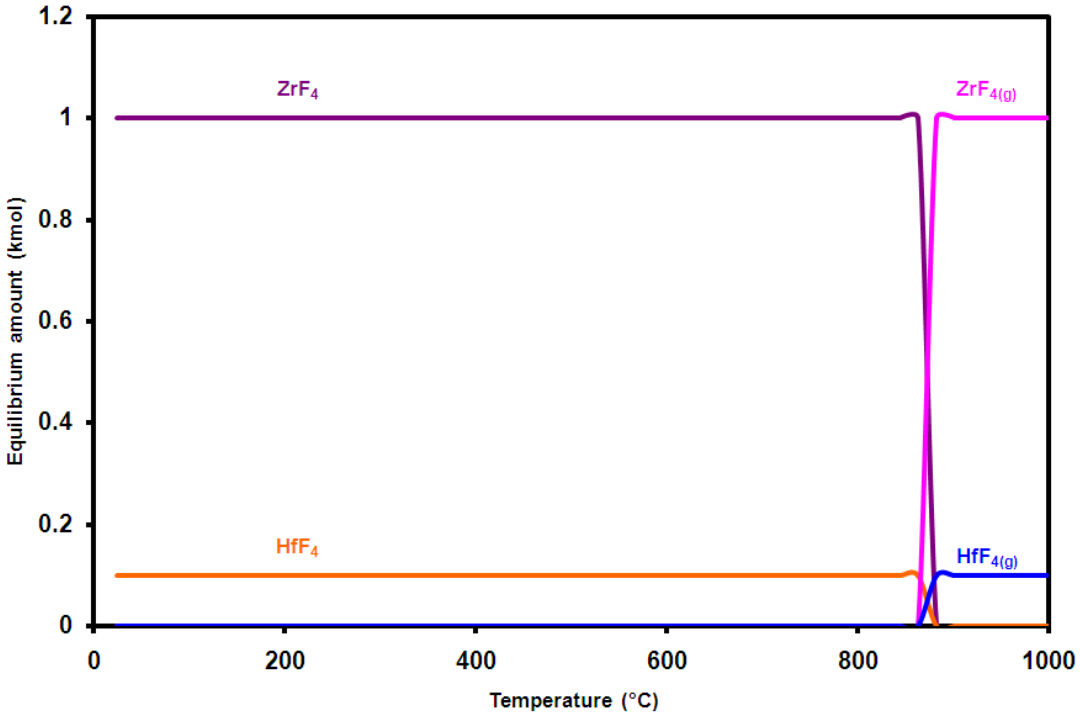

Figure 3.6: The equilibrium compositions originating from the ZrF_4 + HfF_4 system as a function of temperature at 0.5 bar.

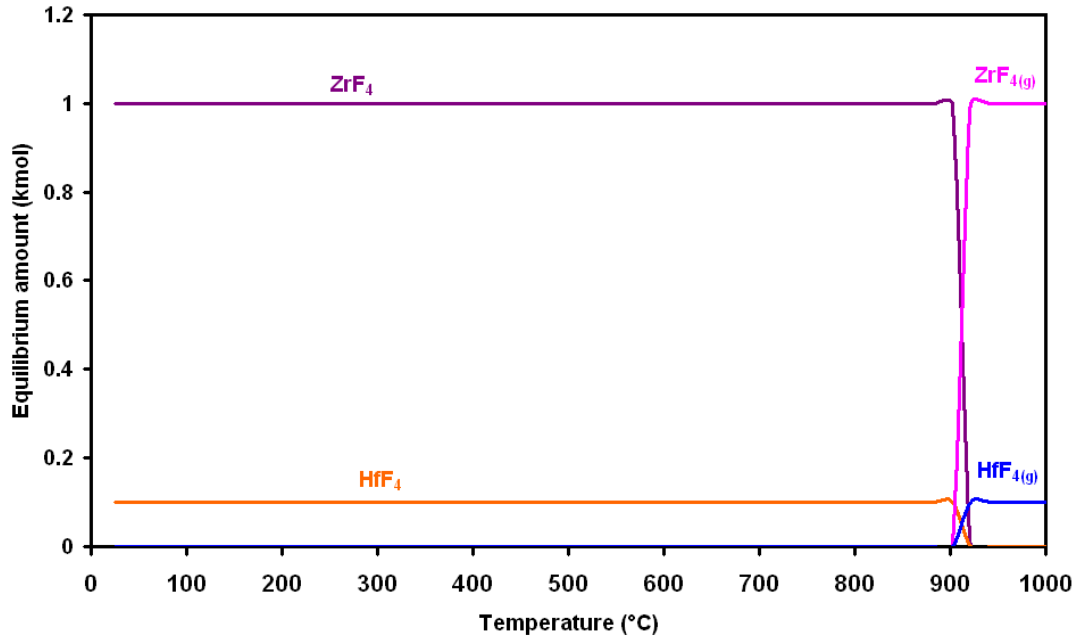

Figure 3.7: The equilibrium compositions originating from the ZrF_4 + HfF_4 system as a function of temperature at 1.0 bar.

The temperature dependence of sublimation-based separation of ZrF_4 and HfF_4 was estimated from thermodynamic studies[97]. The sublimation-based separation of ZrF_4 and HfF_4 reaction in a closed system was simulated as follows:

$$ZrF_{4(s)} + HfF_{4(s)} \rightarrow ZrF_{4(g)} + HfF_{4(g)} \text{ .....3.5}$$

These were performed at pressures of 0.1 bar (Fig. 3.5), 0.5 bar (Fig. 3.6) and 1.0 bar (Fig. 3.7). A 10:1 mole ratio of ZrF_4 and HfF_4 was used. The temperature domain between 25 to 1000 °C was considered. These conditions were used in a closed simulation. The following table was constructed from the thermodynamic study.

Table 3.1: The thermodynamic estimates from Figs. 3.5, 3.6 and 3.7.

Pressure [bar]	$T_s(HfF_4)$ [°C]	$T_s(ZrF_4)$ [°C]	$T_s(HfF_4) - T_s(ZrF_4)$ [°C]
0.1	780	780	0
0.5	850	850	0
1.0	900	900	0

From Table 3.1 the following observations can be made:

a) It is evident that the sublimation temperature of the compounds studied increases with the operating pressure.
b) No difference in the sublimation temperatures between ZrF_4 and HfF_4, irrespective of pressure, was observed.

It is concluded that a closed system cannot be used to effect separation of ZrF_4 and HfF_4.

3.5.2 The Zr-Hf-F-N system

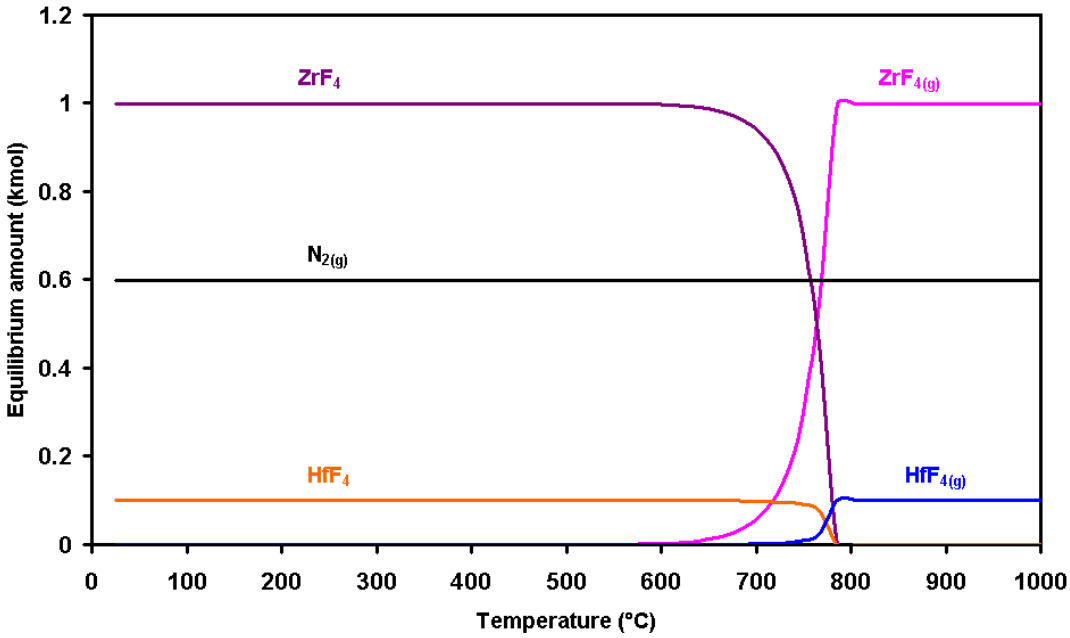

Figure 3.8: Equilibrium compositions originating from the ZrF_4 + HfF_4 + N_2 system as a function of temperature at 0.1 bar.

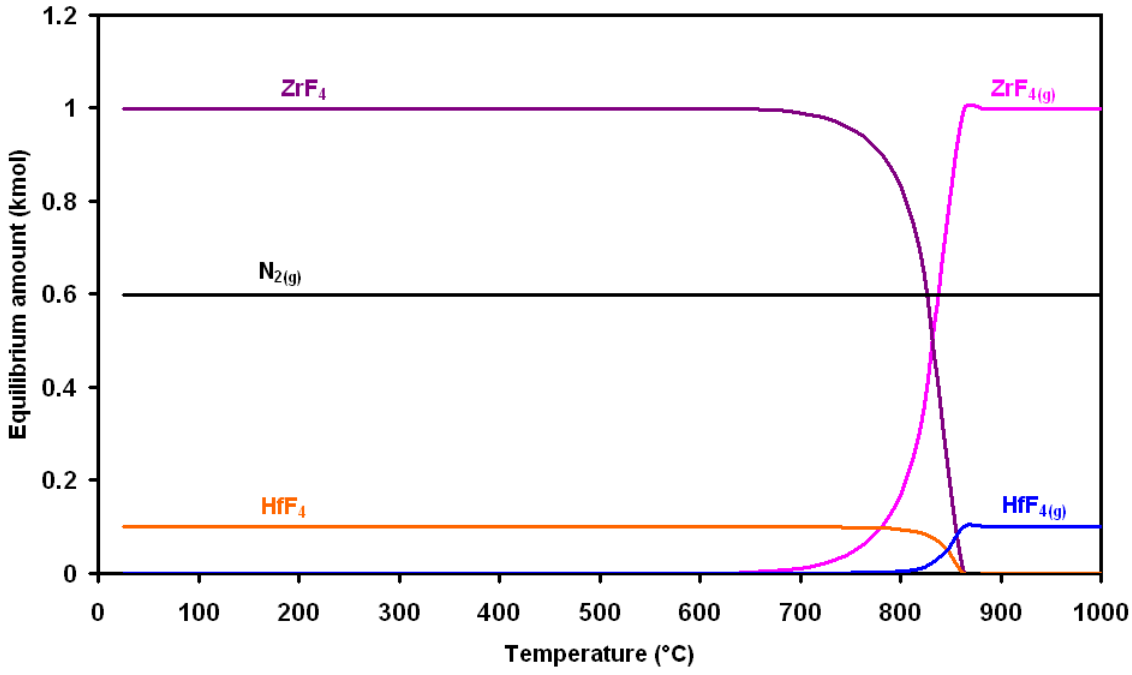

Figure 3.9: Equilibrium compositions originating from the ZrF_4 + HfF_4 + N_2 system as a function of temperature at 0.5 bar.

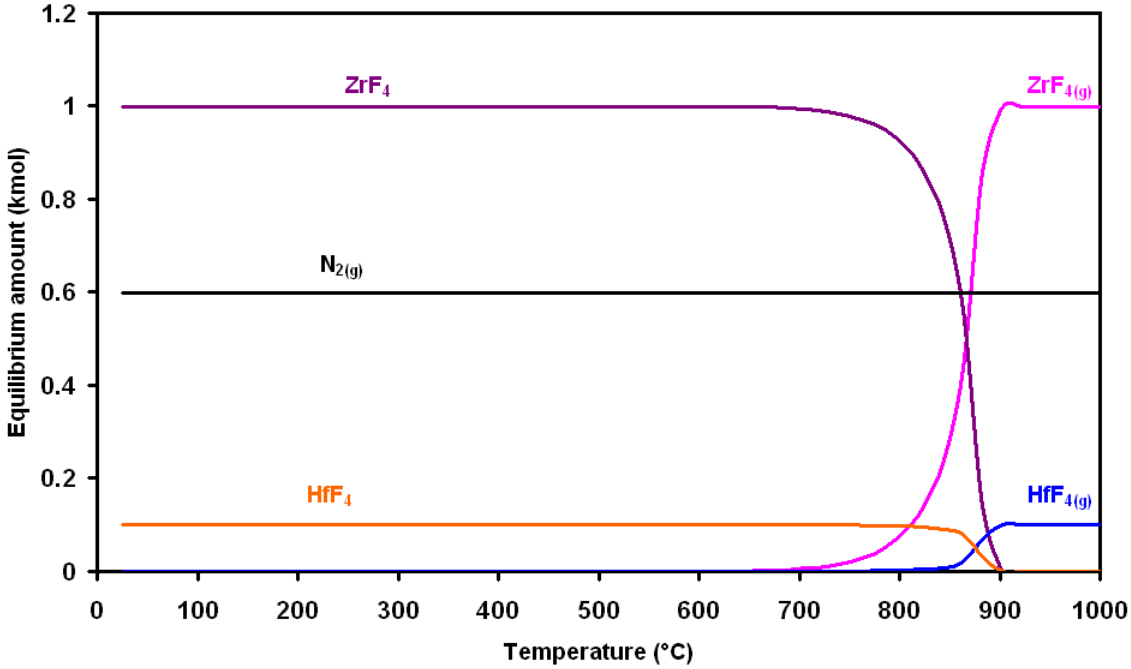

Figure 3.10: Equilibrium compositions originating from the ZrF_4 + HfF_4 + N_2 system as a function of temperature at 1.0 bar.

The temperature dependence of sublimation-based separation of ZrF_4 and HfF_4 was estimated from thermodynamic studies using $N_2(g)$ as an inert additive. The sublimation-based separation of ZrF_4 and HfF_4 reaction in an open system was simulated as follows:

$$ZrF_{4(s)} + HfF_{4(s)} \rightarrow ZrF_{4(g)} + HfF_{4(g)} \quad \text{.....3.6}$$

Studies were performed at three different pressures viz. 0.1 bar (Fig. 3.8), 0.5 bar (Fig. 3.9) and 1.0 bar (Fig. 3.10). These pressures were chosen arbitrarily to establish the effect on simulations. A 10:1 ratio of ZrF_4 and HfF_4 was used which corresponds roughly to the respective metal's ratio in the original ore. The $N_2(g)$ was added to the initial conditions of the study so as to simulate open-system conditions, while maintaining mass balance. This study is therefore more representative of true process conditions compared to the previous closed-system study. From this study, the following tabulated derivation can be made:

Table 3.2: The thermodynamic estimates from Figs. 3.8, 3.9 and 3.10.

Pressure [bar]	$T_s(HfF_4)$ [°C]	$T_s(ZrF_4)$ [°C]	$T_s(HfF_4) - T_s(ZrF_4)$ [°C]
0.1	720	620	100
0.5	780	630	150
1.0	780	650	130

From Table 3.2 data, the following observations can be made:

a) The sublimation temperature of both ZrF_4 and HfF_4 increases with operating pressure.
b) The isobaric difference in sublimation temperature between the two compounds appears to pass through a maximum (150 °C) in the region of 0.5 bar for the discrete pressures investigated. This sublimation temperature difference seemingly represents a practical value to base a practical process on.
c) Open system sublimation is (as expected from Le Chatelier's principle) more efficient (and practical) in effecting sublimation separation of the compounds than closed system sublimation.

3.5.3 The Zr-Hf-F-O system

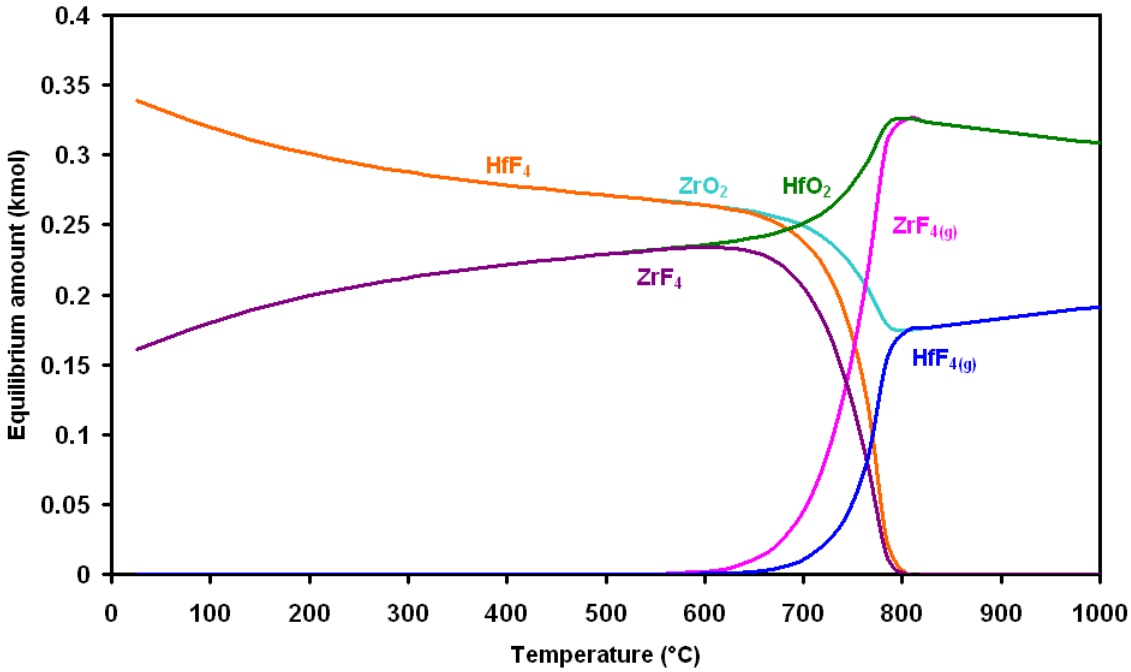

Figure 3.11: Equilibrium compositions originating from the ZrO_2 + HfF_4 + N_2 system as function of temperature.

These simulations were undertaken with the intent of investigating the feasibility of using ZrO_2 as a **getter** to enhance the separation of ZrF_4 and HfF_4. The following reaction was estimated to be viable:

$$ZrO_{2(s)} + HfF_{4(s)} \rightarrow ZrF_{4(g)} + HfO_{2(s)} \quad .....3.7$$

Fig. 3.11 shows equilibrium compositions of equimolar amounts of ZrO_2 and HfF_4 as starting materials as a function of temperature in an open-system. From this study it can be deduced that:

The zirconium oxide reacts stoichiometrically on a 1:1 basis with the hafnium tetrafluoride in an exchange reaction rendering a non-volatile residue at elevated temperatures (T > 800 °C) that is enriched in HfO_2 over ZrO_2. Correspondingly, the sublimed vapours are enriched with ZrF_4 over HfF_4. Process-synthesis-wise, it can be anticipated that enhanced separation will be achieved in a multistage application of the strategy.

The separation efficiency of the getter strategy is limited on a single-stage basis due to the unfavourable equilibrium that exists.

3.5.4 The Zr-Hf-F-O system with excess ZrO_2

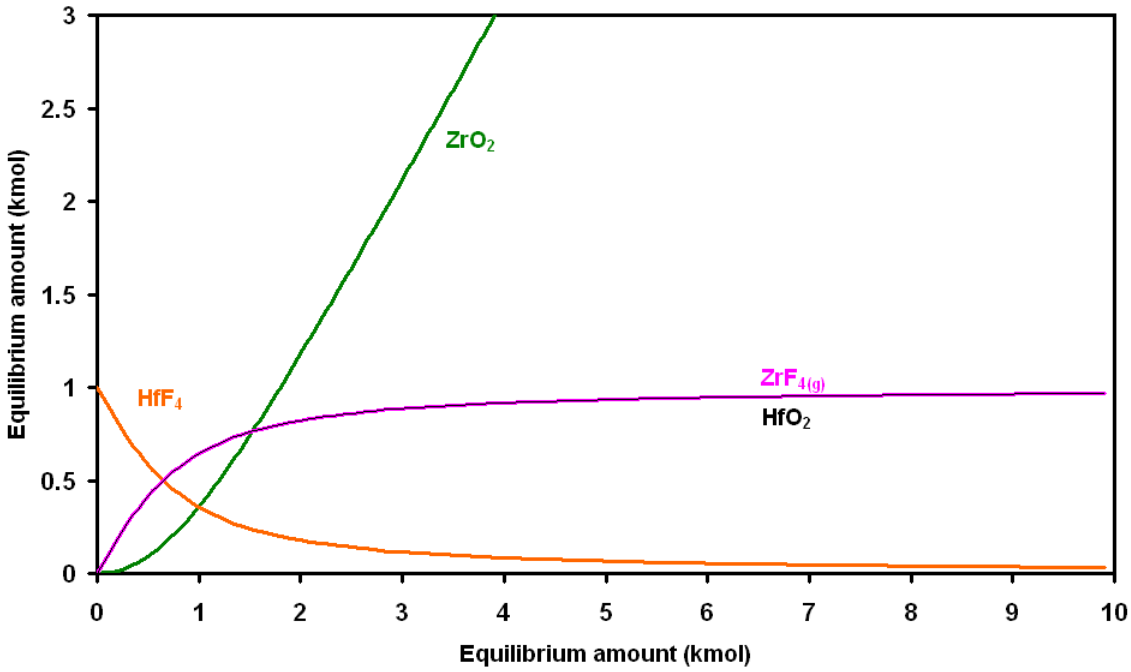

Figure 3.12: Equilibrium composition originating from the ZrO_2 + HfF_4 system.

The equilibrium composition in Fig. 3.12 was simulated with excess ZrO_2 in an exchange reaction with HfF_4. This study was done to validate the results in the above-mentioned paragraph 3.5.3, where the feasibility of the getter effect was simulated. In the study the following was done:

a. The excess zirconium oxide was simulated at an isothermal temperature of 850 °C.
b. The study was simulated with a 0.5 kmol basis increase of ZrO_2 during the exchange reaction.

From the study it is evident that an estimate of an excess of 9 kmol of ZrO_2 will be sufficient to convert the volatile HfF_4 to non-volatile HfO_2. Therefore ZrO_2 will be an effective getter for HfF_4.

3.6 EQUILIBRIUM COMPOSITION FOR REDUCTION OF ZrF_4

The end-goal of this project is to produce pure Zr metal. The reduction of ZrF_4 was estimated to be very difficult and also needs a high-temperature system because of lower volatility. However, also needs was perceived to convert ZrF_4 to a reducible ZrC_4 with CH_4 or C.

3.6.1 The Zr-F-C-H system

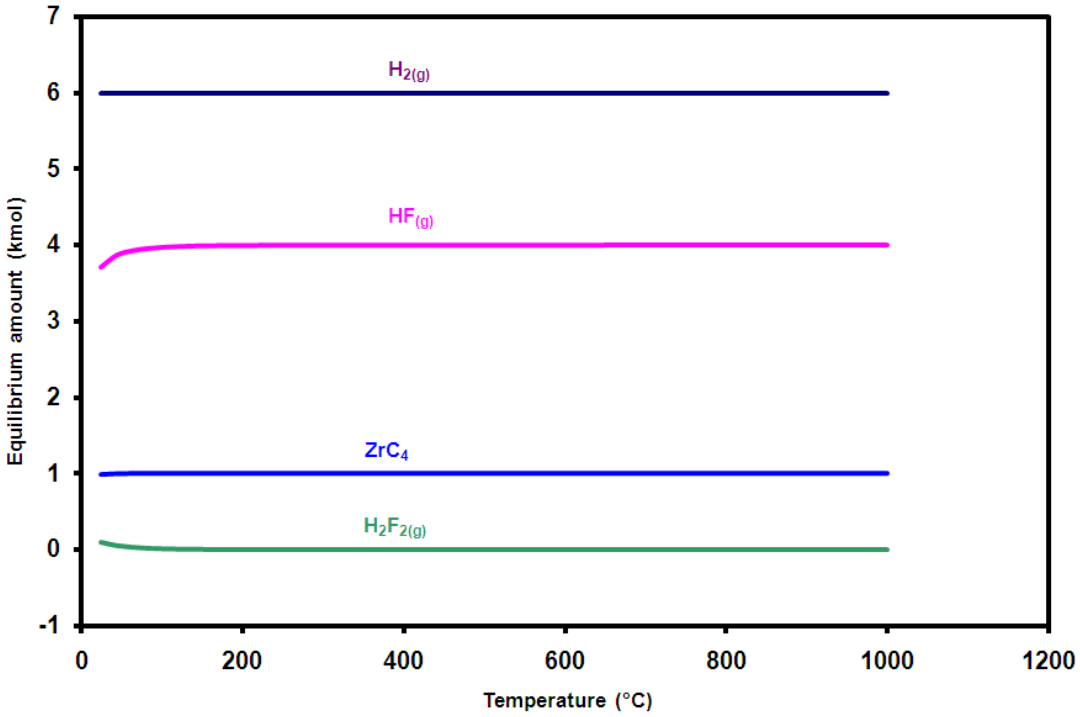

Figure 3.13: Equilibrium compositions originating from the ZrF_4 + CH_4 systems as a function of temperature.

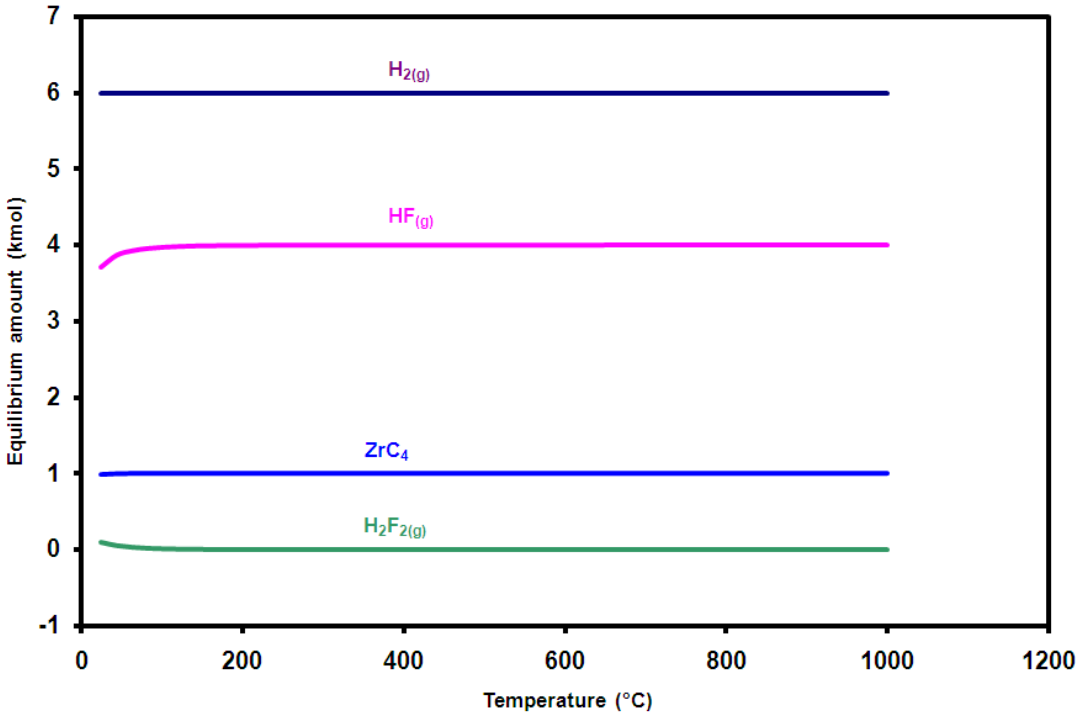

Figure 3.14: Equilibrium compositions originating from the ZrF_4 + C + H_2 systems as a function of temperature.

Fig. 3.13 shows equilibrium compositions originating from the reaction of ZrF_4 (1 kmol) with CH_4 (4 kmol) while Fig. 3.14 is the evaluation of ZrF_4 (1 kmol), C (4 kmol) and H_2 (8 kmol). The simulations were done to estimate the following reactions:

$$ZrF_{4(s)} + 4CH_{4(g)} \rightarrow ZrC_{4(s)} + 4HF_{(g)} + 5H_{2(g)} \quad \text{.....3.8}$$

$$ZrF_{4(s)} + 4C + 4H_{2(g)} \rightarrow ZrC_{4(s)} + 4HF_{(g)} + 2H_{2(g)} \quad \text{.....3.9}$$

These evaluations were done at standard pressure conditions. Even though different reducing species were used (CH_4 versus H_2 + C), identical thermodynamic behaviour was observed. This is because CH_4 is the source of, hydrogen and carbon, so that thermodynamically there is no difference whether it was a reaction between (ZrF_4 and CH_4) or (ZrF_4 + C + H_2).

From the diagrams Figs. 3.13 and 3.14 hydrogen fluoride and zirconium tetracarbide are thermodynamically predicted to form at room temperature.

Upon increasing the temperature no change in the products are predicted thermodynamically, which is ascribed to the chemical stability of the ZrC_4 up to 1000 °C.

The overall conclusion to be drawn is that reduction of ZrF_4 by means of CH_4 is not viable.

3.6.2 The Zr-Hf-H system

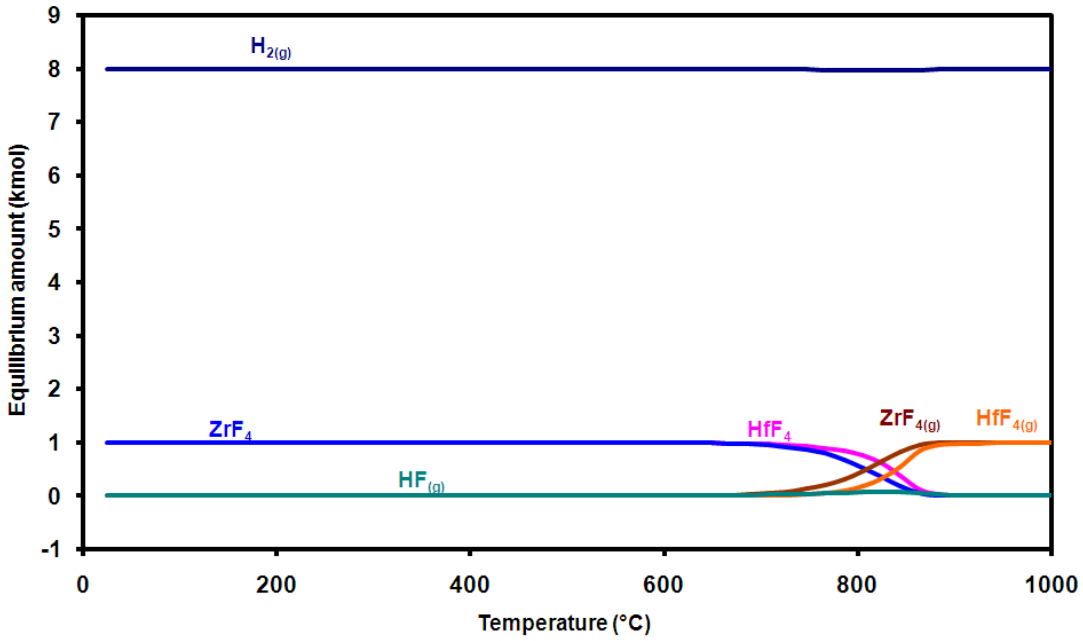

Figure 3.15: Equilibrium compositions originating from the ZrF_4 + HfF_4 + H_2 systems as a function of temperature.

Fig. 3.15 shows an equilibrium simulation result of the following reaction:

$$ZrF_{4(s)} + HfF_{4(s)} + 8H_{2(g)} \rightarrow ZrF_{4(g)} + HfF_{4(g)} + 8H_{2(g)} \quad .....3.10$$

ZrF_4 and HfF_4 were evaluated as to whether they can be reduced with hydrogen and it was found that the reactions were thermodynamically not feasible. Therefore carbon would have to be added in the case of ZrF_4 since it plays an important role during the reduction of ZrF_4.

3.6.3 The Hf-F-C-H system

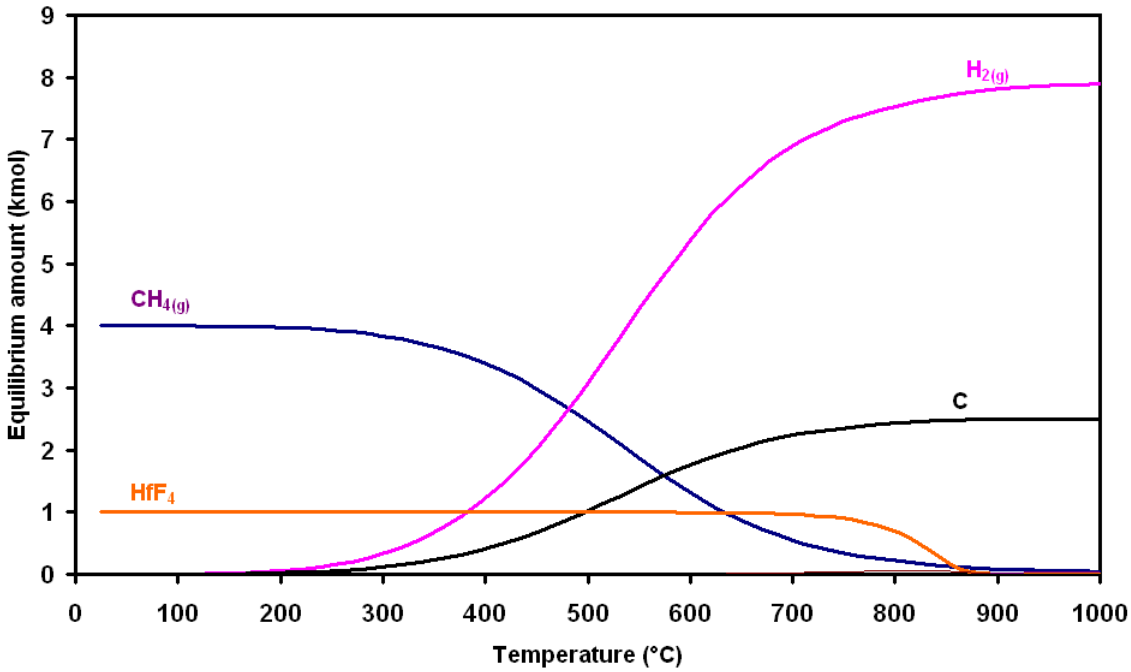

Figure 3.16: Equilibrium compositions originating from the HfF_4 + CH_4 systems as a function of temperature.

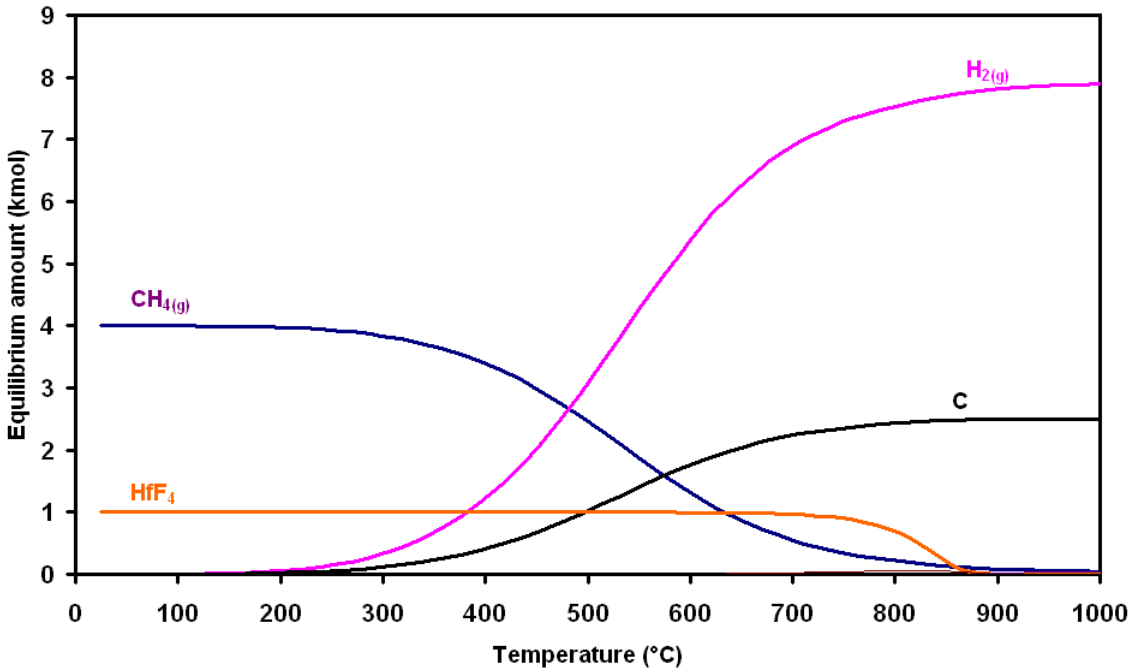

Figure 3.17: Equilibrium compositions originating from the HfF_4 + C + H_2 systems as a function of temperature.

Fig. 3.16 shows the equilibrium compositions originating from the reaction of HfF_4 (1 kmol) with methane (4 kmol) while Fig. 3.17 is the evaluation of HfF_4 (1 kmol), carbon (4 kmol) and hydrogen (8 kmol). The simulations show that the following reactions are not feasible:

$$HfF_{4(s)} + 4CH_{4(g)} \rightarrow HfF_{4(g)} + 4C + 8H_{2(g)} \text{ .....3.11}$$

$$HfF_4(s) + 4C + 8H_{2(g)} \rightarrow HfF_{4(g)} + 4C + 8H_{2(g)} \text{ .....3.12}$$

From these Figs. 3.16 and 3.17 it is evident that the only reaction that is thermodynamically feasible is the decomposition of methane at 200 °C to form carbon and hydrogen. The two figures show identical thermodynamic behavior, irrespective of different reducing species (CH_4 and C + H_2) used.

3.7 EQUILIBRIUM COMPOSITION FOR CONVERSION OF ZrF_4 WITH $MgCl_2$

Since the kinetic constraints contributed negatively to the success of reducing ZrF_4 with CH_4, a new idea was conceived to convert a lower volatile ZrF_4 to a highly volatile $ZrCl_4$ with $MgCl_2$[67]. It is expected that $ZrCl_4$ will be easier to reduce. It was also understood that $MgCl_2$ was very hygroscopic and therefore maintaining anhydrous conditions should be of the order of the day.

3.7.1 The Zr-Mg-F-Cl system

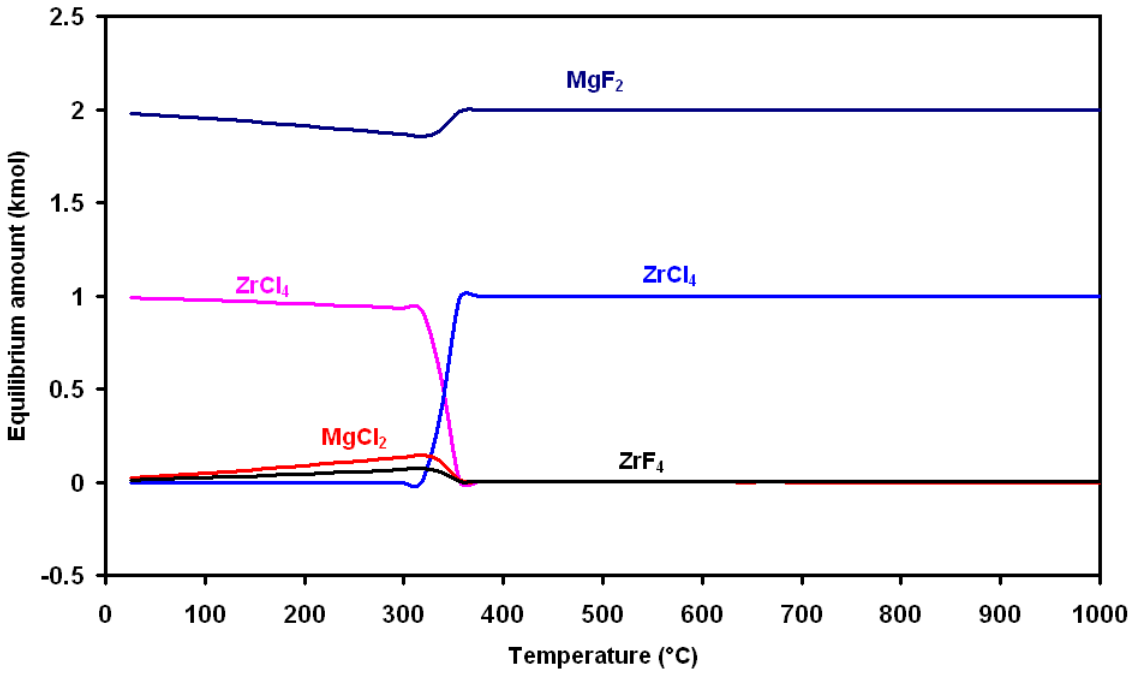

Figure 3.18: Equilibrium composition originating from the ZrF_4 + $MgCl_2$ system as a function of temperature.

Fig. 3.18 depicts an equilibrium composition originating from the reaction of ZrF_4 (1 kmol) with $MgCl_2$ (2 kmol). The simulation shows that the following reaction is feasible:

$$ZrF_{4(s)} + 2MgCl_{2(s)} \rightarrow ZrCl_{4(g)} + 2MgF_{2(s)} \quad \text{.....3.13}$$

The formation of $ZrCl_4$ is mostly estimated in the solid phase until at approximately 320 °C. At temperatures higher than 320 °C the equilibrium is totally estimated in the zirconium tetrachloride gaseous phase. It is therefore thermodynamically concluded that ZrF_4 can be converted to $ZrCl_4$ for metal reduction purposes.

3.8 INTEGRATION OF RESULTS

By integrating the results of paragraph 3.6.1, where there is no difference in sublimation temperatures between ZrF_4 and HfF_4 with respect to increased

pressure, and paragraph 3.6.2 where separation is effected by simulating an open system, a conceptual design proposal for a sublimation separation process can be derived. Such a process is represented schematically in Fig. 3.19 below.

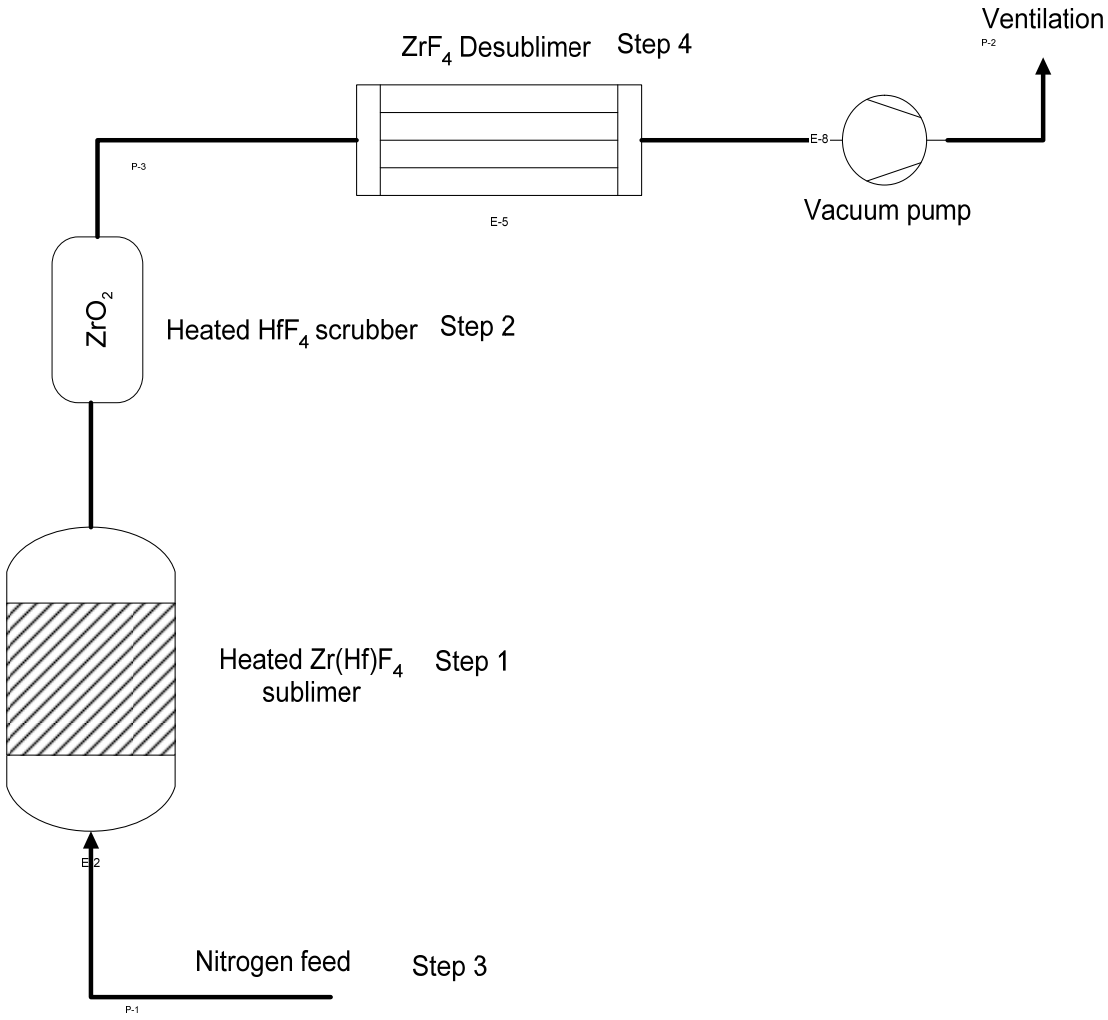

Figure 3.19: Schematic representation of ZrF_4 sublimer based on thermodynamic equilibrium calculations.

A typical batch reaction will be conducted via the following steps:

1. Charge the sublimer with crude $Zr(Hf)F_4$, at an operating temperature of 700 to 750 °C and a pressure of 0.5 to 1 bar.
2. Charge the HfF_4 scrubber with crude ZrO_2 at an operating temperature of 800 °C.

3. Purge the system with nitrogen gas.
4. Recover purified ZrF_4 at ZrF_4-desublimer.

Conceptually, the ZrF_4 sublimer will be charged with crude ZrF_4 containing HfF_4 impurity. The sublimer, operating at a temperature ranging from 700 to 750 °C and a pressure ranging from 0.5 to 1 bar will then be purged with nitrogen gas to effect transfer of the ZrF_4 enriched sublimation vapour to the HfF_4 scrubber. The scrubber, charged with ZrO_2 packing and operating at T > 800 °C, will convert residual volatile HfF_4 to volatile ZrF_4 and non-volatile HfO_2. The purified ZrF_4 stream will then be transferred to the ZrF_4 desublimer for recovery.

3.9 ELEMENTAL ANALYSES OF PDZ AND ZrO_2

The elemental analyses were done at Pelindaba Analytical Laboratories (PAL) at Necsa and the chemical composition of the crude PDZ and ZrO_2 products as determined by X-Ray Fluorescence Spectroscopy (XRF) are given in the following Table:

Table 3.3: Typical analysis of crude PDZ and ZrO_2.

Element	Unit	PDZ[a]	ZrO_2[b]	ASTM[c]
P	ppm	281.22	27.85	-
Ni	ppm	54.60	35.46	70
Cu	ppm	1207.32	1411.92	30
Zr	%	46.27	71.18	-
Hf	%	1.17	1.41	100
Th	ppm	154.00	3.18	3.0
U	ppm	304.76	16.29	3.0
Si	%	14.37	0.03	120
Ca	ppm	347.10	58.92	-
Ti	ppm	773.22	1293.33	50
Fe	ppm	537.77	11.17	1500
Al	ppm	6436.85	17.63	75
Cr	ppm	16.58	13.08	200

[a] PDZ Sample supplied by Necsa.
[b] ZrO_2 Sample supplied by Sigma-Aldrich.
[c] Maximum permissible contaminant levels (ppm) according to ASTM number B350.

The PDZ analysis results are representative of what could be expected for real samples derived from zircon ore. The analyses were done to have an understanding of the chemical composition and concentration of contaminants in PDZ and ZrO_2. This information is highly important, as it will be used in the theoretical calculations for separation coefficients of the impurity fluorides.

3.10 SEPARATION COEFFICIENTS

The purpose of calculating the theoretical separation coefficients was to provide an understanding on the difficulties of purifying ZrF_4 of metal impurity fluorides. These separation coefficients will also become of great guidance at a later stage when a sublimator unit is operational. The separation coefficients are calculated using equation 2 from Kotsar' et al.[98], which is given as follows:

$$\beta = \frac{p^{o}_{ZrF_4}}{N_{MF_n} p^{o}_{MF_n}} \sqrt{\frac{M_{MF_n}}{M_{ZrF_4}}} \quad \text{.....3.14 ,}$$

where β is the separation coefficient, $p^{o}_{ZrF_4}$ and $p^{o}_{MF_n}$ are the equilibrium vapour pressures over ZrF_4 and the fluoride impurity (M = Hf, Fe, Cu, etc), N_{MF_n} is the mole fraction of the fluoride impurity and M_{ZrF_4} and M_{MF_n} are the molecular weights of ZrF_4 and the impurity. The vapour pressures were calculated using the following equation:

$$\log P_{(atm)} = A - \frac{B}{T} \quad \text{.....3.15}$$

Table 3.4: Vapour pressure data for metal fluorides.

Compound	A	B	Reference
ZrF_4	12.569	11450	[99]
HfF_4	12.31	11895	[100]
FeF_3	11.10	14000	[101]
CuF_2	8.58	13000	[101]
CdF_2	7.391	14090	[101]
TiF_3	9.60	15700	[101]
UF_4	12.03	15994	[102]
MnF_2	8.70	15960	[101]
FeF_2	9.42	15820	[101]
NiF_2	10.63	15496	[103]
CoF_2	10.55	15230	[103]
ThF_4	9.19	16965	[104]
TiF_2	9.00	16500	[101]
CrF_2	9.14	18820	[101]
AlF_3	11.70	14950	[105]

Table 3.5: Separation coefficients of ZrF_4 and metal fluoride impurities (N_{MF_n} = 0.01) at 773 to 923 K.

	Separation Coefficient (β)			
Fluoride	773 K	823 K	873 K	923 K
HfF_4 (x 10^2)	9.24	8.42	7.25	6.81
FeF_3 (x 10^3)	6.33	3.99	2.65	1.84
CuF_2 (x 10^4)	10.1	7.65	5.97	4.78
CdF_2 (x 10^5)	18.6	8.94	4.68	2.62
TiF_3 (x 10^6)	30.5	1.41	7.16	3.90
UF_4 (x 10^6)	47.6	21.0	10.1	5.29
CoF_2 (x 10^7)	8.23	4.17	2.26	1.32
CrF_5 (x 10^7)	28.2	3.27	0.488	0.0896
FeF_2 (x 10^7)	14.9	2.83	1.41	0.753
NiF_2 (x 10^7)	15.1	7.26	3.80	2.13
MnF_2(x 10^7)	49.5	21.9	10.6	5.59
ThF_4(x 10^8)	58.2	21.5	8.89	4.04
TiF_2(x 10^8)	11.9	4.78	2.12	1.03
CrF_2(x 10^{10})	88.7	23.4	7.18	2.51
AlF_3(x 10^6)	2.35	1.25	0.714	0.433

Table 3.6: Separation coefficient of ZrF_4 and HfF_4 (x 10^2).

Mole Fraction	773 K	823 K	873 K	923 K
0.005	16.8	15.6	14.5	13.6
0.00621	13.6	12.5	11.7	11.0
0.01	8.42	7.79	7.25	6.81
0.015	5.61	5.19	4.85	4.54

Table 3.7: Separation coefficients of ZrF_4 and fluoride impurities.

		Separation coefficients			
Fluoride	Mole %	773 K	823 K	873 K	923 K
HfF_4 (x 10^3)	0.62083	1.36	1.25	1.17	1.10
FeF_3 (x 10^4)	0.09120	6.95	4.37	2.90	2.02
TiF_3 (x 10^7)	0.15362	19.8	9.21	4.66	2.54
FeF_2 (x 10^7)	0.09120	163	31.0	15.4	8.26
UF_4 (x 10^8)	0.01213	394	17.4	8.29	4.38
TiF_2 (x 10^8)	0.15362	77.6	31.1	13.8	6.73
NiF_4 (x 10^9)	0.00881	17.1	8.24	4.32	2.42
ThF_4 (x 10^{10})	0.00629	92.7	34.2	14.2	6.43
CrF_2 (x 10^{12})	0.00302	294	77.6	23.8	8.30

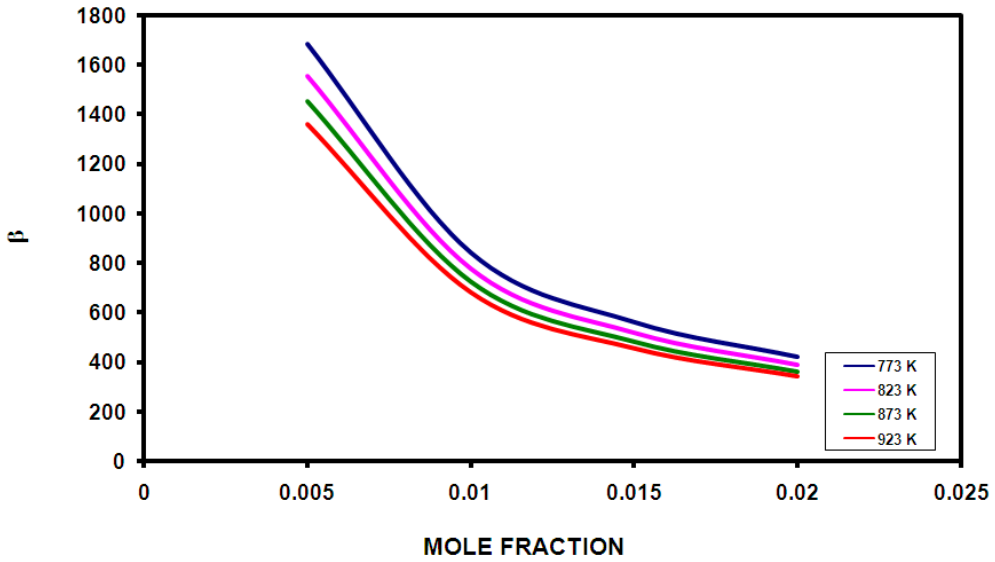

Figure 3.20: Separation coefficients of HfF_4 vs. mole fraction at 773, 823, 873 and 923 K.

The β values calculated from equation 3.14 for 773 to 923 K, and N_{MF_n} = 0.01 (1 mole %) are listed in Table 3.5. Table 3.4 depicts the vapour pressure data for the metal fluorides and Table 3.5 the separation coefficients for HfF_4 at different mole percentages. Hafnium is specifically emphasized since it is a major contaminant. Table 3.6 outlines the separation coefficients and mole percent calculations for the elemental composition of a PDZ sample. However it is important to note that lower temperatures were used for the calculations of the separation coefficients as compared to those used in their range of vapour pressure equations. A degree of extrapolation was therefore needed, which might compromise the accuracy of the results.

It follows from Tables 3.5, 3.6 and 3.7 that the separation coefficients decrease with increasing sublimation temperature of the fluoride impurity. As a higher separation coefficient implies better separation, it follows that if sublimation is used for purification, it should be done at as low a temperature as practically possible. A higher mole fraction also leads to lower separation coefficients (Tables 3.6 and 3.7). However, this is also represented graphically in Fig. 3.20. This can be deduced intuitively as higher levels of impurities will lead to more difficult purification. The separation coefficient values for the equilibrium in the system ZrF_4-impurity show that the difluoride type impurities such as chromium, iron, titanium, nickel, manganese and cobalt should be easily separable from the base compound. Other impurities, such as copper difluoride, iron trifluoride and hafnium tetrafluoride have a lower potential for separation, making them the most difficult to separate. The dominating feature of consideration specifically for the elements zirconium and hafnium, is the unique similarity of their chemistries. This is reflected in the difficulty of separation of these elements.

3.11 CONCLUSIONS

From the equilibrium composition calculations, it was concluded that thermodynamically, it is possible that HF can be used as a fluorinating agent

to fluorinate ZrO_2 or HfO_2, but H_2O will have to be removed as quickly as possible as soon as it forms, to prevent the formation of oxyfluorides. It was also concluded that F_2 was a better fluorinating agent than HF as there were no reversible reactions predicted.

From the theoretical separation coefficients it can be concluded that purification of ZrF_4 of some of the impurities will be fairly achievable, while for others (especially HfF_4) it will be relatively challenging, leading to a multi-step purification process.

CHAPTER 4

ANHYDROUS HYDROGEN FLUORIDE AS A FLUORINATING AGENT

4.1 INTRODUCTION

The overall purpose of this chapter was to investigate the following in a gaseous hydrogen fluoride atmosphere:

- To determine the optimum synthesis conditions for the formation of pure ZrF_4;
- To determine whether formation of ZrF_4 occurs via intermediates;
- To determine whether fluorination conditions could be used for a purification method for the synthesis of high-purity ZrF_4.

Hydrogen fluoride and fluorine gas have been widely used for obtaining higher fluorides as well as being the most useful fluorinating reagents[106]. However, hydrogen fluoride has one disadvantage for fluorinating zirconium and hafnium oxides: all fluorination reactions with HF above approximately 200 °C are reversible as illustrated in the previous chapter.

This study was performed to understand the chemical behaviour of the tetrafluoride species prior to separation and whether this behaviour cannot be manipulated to effect separation. The study is mainly concerned with the purification of zirconium compounds, but hafnium compounds were also studied for the purpose of comparison with the zirconium fluoride species.

These reaction studies were performed using a modified thermogravimetric analyzer instrument with the capabilities of handling corrosive gases. The technique is used to monitor the mass change of a substance as a function of temperature or time in a reactive or non-reactive atmosphere.

In order to study the possible reactions between the sample and the gas atmosphere at a specific temperature, a so-called isothermal analysis was carried out, where the sample is first heated to the desired temperature under nitrogen and allowed to equilibrate before being exposed to the specific gas medium. In this way, reaction isotherms are obtained.

4.2 EXPERIMENTAL PROCEDURES

4.2.1 Experimental investigation using a thermogravimetric analyzer

Thermogravimetry was used as the principal experimental tool to study the reaction of ZrO_2 and PDZ with anhydrous hydrogen fluoride. A commercial thermogravimetric analyzer (TGA) was modified to permit the use of corrosive gases such as HF, F_2 etc. Considering the corrosiveness and toxicity of HF and F_2, a high measure of safety has to be primarily considered, hence 10 % diluted mixtures of these gases had to be used. The diluted mixture was also used to minimize the impurities transfer from the gas during the fluorination process (due to impurities present in the HF). The entire thermobalance was housed in a glove box to allow for a controlled atmosphere. A detailed description of the modified instrument (TGA) is outlined by Rampersadh[107] .

Isothermal thermogravimetric experiments were conducted according to the following general procedure:

1. Approximately 10 mg of a sample was placed in a Ni TG pan.
2. The sample was heated at a rate of 10 °C/min to the desired temperature and then held constant.
3. A mixture of 10 % HF in N_2 was introduced and allowed to react with the sample, while the mass change was recorded as a function of time.
4. A thermogravimetric curve was obtained.

Dynamic thermogravimetric experiments were conducted in a similar fashion, but the reactive gas was introduced at the start of the experiment after which the temperature was increased at a steady rate (normally 10 °C/min) while the thermogravimetric curve was recorded.

The extent of reaction of a solid and HF (or F_2) gas was manifested in a weight change that can be continuously recorded as a function of temperature and/or time.

The MO_2 (e.g. M = Zr (pure, 14603-100G), Hf (Powder 98 %, product/unit 202118-25G)) and MF_4 (e.g. M = Zr (99.9 %, product/unit 311464-100G), Hf (product/unit 157-15EI-25G)) used in this investigation were received from Sigma-Aldrich. Compounds were used as received without any further treatment. The crystal structure of ZrO_2 and desilicated PDZ were analyzed by XRD to confirm a monoclinic structure. Pelchem, the chemical manufacturing division of Necsa, supplied the anhydrous hydrogen fluoride (>99.99 %) and fluorine (>99.4 %) used in this study.

Note: These compounds were used throughout this study unless stated otherwise.

In order to interpret the results, the theoretical transformation of ZrO_2 to ZrF_4 can be described by the following reaction:

$$ZrO_2 + 4HF \rightarrow ZrF_4 + 2H_2O \quad \text{..... 4.1}$$

In a system of flowing HF, the $H_2O_{(g)}$ formed is rapidly removed, which drives the reaction strongly to the right. The theoretical mass increase accompanying this reaction is approximately 35.7 % and is calculated as follows:

$$\text{Theoretical mass increase}(\%) = \left(\frac{m_f - m_i}{m_i}\right) \times 100$$
$$= \left(\frac{167.22 - 123.22}{123.22}\right) \times 100$$
$$= 35.7\ \%$$

$m_i = \text{Initial mass}$
$m_f = \text{Final mass}$

4.2.2 X-ray diffraction

The X-ray diffraction analyses were conducted according to the following description: The samples were prepared for XRD analysis using a zero background sample disc with top loading preparation method at the University of Pretoria[108]. Compounds were analyzed with a PANalytical X'Pert Pro powder diffractometer with X'Celerator detector and variable divergence and receiving slits with Fe-filtered Co-Kα radiation. The phases were identified using X'Pert Highscore plus software.

4.2.3 Raman Spectroscopy

Raman spectra were recorded between 100 and 3500 cm^{-1} for samples of pure ZrO_2 and ZrF_4 using a Bruker FT-Raman RFS 100 at the University of South Africa (UNISA)[109, 110]. Laser excitation was achieved with 1064 nm, and was used at a power of 30 and 450mW, while the number of scans varied between 128, 256 or 512, depending on the sample requirements.

4.3 RESULTS AND DISCUSSION

Fluorinations of ZrO_2 with anhydrous hydrogen fluoride were investigated by means of thermogravimetry.

4.3.1 Adsorption of HF on ZrO_2

HF is a highly polar molecule and has a tendency to adsorb on any surface. An isothermal thermogravimetric run was done at room temperature (30 °C) with 10 % HF/N_2 to study the absorption behaviour of HF on ZrO_2. After approximately 110 minutes the gas flow was changed to pure N_2 (Fig. 4.1).

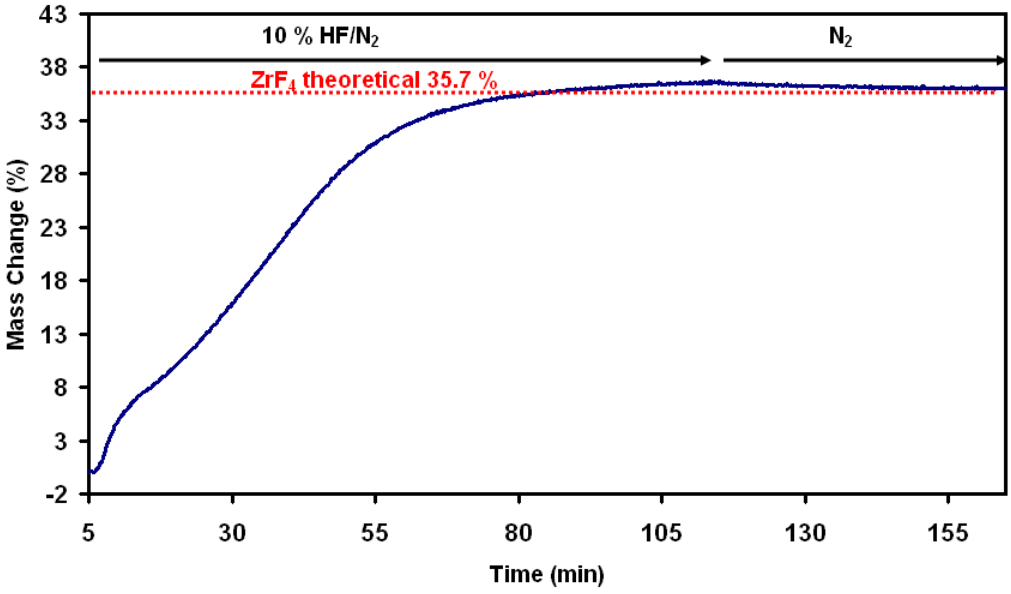

Figure 4.1: Thermogravimetric curve for the isothermal interaction of ZrO_2 with HF at 30 °C.

From Fig. 4.1 the following can be observed:

a. A small initial apparent rate of mass increase, followed by a region of slightly lower mass increase rate, which can possibly be ascribed to the rate change in absorption of HF.
b. A total mass increase of approximate 36 % was observed, which is in accordance with the theoretical value of 35.7 % (indicated by a horizontal line), were the ZrO_2 to have reacted with the HF to form ZrF_4.
c. After approximately 110 min the HF/N_2 was replaced by N_2, there was virtually no mass loss.

This sample was submitted for X-ray powder diffraction analysis and only ZrO_2 was detected. Therefore it is likely that no chemical reaction took place, and the HF was only absorbed, albeit strongly. Nel[111] confirms that "at relatively low temperatures, typically in the region of about 50 °C at atmospheric pressure, zirconia, ZrO_2, adsorbs hydrogen fluoride". Robinson et al.[112] cites that "The hydrofluorination of ZrO_2 proceeds rapidly at 25 °C to yield ZrF_4", however this was not in accordance with our findings.

This sample (the fluorinated ZrO_2 at 30 °C) was re-exposed to HF under the same conditions and no further mass increase was observed. The sample was submitted for X-ray powder diffraction analysis and mixtures of ZrO_2 and $ZrF_4.H_2O$ patterns were observed (See Fig. 4.11) as a possible match.

Fig. 4.1 depicts a high uptake of HF by the zirconium oxide sample. It is assumed that the HF is taken up as a multi-layer on the internal and external surface of ZrO_2. The kinetic diameter of an HF molecule is 3.148 Å[107] . However when four HF molecules are placed together the area between them also has to be factored in as part of the total occupied area, hence the area occupied by the HF molecules was taken as d^2 i.e. $(3.148 \times 10^{-10})^2$ or 9.91×10^{-20} m^2. If ZrO_2 has a 35 % mass uptake then a 1g ZrO_2 sample takes up 0.35g of HF, which is equal to 0.35/20 moles of HF (20 g/mol being the molar mass of HF). Using Avogadro's number of 6.022×10^{23} molecules per mole there is a total of 1.05×10^{22} molecules of HF that cover the surface of ZrO_2. Now considering that each molecule of hydrogen fluoride covers a surface area of 9.91×10^{-20} m^2, the total area covered by all the HF molecules adsorbed on 1g ZrO_2 sample can be calculated. This totals 1041 m^2, a clear indication of a multi-layer, considering that the surface area of the ZrO_2 is 5.87 m^2/g.

In order to test the adsorption hypothesis, a stepwise HF adsorption/desorption thermogravimetric run was done.

4.3.2 Step-wise reaction of ZrO_2 with HF

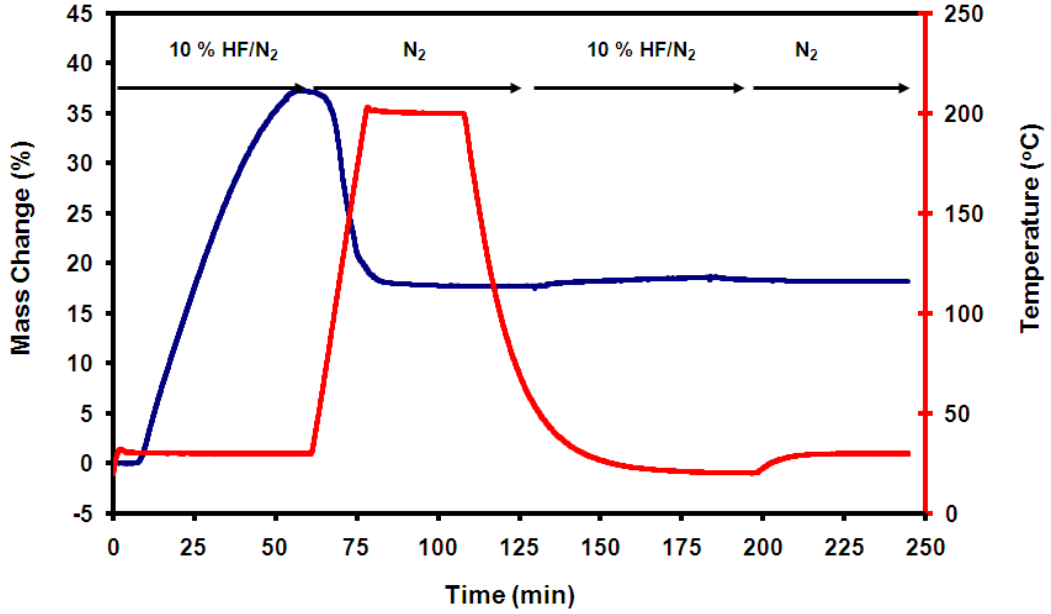

Figure 4.2: Thermogravimetric curve for the isothermal interaction of ZrO_2 with HF at 30 °C and then 200 °C.

Fig. 4.2 depicts a stepwise interaction performed at room temperature (30 °C) in a HF atmosphere, continued until the reaction time reached ca. 60 min, where the hydrogen fluoride was replaced with nitrogen and the temperature elevated to 200 °C until the mass change reached a plateau at ca. 110 min. The temperature was allowed to drop and at ca. 130 min HF was introduced to allow any further adsorption. However no further mass increase was observed. Furthermore, at approximately 190 min HF was replaced with nitrogen at 30 °C and no further desorption was observed.

This was to illustrate that the HF that was probably adsorbed at room temperature was partially desorbed at elevated temperature. However it could not be proven experimentally that ZrO_2 does/does not react with HF at 200 °C. A ZrO_2 sample that was exposed to HF at 200 °C was submitted for X-ray powder diffraction analysis and the results show the presence of ZrO_2. Since HF is polar, partial desorption (if that is indeed what takes place) could be attributed to physio-sorption.

4.3.3 Thermogravimetric analysis of the reaction between ZrO_2 and HF

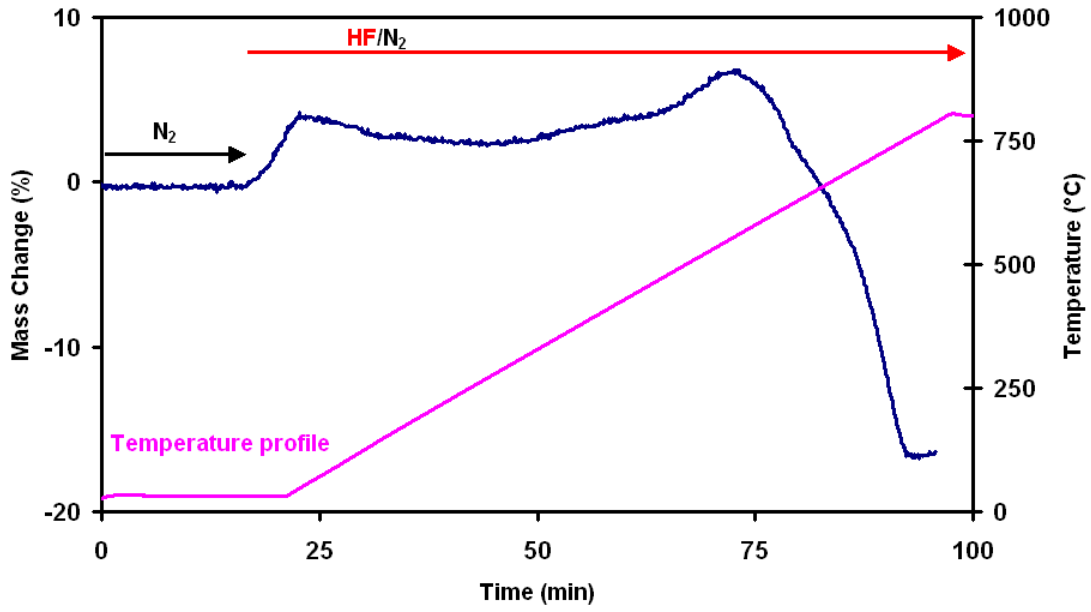

Figure 4.3: Thermogravimetric curve of the reaction of ZrO_2 in a 10 % HF/N_2 atmosphere.

A ZrO_2 sample was heated from room temperature to 800 °C in a 10 % HF/N_2 atmosphere. The thermogravimetric curve of this ZrO_2/HF reaction is depicted in Fig. 4.3. In a HF stream at elevated temperature, the ZrO_2 would be converted to ZrF_4 and H_2O released as a possible contaminant into the gas stream. From this figure the following can be observed; After introduction of the HF at room temperature a mass increase of approximately 5 % was observed. This mass increase can possibly be ascribed to the adsorption of $HF_{(g)}$ onto the ZrO_2 sample. Upon further heating, a small, slow mass loss was observed. This slow mass loss may be ascribed to desorption of the HF from the ZrO_2 sample. From about 350 °C onwards a slow mass increase was observed, passing through a maximum at about 550 °C. Sublimation (mass loss) was observed upon further heating.

Contrary to the expected mass gain of 35.7 %, which accompanies the complete fluorination of ZrO_2 to ZrF_4, a gain of only approximately 5 % was observed with a maximum at 550 °C. This can be postulated to the formation of an intermediate fluoride compound which formed on the ZrO_2 sample surface and which prevented further reactions taking place. This situation continued until the temperature was sufficiently high enough to initiate sublimation of the formed ZrF_4. From this temperature onwards though, the sublimation of the ZrF_4 started to compete with the formation thereof, limiting the observed mass increase due to ZrF_4 formation.

This sample (the fluorinated ZrO_2 from room temperature to 800 °C) was ground and re-exposed to HF under the same conditions and no further mass increase was observed. This reaction eliminated the possibility of any product skin formation. However, this unexpected behaviour could be due to the formation of stable oxyfluoride intermediates.

Note: The shortcomings of current TGA system: Sublimation occurs concurrently with condensation on the hang-down wire.

4.3.4 Isothermal reactions of ZrO_2 with HF

Thermogravimetric curves for the isothermal reaction of ZrO_2 with HF at 400, 450, 500, 550 and 600 °C were recorded.

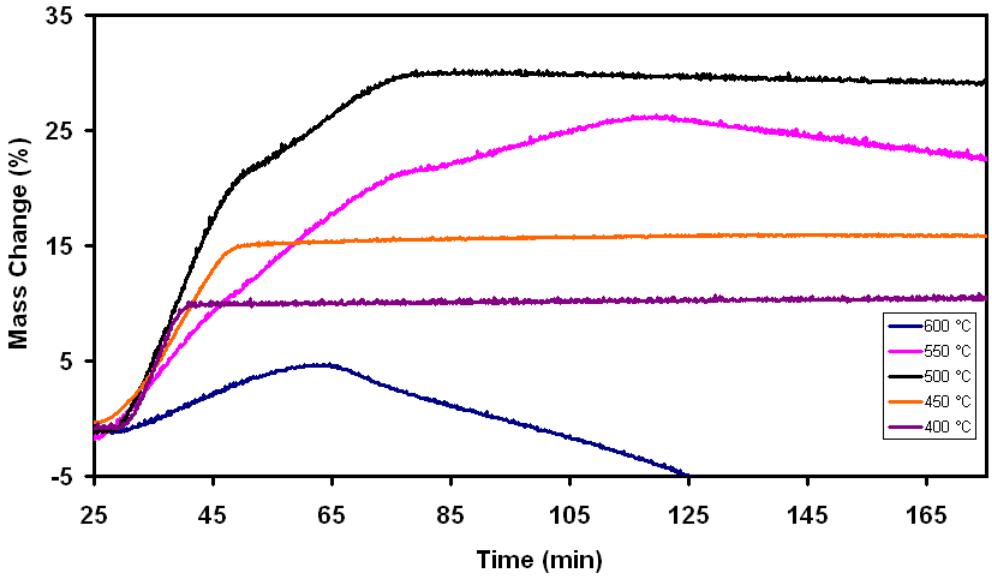

Figure 4.4: Thermogravimetric curves for the isothermal reaction of ZrO_2 with HF at 400, 450, 500, 550 and 600 °C.

In order to interpret the data from the different isotherms, it is necessary to define the possible reactions that could have taken place.

- **Zirconium oxyfluoride ($ZrOF_2$) formation.**

$$ZrO_{2(s)} + 2HF_{(g)} \rightarrow ZrOF_{2(s)} + H_2O_{(g)} \quad \text{.....4.2}$$

The theoretical mass increase accompanying this reaction is ca. 18 %.

- **Zirconium oxyfluoride (Zr_2OF_6) formation.**

$$2ZrO_{2(s)} + 6HF_{(g)} \rightarrow Zr_2OF_{6(s)} + 3H_2O_{(g)} \quad \text{.....4.3}$$

The theoretical mass increase accompanying this reaction is ca. 27 %.

- **Zirconium oxyfluoride ($Zr_3O_2F_8$) formation.**

$$3ZrO_{2(s)} + 8HF_{(g)} \rightarrow Zr_3O_2F_{8(s)} + 4H_2O_{(g)} \quad \text{.....4.4}$$

The theoretical mass increase accompanying this reaction is ca. 24 %.

- **Zirconium oxyfluoride ($Zr_7O_9F_{10}$) formation.**

$$7ZrO_{2(s)} + 10HF_{(g)} \rightarrow Zr_7O_9F_{10(s)} + 5H_2O_{(g)} \quad \text{.....4.5}$$

The theoretical mass increase accompanying this reaction is ca. 13 %.

- **Conversion of $ZrOF_2$ to ZrF_4.**

$$ZrOF_{2(s)} + 2HF_{(g)} \rightarrow ZrF_{4(s)} + H_2O_{(g)} \quad \text{.....4.6}$$

The theoretical mass increase accompanying this reaction is ca. 16 %.

- **Direct formation of ZrF_4.**

$$ZrO_{2(s)} + 4HF_{(g)} \rightarrow ZrF_{4(s)} + 2H_2O_{(g)} \quad \text{.....4.7}$$

The theoretical mass increase accompanying this reaction is ca. 35.7 %.

- **Sublimation of ZrF_4.**

$$ZrF_{4(s)} \rightarrow ZrF_{4(g)} \quad \text{.....4.8}$$

The theoretical mass loss accompanying this reaction is 100 %.

The theoretical mass changes for the possible reactions are summarized as follows:

Table 4.1: The theoretical mass changes for the possible reactions of ZrO_2 with HF.

Equations	Percentage
4.2	+ 18 %
4.3	+ 27 %
4.4	+ 24 %
4.5	+ 13 %
4.6	+ 16 %
4.7	+ 36 %
4.8	- 100 %

The results from Fig. 4.4 can be summarized as follows:

Table 4.2: Summary of results obtained during the isothermal reaction between ZrO_2 and HF, refer to Fig. 4.6.

Isothermal Temperature (°C)	Experimental Mass change (%)	Notes
400	+ 10	Relatively high reaction rate. Formation of stable products at this temperature.
450	+ 15	Relatively high reaction rate. Formation of stable products at this temperature.
500	+ 30	High reaction rate followed by region of lower rate indicating double-step reaction – possible formation of intermediate. Final product shows low rate of mass loss.
550	+ 26	TG curve shows initial slower apparent rate than at 500 °C, and presence of double-step reaction. Higher final mass loss region. Mass increase followed by decrease indicate two possible consecutive reactions (mass increase = product formation, mass loss = sublimation. TG curves the resultant of both processes)
600 600	+ 4 - 30	Lower apparent reaction rate followed by mass loss (sublimation of ZrF_4) indicating overlapping consecutive reactions.

Note: Initial reaction rates at 400, 450 and 500 °C are the same.

Reaction at 400 °C

It seems obvious that this reaction is that of ZrO_2 reacting with HF to possibly form zirconium oxyfluoride after which the mass increase reaches a plateau. The fact that the theoretical mass increase of 18 % was not reached, indicates that the reaction was not completed at this temperature, possibly due to product skin formation preventing HF from reacting further with the unreacted ZrO_2. An alternative interpretation is that a hitherto unknown stable

oxyfluoride was formed, e.g. if $Zr_7O_{10}F_8$ was formed the mass increase would be 10.2 %.

Reaction at 450 °C

Again, the result suggests the formation of zirconium oxyfluoride. The reasonably good correlation between the experimental and theoretical mass increase (15 vs. 18 %) indicates that the almost complete conversion to $ZrOF_2$ was possibly reached. Again, product skin formation could have prevented complete reaction of ZrO_2 to $ZrOF_2$. Once again, an as yet unidentified oxyfluoride could have formed; if $Zr_7O_8F_{12}$ was formed the mass increase would be 15.3 %.

Reaction at 500 °C

Changes in the reaction indicate the formation of ZrF_4 via the formation of an intermediate product. Apparently 500 °C is a favourable temperature for the conversion of the postulated $ZrOF_2$ to ZrF_4. The mass decrease that was observed after the formation of ZrF_4 may be attributed to the early onset of sublimation of ZrF_4.

Reaction at 550 °C

Exactly the same trend as at 500 °C was observed with the exception that the eventual mass loss rate after the maximum mass gain was more pronounced than the lower mass loss rate at 500 °C, again supporting the fact that sublimation of ZrF_4 is becoming more prominent.

Reaction at 600 °C

A lower apparent initial rate was observed in the case of 550 °C in comparison to the rate at 500 °C. The decreased rate could indicate the presence of intermediate products reacting at different reaction rates. However, it is likely that the formation reaction and ZrF_4 sublimation occur simultaneously, resulting in a resultant thermogravimetric curve. Sublimation is playing an ever-increasing role, competing with the formation reaction. Eventually the sublimation process dominates, leading to the final higher mass loss rate.

4.3.5 Isothermal reaction of ZrO_2 with HF at 525 °C

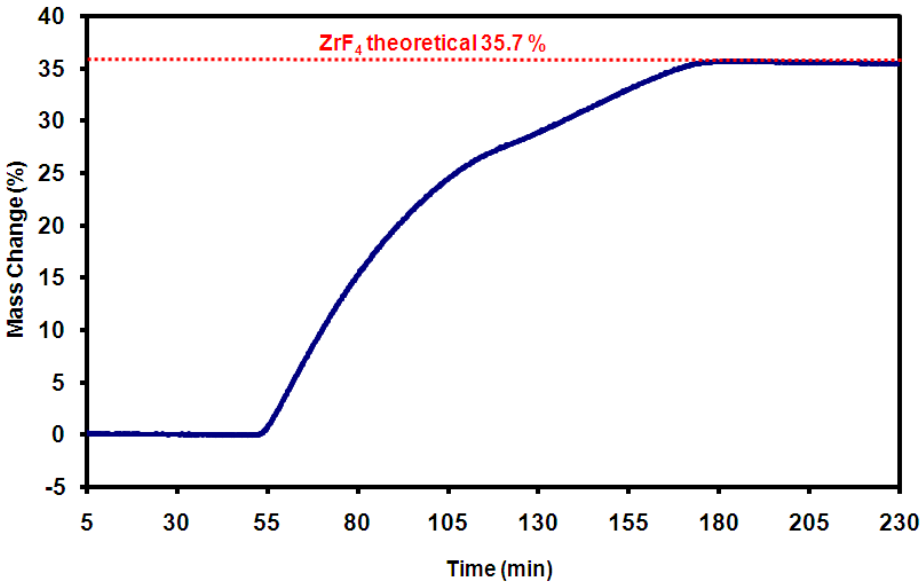

Figure 4.5: Thermogravimetric curve of the reaction between ZrO_2 with HF at 525 °C.

Fig. 4.5 depicts a thermogravimetric curve of the isothermal reaction between ZrO_2 and HF at 525 °C. The formation of ZrF_4 is via a double step reaction, which shows an initial fast mass increase rate followed by a slower mass increase rate. However, the conversion is complete with the expected theoretical mass increase of 35.7 %. It seems that 525 °C is the optimum temperature to achieve complete fluorination without sublimation.

4.3.6 TGA investigation of the reaction between PDZ and HF

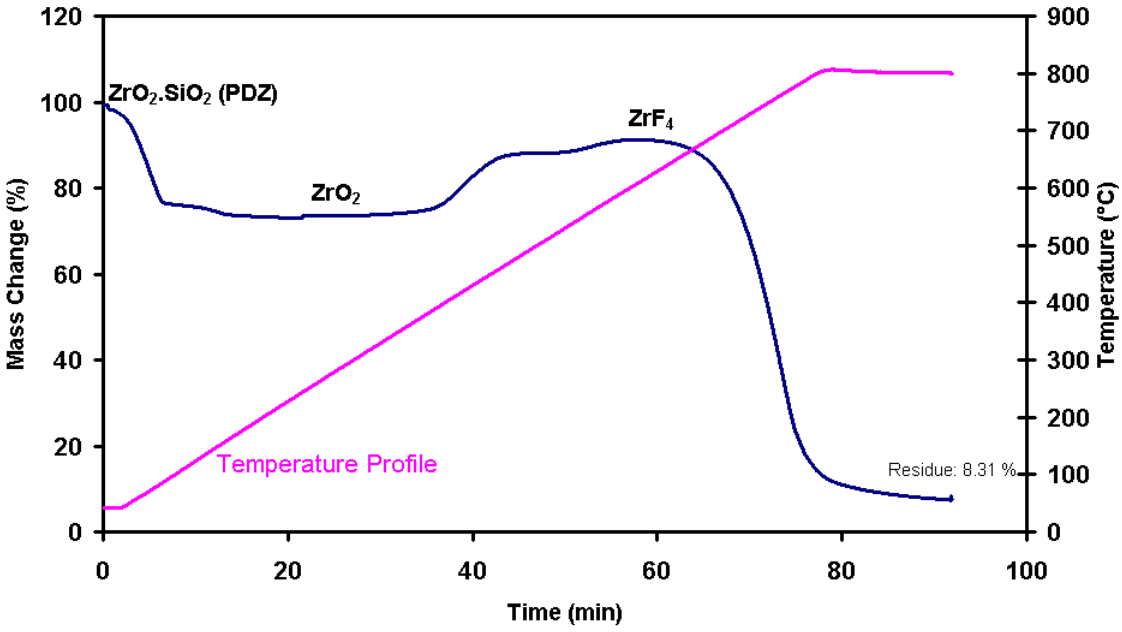

Figure 4.6: Reaction of PDZ with HF.

A PDZ sample was heated from room temperature to 800 °C using a 10 % HF/N_2 gas atmosphere. In Fig. 4.6 the thermogravimetric curve of the reaction between PDZ and HF is outlined. For the interpretation of Fig. 4.6, it is necessary to know that analyses have shown that the thermal conversion of zircon ($ZrSiO_4$) to PDZ ($ZrO_2.SiO_2$) was at utmost only 94 % efficient, thus leaving 6 % unconverted zircon in the matrix of PDZ.

The first mass loss reaction of approximately 27 % at approximately 130 °C is ascribed to the volatilization of the SiO_2 content as $SiF_{4(g)}$, leaving the unreacted ZrO_2 and unconverted zircon behind.

Theoretically, assuming 94 % PDZ formation, one would have expected a total mass loss of 30.81 % for the removal of SiO_2 as SiF_4. It is also clear that the first mass loss reaction is not a single-step loss, but proceeds via at least a double-step reaction.

Upon further heating, a double-step mass increase starting at ca. 400 °C is observed. This is ascribed to the interaction of ZrO_2 with $HF_{(g)}$ forming ZrF_4. Theoretically the total mass loss accompanying the formation of ZrF_4 from PDZ and assuming the total removal of SiO_2, is 8.77 %, which agrees well with the mass loss value at ca. 600 °C. It could be that the two-step mass increase described is because the fluorination of ZrO_2 proceeds via the formation of zirconium oxyfluoride species as intermediates.

Upon further heating the last mass loss is ascribed to the sublimation of ZrF_4, leaving a residue of mostly unconverted zircon. If the assumption of 94 % zircon conversion was true, the residue should have been 6 %, and not the experimentally determined value of 8.31 %, indicating a possible lower percentage conversion of zircon to PDZ (91.69 %), or the small sample used for TG was not representative.

It was experimentally proven that zircon does not react with HF from room temperature until 800 °C.

It is therefore evident that ZrF_4 can be manufactured from PDZ by a two-step process, according to the following reaction:

$$ZrO_2.SiO_2 \xrightarrow{130\,^\circ C/HF} ZrO_2 + SiF_4 \uparrow \xrightarrow{480\,^\circ C/HF} ZrF_4 \xrightarrow{700\,^\circ C} ZrF_4(anhy)....4.9$$

Note: This anhydrous ZrF_4 is still not purified of Hf, and this critical aspect must be addressed by enhanced sublimation techniques.

4.4 SEM ANALYSIS OF ZrO_2

Fig. 4.7 depicts a Scanning Electron Microscope (SEM) micrograph of zirconium oxide, showing an agglomerated structure.

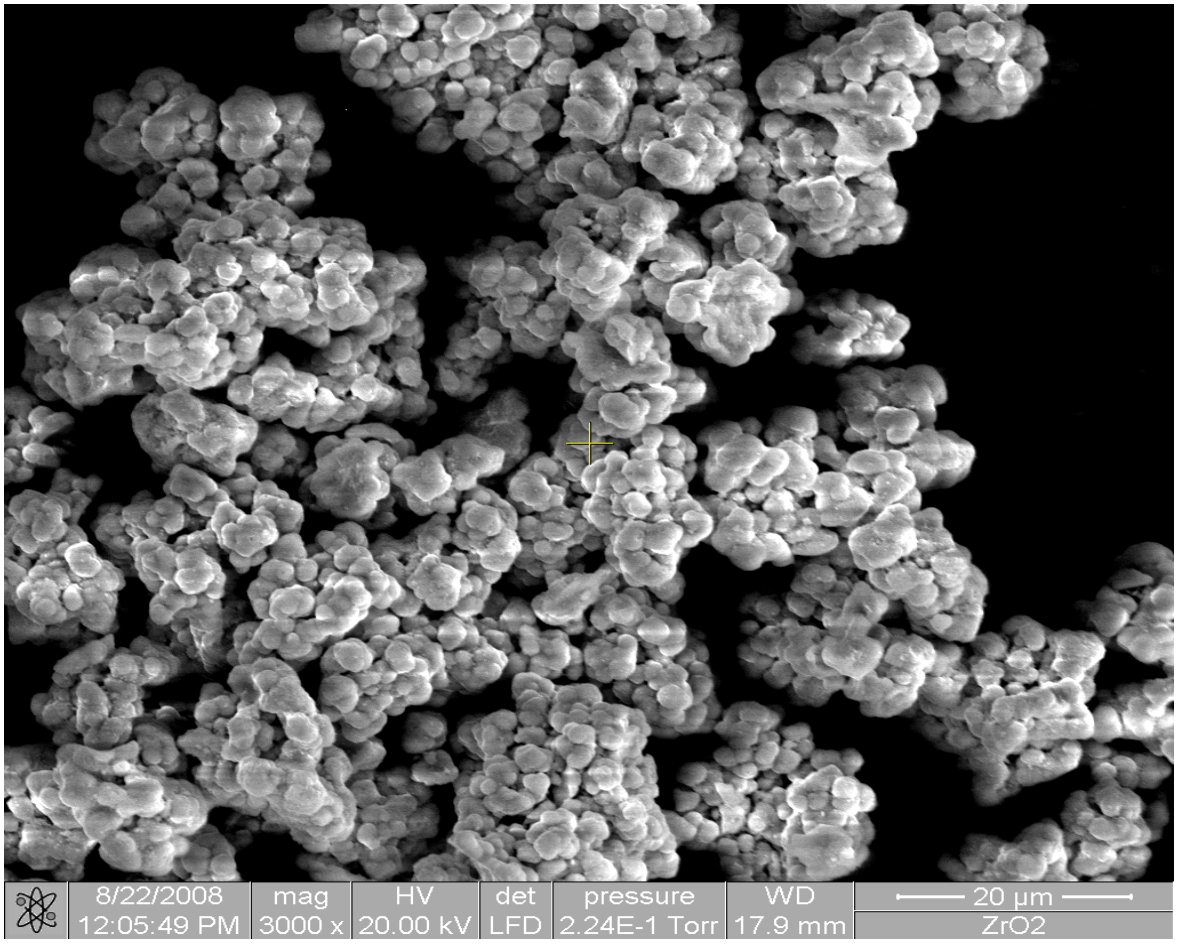

Figure 4.7: ZrO_2 SEM micrograph.

The particle size and particle size distribution of all powdered material affect their physical and chemical properties in many ways. As the particle size diminishes, there is a gradual rate of change in certain properties like specific surface area, diffusivity, rate of coagulation and in case of this study, rate of fluorination. It was difficult to measure the particle size of the ZrO_2 sample particles due to its agglomerated structure. Hard and soft agglomerates present in a powder play a very crucial part on the rheology of the slip, powder packing density, sintering behaviour, microstructure development and mechanical properties of the sintered product.

4.5 X-RAY DIFFRACTION RESULTS

Isothermal reactions of ZrO_2 in HF atmospheres were studied at different temperatures using a TGA. These samples were submitted for XRD

analyses. ZrF_4 and possibly zirconium oxyfluorides are hygroscopic and the X-ray analyses were performed on samples exposed to atmospheric moisture, therefore hydration is expected.

The following table comprises a summary of the best matching XRD results.

Table 4.3: Summary of the possible XRD patterns of Zr compounds.

Number	Reaction	Temperature °C	XRD Results	Figures
1	ZrO_2 + HF	30	ZrO_2	4.10
2	ZrO_2 + HF	Re-exposed at 30	Mixture ZrO_2 & $ZrF_4.H_2O$	4.11
3	ZrO_2 + HF	100	ZrO_2	4.12
4	ZrO_2 + HF	200	ZrO_2	4.13
5	ZrO_2 + HF	300	Mixture ZrO_2 & $ZrF_4.H_2O$	4.14
6	ZrO_2 + HF	400	?	4.15
7	ZrO_2 + HF	450	Mixture ZrO_2 & ZrF_4	4.16
8	ZrO_2 + HF	200-500	?	4.17
9	ZrO_2 + HF	530	ZrF_4	4.18
10	ZrO_2 + HF	550	$ZrF_{3.33}O_{0.33}$ & ?	4.19
11	ZrO_2 + HF	600	$ZrF_{3.33}O_{0.33}$ & ?	4.20

? = Unknown patterns

From Table 4.3 it is observed that a ZrO_2 pattern was identified from reactions between 30 to 450 °C. The XRD results also show an inconclusive ZrF_4 match at 530 °C and a possible match of zirconium oxyfluoride and the unknown patterns at 550 and 600 °C.

4.6 RAMAN SPECTROSCOPY RESULTS

Figs. 4.8 and 4.9 illustrate Raman spectra of the reaction products of the ZrO_2/HF reaction at three temperatures, namely 450, 500 and 600 °C. The Raman bands observed for products of the ZrO_2/HF reaction are listed and compared in Table 4.4.

4.6.1 Raman spectra of the products formed in the reaction between ZrO_2 and HF

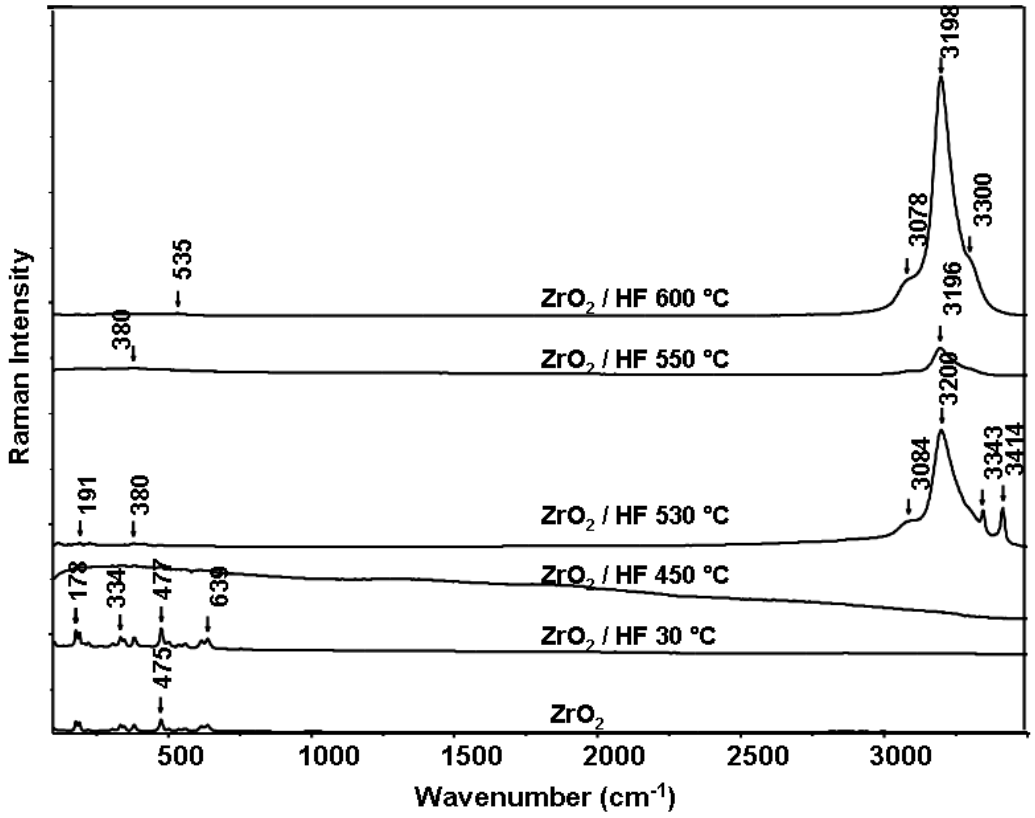

Figure 4.8: Raman spectra of the products of the reaction between ZrO_2 and HF at different temperatures, in the spectral region between 100 to 3500 cm^{-1}.

4.6.2 Comparison of the Raman spectra of the products of the reaction between ZrO_2 and HF at different temperatures, with those of ZrO_2 and ZrF_4

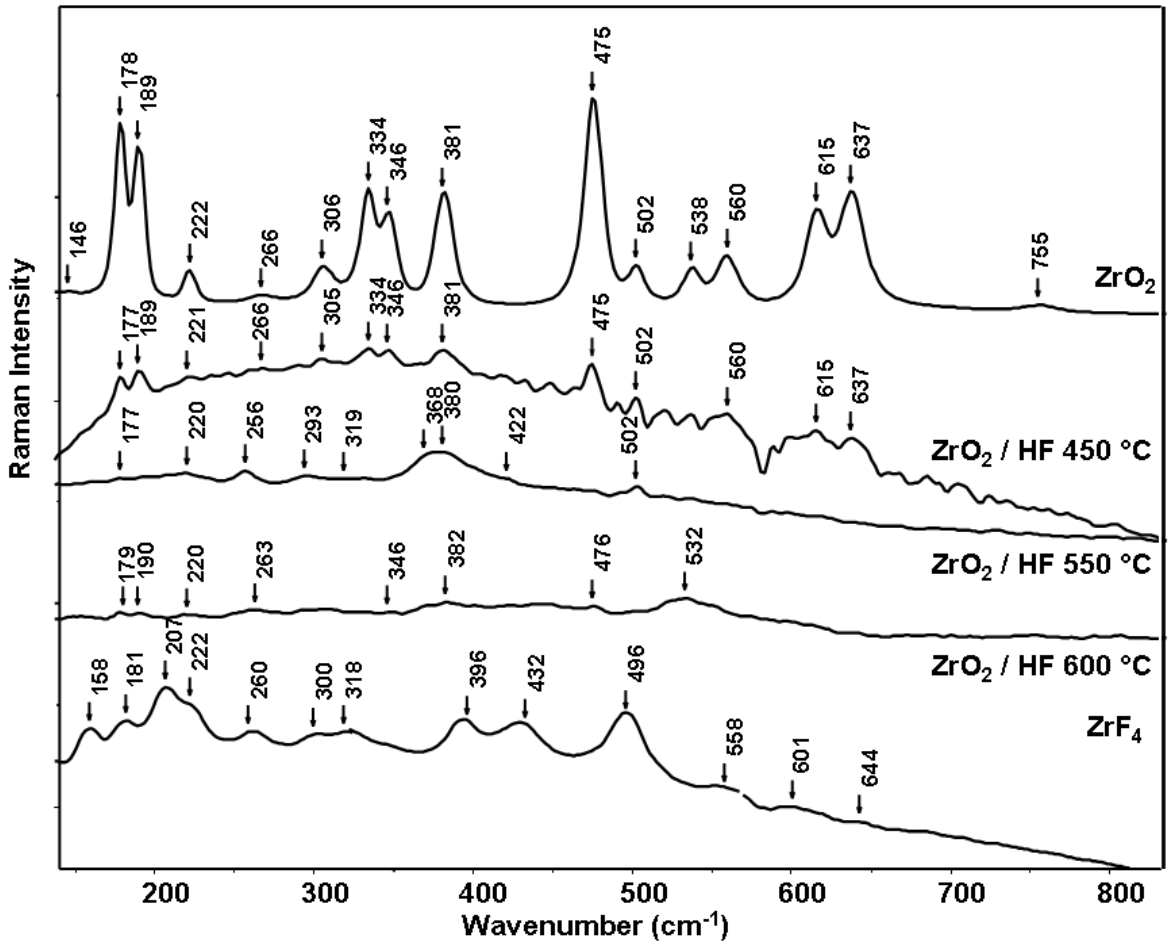

Figure 4.9: Comparison of the Raman spectra of the reaction products of ZrO_2/HF at 450, 500 and 600 °C, with the starting material ZrO_2, and the reaction product, ZrF_4.

Fig. 4.8 shows the Raman spectra of the entire region between 100 and 3500 cm^{-1}. Fig. 4.9 shows the Raman spectra between 100 and 800 cm^{-1} of the reaction products at three different temperatures: 450, 550 and 600 °C, compared to Raman spectra of the starting material (ZrO_2) and the final reaction product that could be identified as ZrF_4 from the Raman spectra (corresponding Raman bands at 260 and 318 cm^{-1}) and X-ray powder diffraction data. These spectra show new Raman bands in the higher wavenumber region (between 3000 and 3400 cm^{-1}) at temperatures above 500 °C, with an increase in band intensity with higher temperatures. A broad band and shoulders on both sides of the band and with very high intensity

around 3200 cm^{-1} are observed for the highest temperature sample, this can probably be attributed to HF adsorption on the sample. Maybury et al.[113] reported that, the IR spectrum of liquid hydrogen fluoride consists mainly of a band of almost complete absorption in the 3000-3600 cm^{-1} region and a broad absorption band between 400 and 1000 cm^{-1}.

Corresponding Raman bands for solid HF at 18 K occur at about 3050 cm^{-1}, with medium shoulders at 3000 and 3100 cm^{-1}[114, 115]. The Raman bands on these samples that can possibly be attributed to adsorbed HF, are shifted by about 80, 150 and 200 cm^{-1} to 3198 cm^{-1} for the highest intensity band, and 3078 and 3300 cm^{-1} for the shoulders.

Table 4.4: Summary of Raman bands in wavenumbers (cm^{-1}) observed for ZrO_2, ZrO_2 reacted with HF at 450, 550 and 600 ˚C, and ZrF_4.

ZrO_2	**ZrO_2 reacted with HF at 450 ˚C**	**ZrO_2 reacted with HF at 550 ˚C**	**ZrO_2 reacted with HF at 600 ˚C**	**ZrF_4**	**ZrF_4[116]**	**Solid phase HF 18 K[114, 115].**
		158 vw		**158 w**	**163 m**	
178 vs	177 w	177 vw	179 vw	**181w**	**178 w**	
189 vs	189 w		190 vw		**198 w**	
222 m	221 vw	220 vw	220 vw	**222 m sh**	**222 w**	
		256 w	**263 vw**	**260 w**	**260m**	
266 vw	266 vw					
306 m	305 vw	293 vw		**300 w**		
		319 vvw		**318 w**		
334 s	334 vw					
346 s	346 vw	368 m			**345 w**	
381 s	381 w	380 m	382 vw	**396 m**	**391 w**	
		422 w			**425 w**	
				432 m		
475 vs	475 w		475 w			
502 m	502 w	502 w		**496 m**	**505 w**	
538 m	538 vw					
560 m	560 w			**558 vw**		
615 s	615 vw			**601 vw**		
637 s	637 vw			**644 vw**	**655 w**	
755 w	-					
-	-	***3080 w sh***	***3079 s sh***			***±3000 m sh***
-	-	***3193 s***	***3198 vs***			***3050 vs***
-	-	***3300 w sh***	***3300 s sh***			***±3100 m sh***
						3260 w
						3360 w

w = weak; m= medium; s = strong; v = very; sh = shoulder

4.7 CONCLUSIONS

The conversion of ZrO_2 to ZrF_4 was achieved with anhydrous hydrogen fluoride at 525 ˚C with respect to the theoretical mass increase of 35.7 %. It is suspected that the temperature at which ZrF_4 forms could be the same as where it starts to sublime.

It is concluded that ZrF_4 can be manufactured from plasma dissociated zircon by a two-step process using hydrogen fluoride.

4.8 X-RAY DIFFRACTOGRAMS

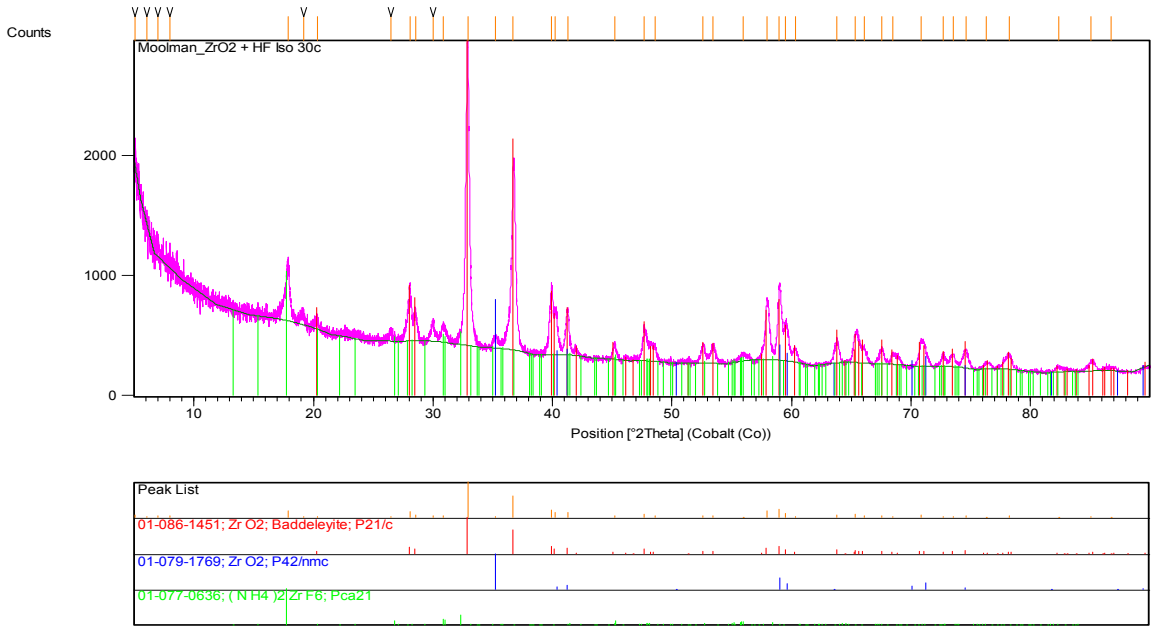

Figure 4.10: Diffraction pattern of the products from the ZrO_2/HF reaction at 30 °C (isothermal).

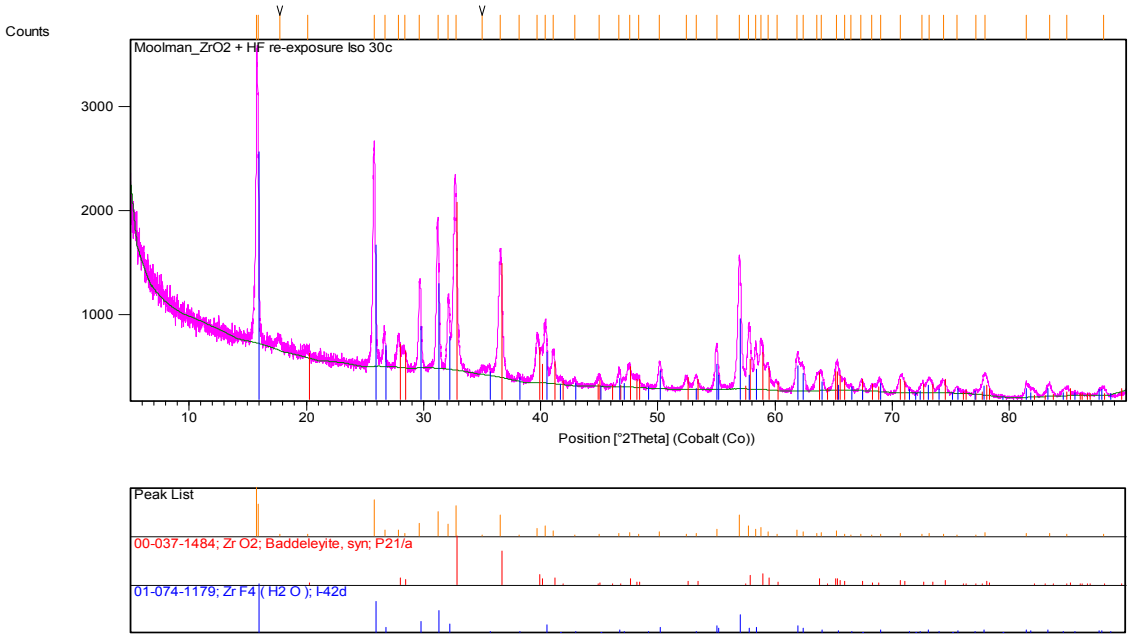

Figure 4.11: Diffraction pattern of the products from the ZrO_2/HF reaction at 30 °C, after re-exposure to HF.

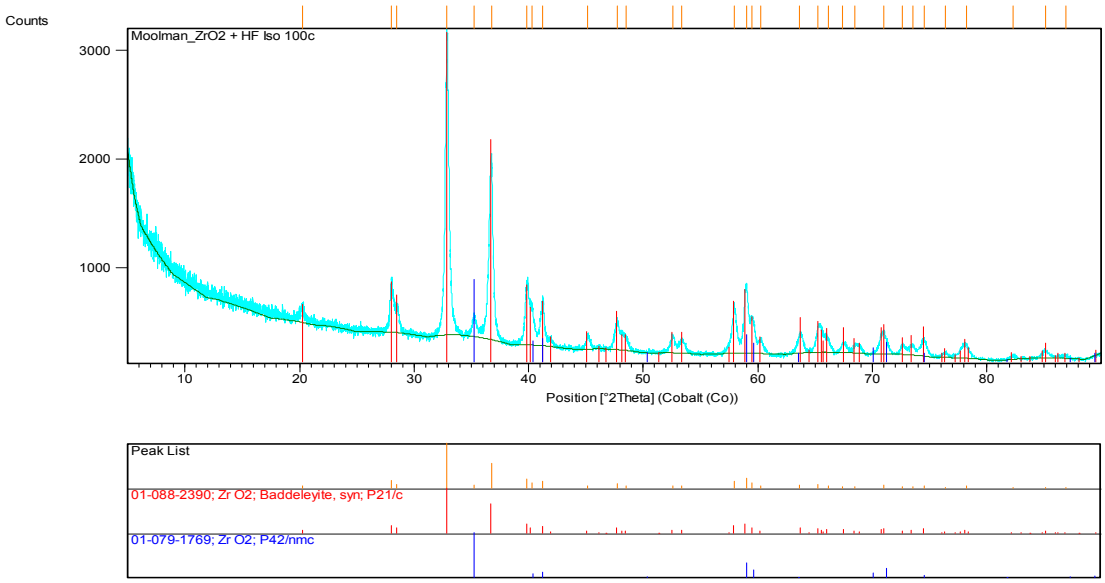

Figure 4.12: Diffraction pattern of the products from the ZrO_2/HF reaction at 100 °C.

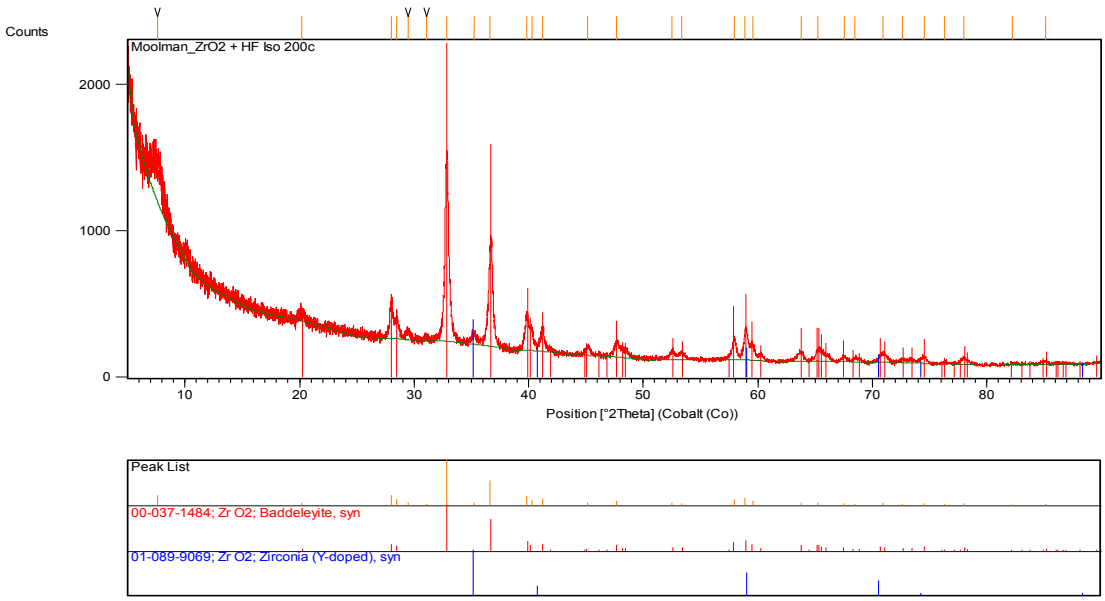

Figure 4.13: Diffraction pattern of the products from the ZrO_2/HF reaction at 200 °C.

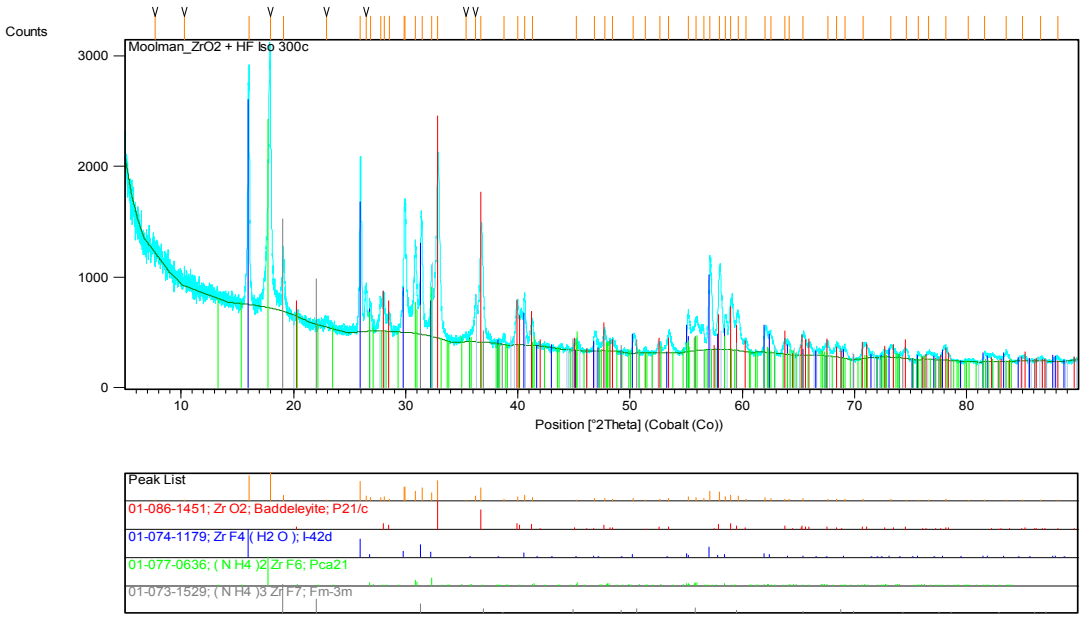

Figure 4.14: Diffraction pattern spectra of the products from the ZrO_2/HF reaction at 300 °C.

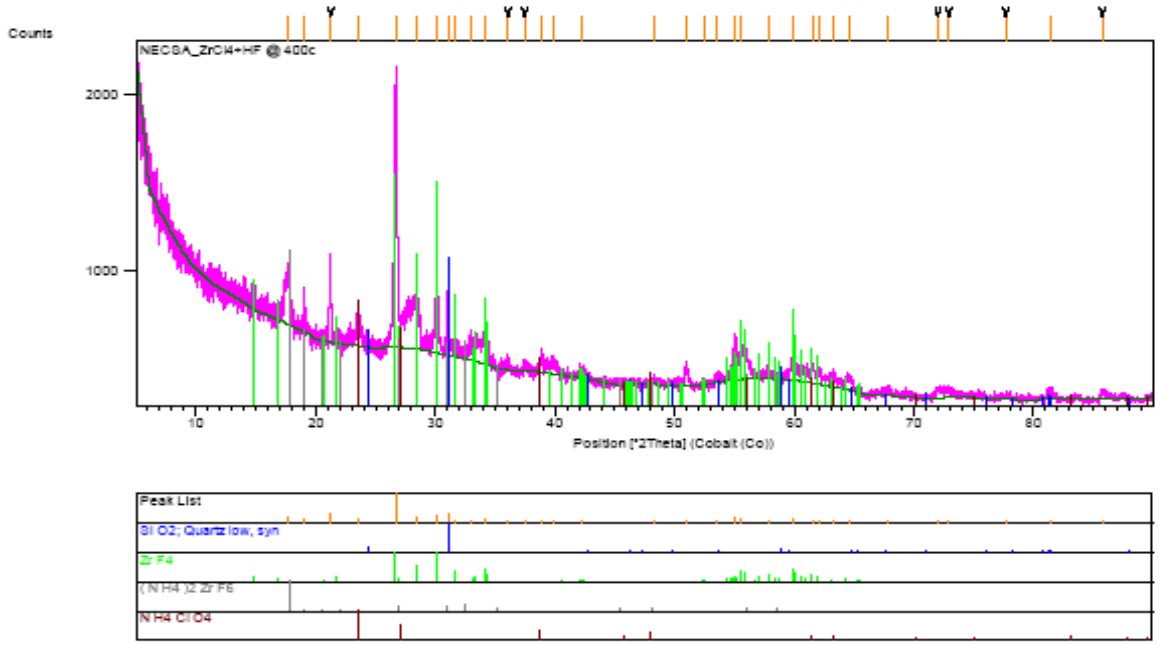

Figure 4.15: Diffraction pattern of the products from the ZrO_2/HF reaction at 400 °C.

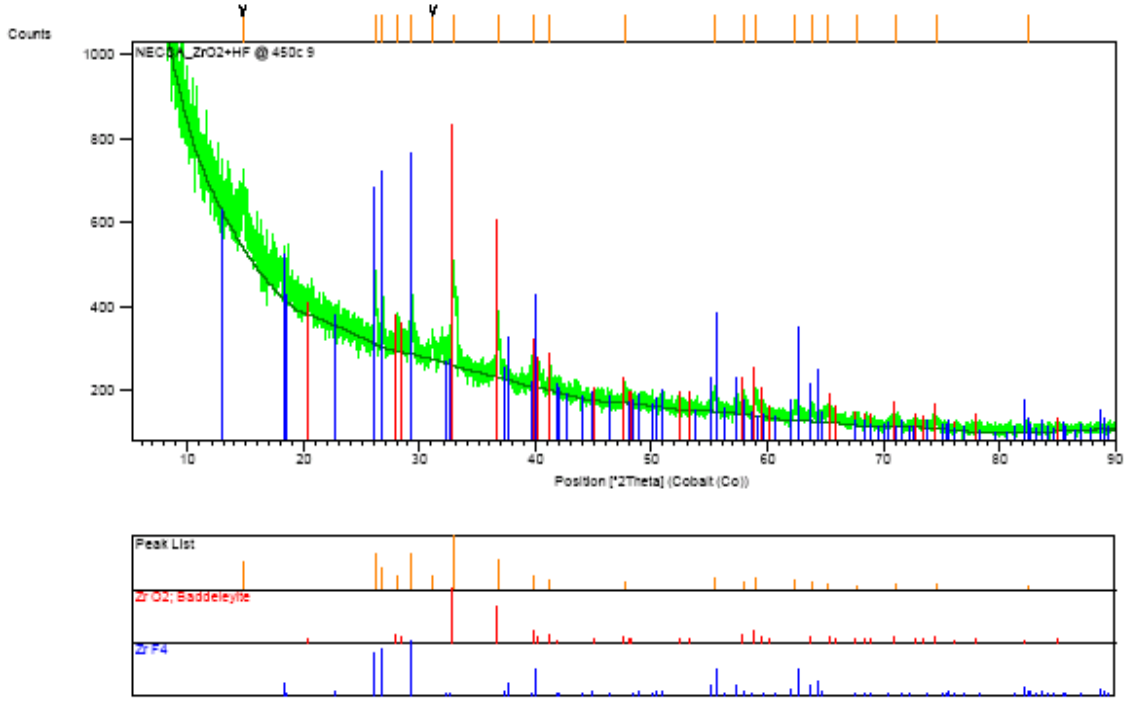

Figure 4.16: Diffraction pattern of the products from the ZrO_2/HF reaction at 450 °C.

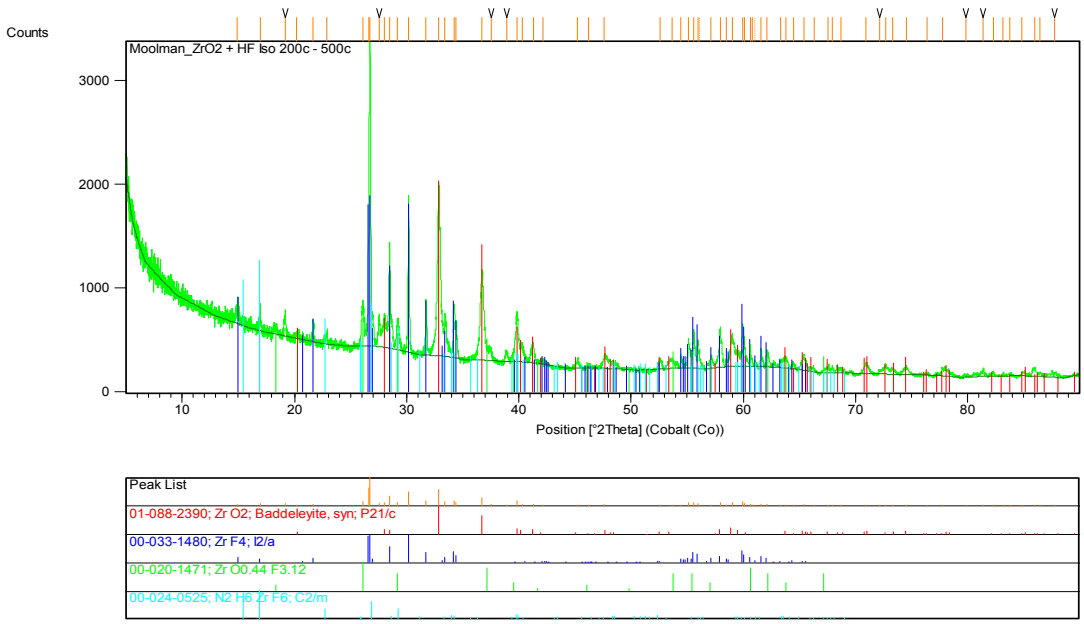

Figure 4.17: Diffraction pattern of the products from the ZrO_2/HF reaction at 500 °C.

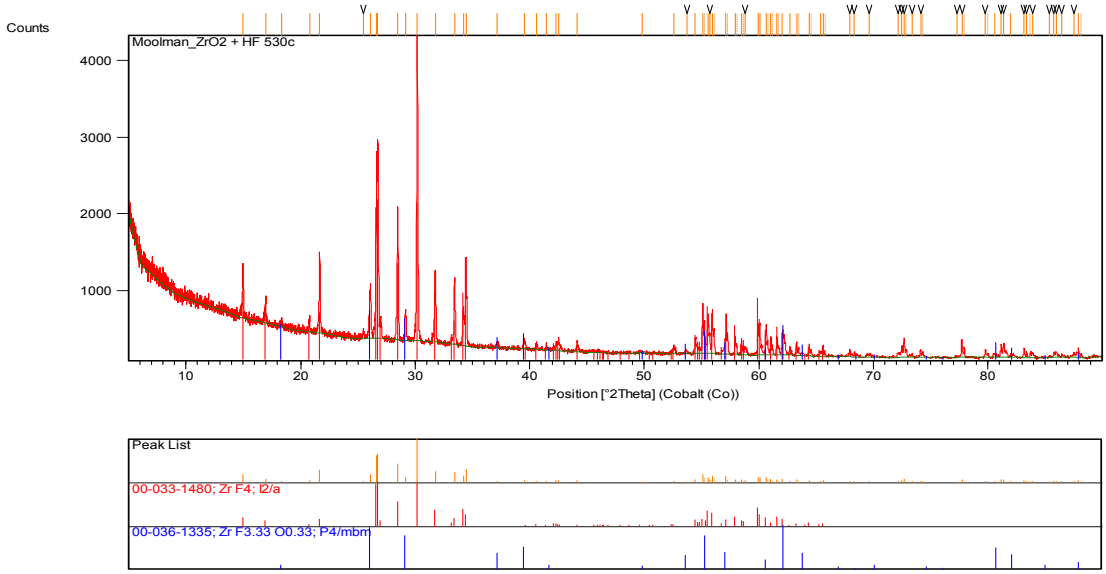

Figure 4.18: Diffraction pattern of the products from the ZrO_2/HF reaction at 530 °C.

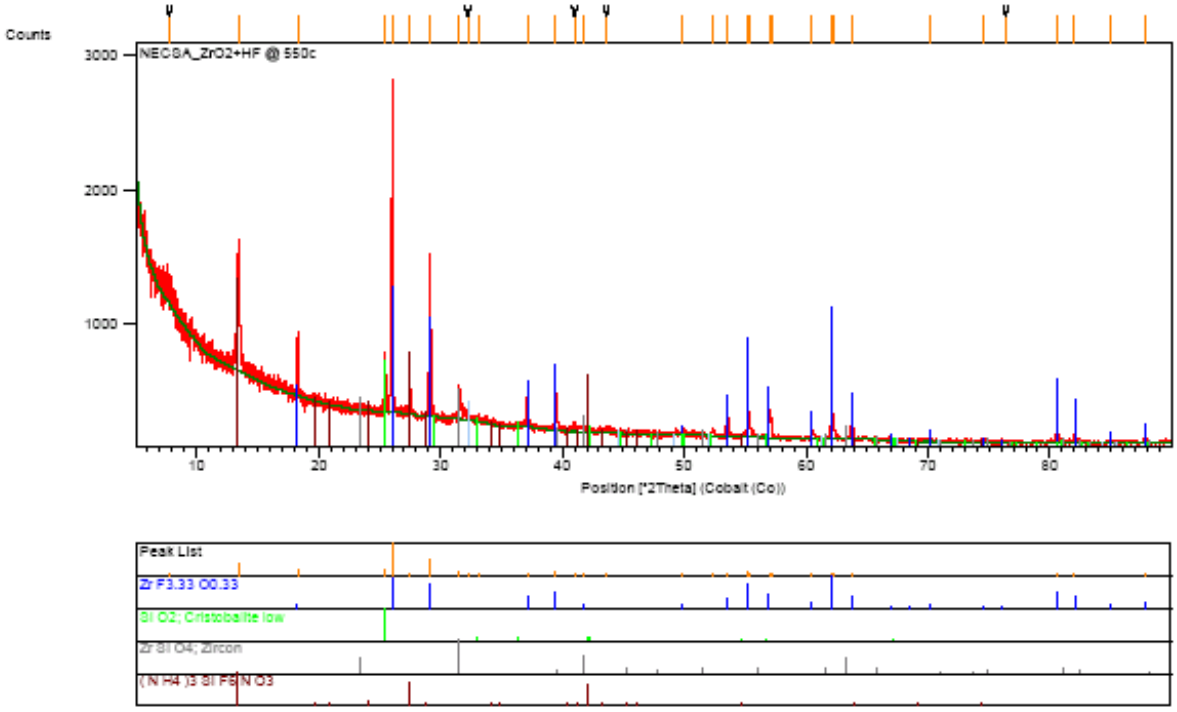

Figure 4.19: Diffraction pattern of the products from the ZrO_2/HF reaction at 550 °C.

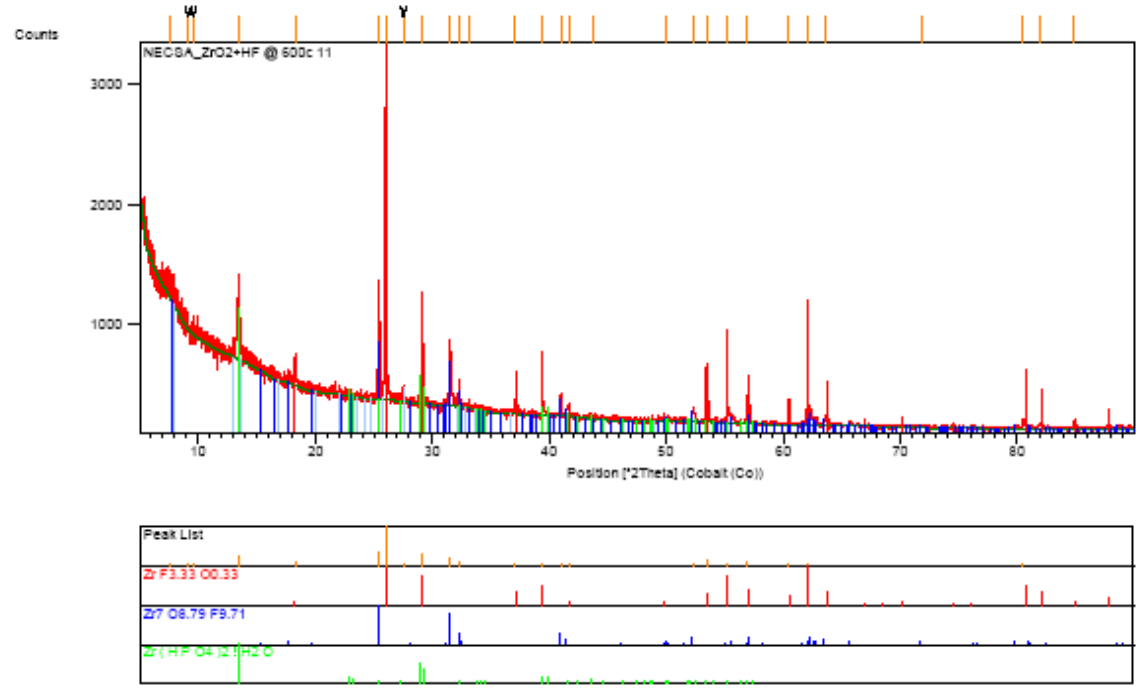

Figure 4.20: Diffraction pattern of the products from the ZrO_2/HF reaction at 600 °C.

CHAPTER 5

FLUORINE GAS AS A FLUORINATING AGENT

5.1 INTRODUCTION

The overall purpose of this chapter was to investigate the following in a F_2 atmosphere:

- Determination of the optimum synthesis conditions for the formation of pure ZrF_4;
- Determination whether formation of ZrF_4 occurs via an intermediate;
- Determination whether fluorination conditions could be used as a purification method for the synthesis of high-purity ZrF_4.

Note: When using this strong fluorinating agent care should be taken as unexpected reactions may occur even when the system might be regarded to be in a relatively safe state.

A dry processing and purification process was investigated as a means of separating zirconium and hafnium.

5.2 EXPERIMENTAL

The experimental procedures are described in full in Chapter four.

5.3 RESULTS AND DISCUSSION

The fluorination of ZrO_2 samples with fluorine gas was investigated by means of thermogravimetry.

5.3.1 Thermogravimetric analysis of the reaction between ZrO_2 and F_2

In Chapter four HF was considered as a fluorinating agent, but fluorine can also be used.

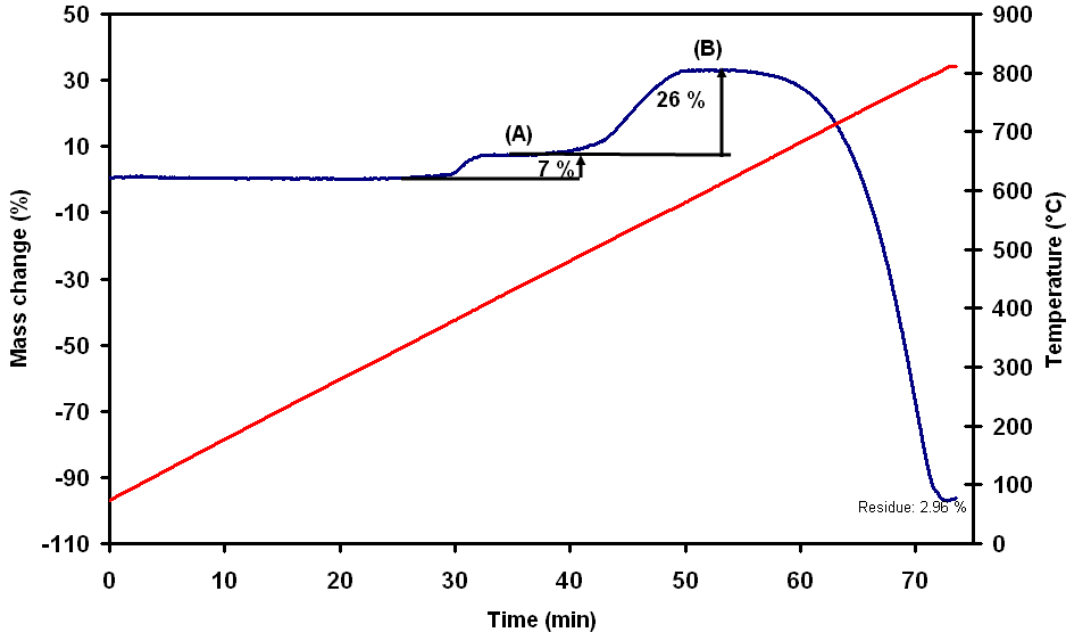

Figure 5.1: Thermogravimetric curve of the reaction of ZrO_2 in a 10 % F_2/N_2 atmosphere.

A ZrO_2 sample was heated from room temperature to 800 °C at a rate of 10 °C/min in a 10 % F_2/N_2 atmosphere. The thermogravimetric curve of this reaction is depicted in Fig. 5.1. It is evident that fluorination was via a double-step reaction, with the initial mass increase of 7 % at approximately 380 °C, and the second 26 % at approximately 480 °C. The initial mass increase of 7 % does not correspond with any of the possible oxyfluorides for which mass increases were calculated in the previous chapter. The double-step reaction could, however, be ascribed to the formation of ZrF_4 (**B**) via a zirconium oxyfluoride (**A**) species as an intermediate, but the species is unknown. A sample of the first fluorination step product was prepared at 350 °C and submitted for XRD analysis, and ZrO_2 and some unknown patterns were detected. The total mass increase of 33 % for both steps corresponds well with the theoretical mass increase of 35.7 % for the conversion of ZrO_2 to ZrF_4. The formed ZrF_4 started to sublime at approximately 625 °C, with a

resultant residue of 2.96 %, which could be ascribed to less volatile impurity fluorides or condensation on the hang-down wire.

5.3.2 Isothermal reactions of ZrO_2 with F_2

In an attempt to isolate the intermediate compounds, fluorinations were carried out at selected isothermal reaction temperatures of 200, 300, 400, 500, 525 and 550 °C. It is important to mention that for the interaction of ZrO_2 with F_2 at room temperature, no mass increase was observed as in the case for HF.

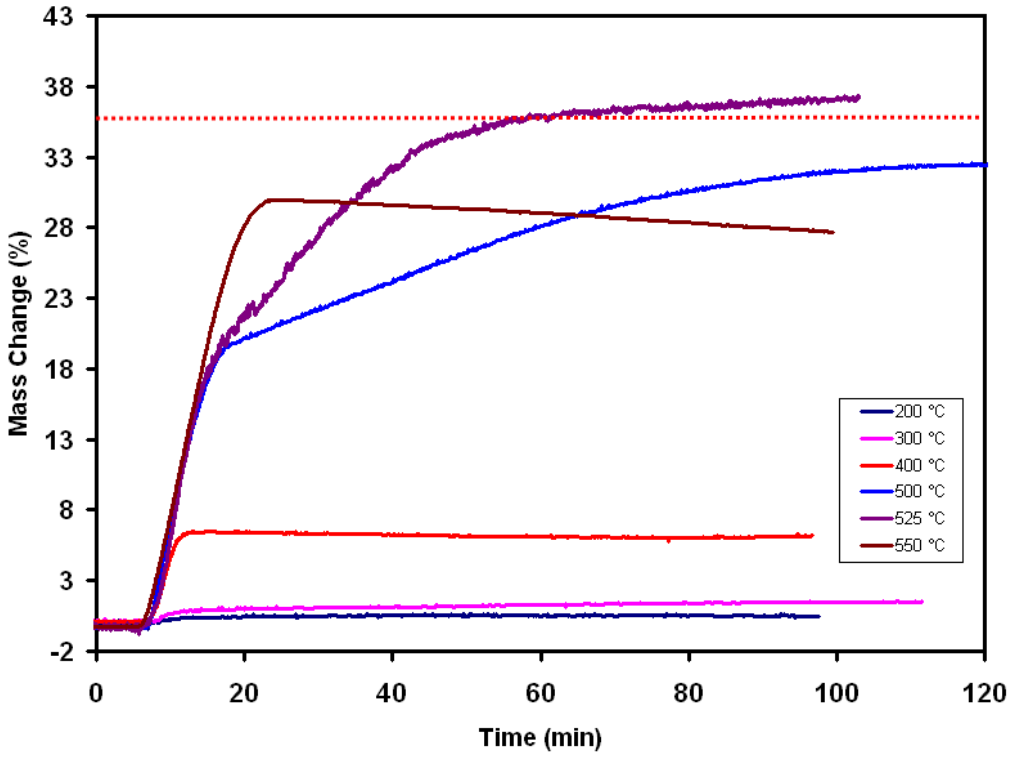

Figure 5.2: Thermogravimetric curves for the isothermal reaction of ZrO_2 with F_2 at 200, 300, 400, 500, 525 and 550 °C.

From Fig. 5.2 the following can be observed:

1. ZrO_2 does not react with F_2 below 300 °C.
2. At 400 °C only a 6 % mass increase due to the formation of oxyfluoride or zirconium tetrafluoride was observed

(this corresponds to the 7 % mass increase observed for the first step in the dynamic run reported above).

3. At 500 °C the observed mass increase was via a double-step reaction with a total mass increase of 34 %.
4. At 525 °C the conversion was complete via a double-step reaction exceeding the expected theoretical mass increase of 35.7 %.

The mass increase due to the reaction of ZrO_2 with F_2 at a temperature of 400 °C seems to be approximately 7 %, this was evident in Figs. 5.1 and 5.2, which might be ascribed to kinetic constraints, or to a hitherto unknown oxyfluoride compound that forms as an intermediate.

At a higher temperature (550 °C) the mass increase was ca. 29 %. The lower than theoretical mass increase could be an indication of two possible consecutive reactions (product formation followed by mass loss). At this temperature (550 °C) sublimation has already started to dominate. The curves only show comparison for the specified temperatures; however if the runs had been allowed for longer times, some of the reactions might have run to completion.

In the literature Haendler et al.[117] cite that zirconium (IV) oxide does not react with fluorine at 100 °C but converts to zirconium (IV) fluoride above 250 °C, which was in accordance with our experimental investigations that show mass increase or conversion at above 200 °C. They further state that the conversion was approximately 28 % at 400 °C, 33.3 % at 450 °C and complete at 525 °C. However Haendler's finding for the specific temperature of 400 °C was not in accordance with our finding, as a lower percentage was obtained by us under isothermal conditions. This could also be influenced by the difference in particle sizes. It was not certain which instrument Haendler used to obtain these results. The surface area of the starting material will also influence the reaction rate and extent, however the surface area is not stated in the reference.

5.4 X-RAY DIFFRACTION RESULTS

In the previous section isothermal reactions of ZrO_2 with F_2 were studied at different temperatures using a TGA. The samples obtained at the end of TGA runs were submitted for XRD analyses. The following table contains the best matching XRD results.

Table 5.1: Summary of the expected XRD patterns of Zr compounds.

Number	Reaction	Temperature °C	XRD Results	Figures
1	$ZrO_2 + F_2$	350	Mixture ZrO_2 & ?	5.8
2	$ZrO_2 + F_2$	400	ZrO_2	5.9
3	$ZrO_2 + F_2$	525	?	5.10
4	$ZrO_2 + F_2$	550	Mixture ZrF_4 & ?	5.11

? = Unknown patterns.

It is evident that unknown patterns are often observed. At the temperatures where thermogravimetric analyzer indicates that the reaction has gone to completion (525 and 550 °C) no ZrO_2 was identified, which indicates that all of the starting material had been converted. ZrF_4 could be identified for the reaction at 550 °C but not for the reaction at 525 °C.

5.5 RAMAN SPECTROSCOPY RESULTS

Figures 5.3 – 5.5 illustrate the Raman spectra for reaction products of ZrO_2 with fluorine gas at various temperatures, between 30 and 600 °C. The Raman bands are listed and compared in Table 5.2.

5.5.1 Raman spectra of the products formed in the reaction between ZrO_2 and F_2

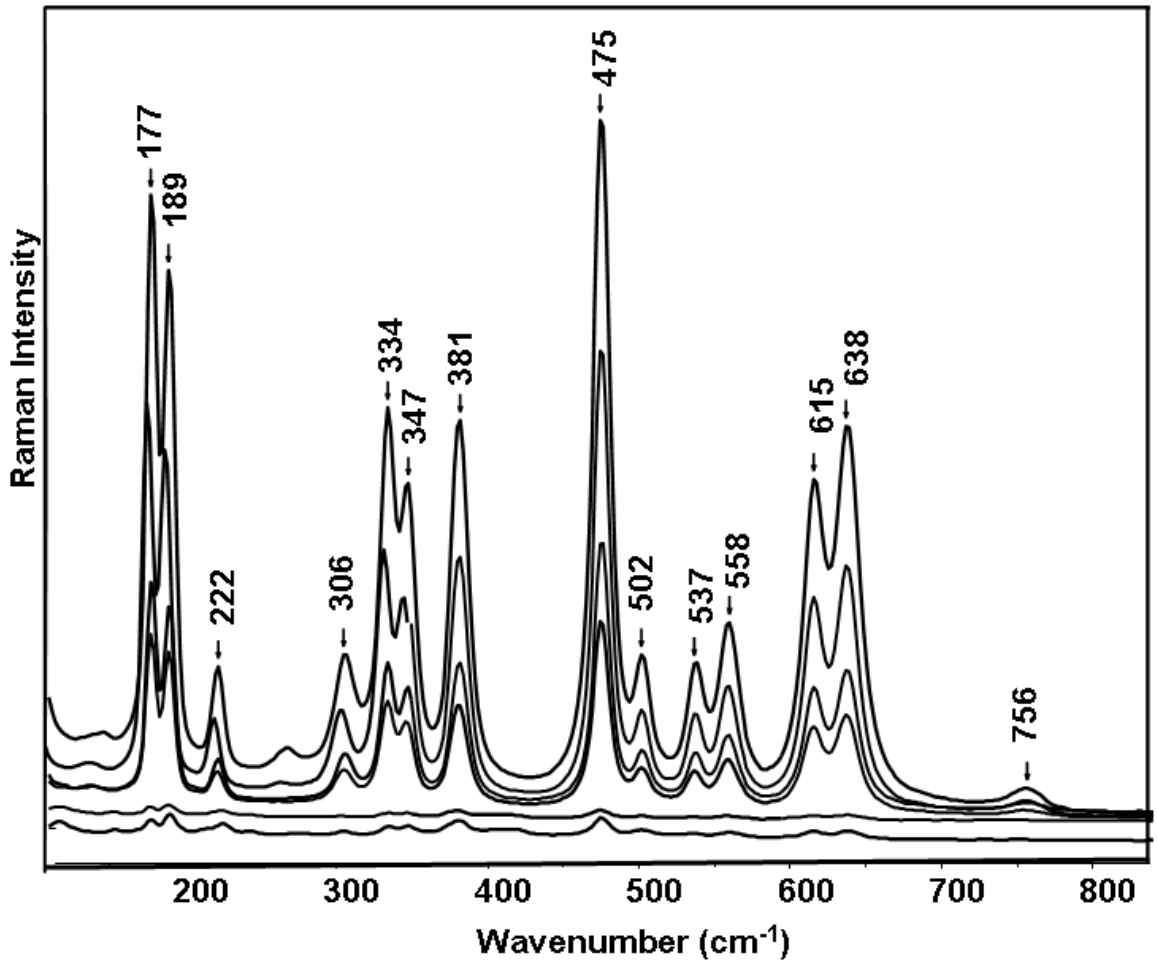

Figure 5.3: Raman spectra of the reaction products of ZrO_2 with F_2 at different temperatures from 30 to 550 °C (top to bottom).

5.5.2 Comparison between the Raman spectra of the products from the reaction between ZrO_2 and F_2 at different temperatures, with those of ZrO_2 and ZrF_4

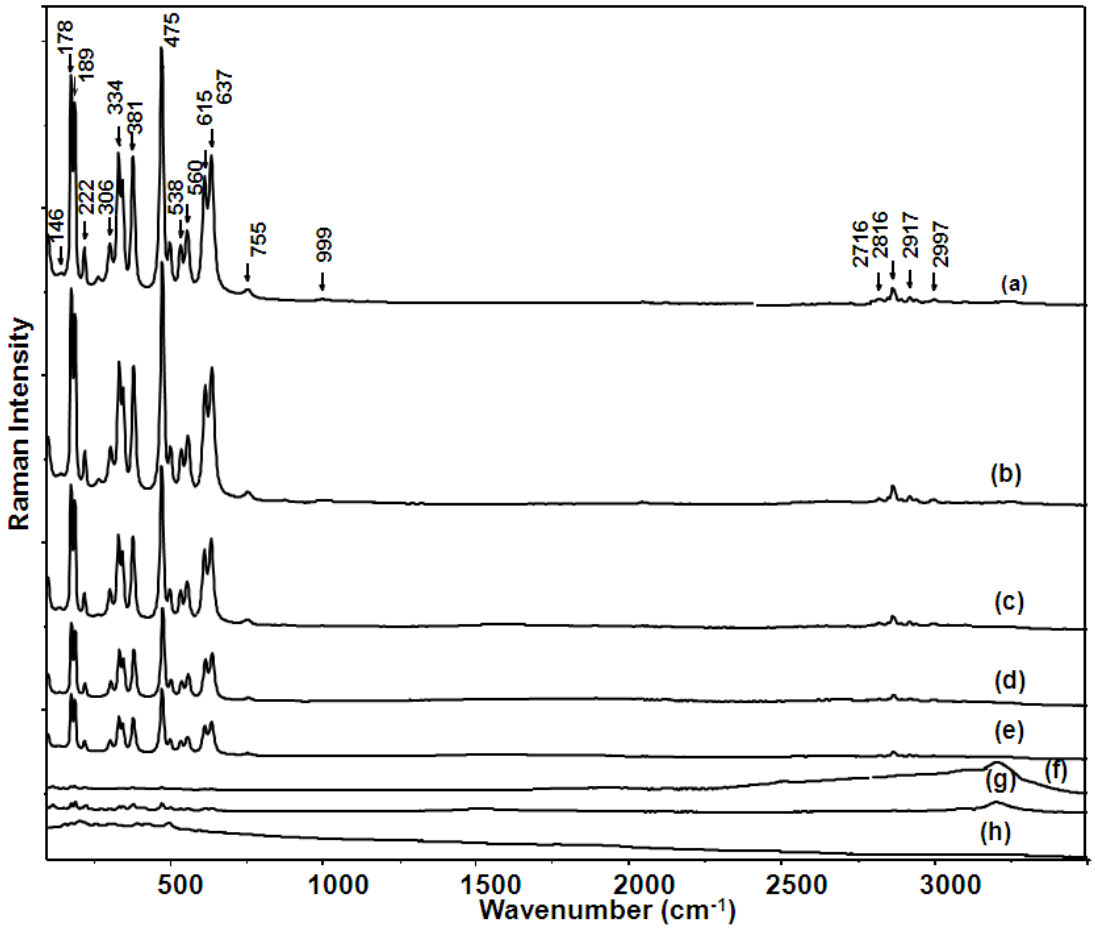

Figure 5.4: Comparison between the Raman spectra of (a) ZrO_2, with the reaction products from ZrO_2 with F_2 at (from top to bottom): (b) 30, (c) 300, (d) 350, (e) 400, (f) 525, (g) 550 °C and (h) ZrF_4.

Fig. 5.3 depicts the Raman spectra of the reaction products, of the reaction between ZrO_2 and F_2 at various temperatures between 30 and 550 °C. In Fig. 5.4 these were compared to Raman spectra of the starting material (ZrO_2) and the final reaction product that could be identified as ZrF_4 from the Raman spectra and X-ray powder diffraction data. The spectra clearly illustrate how the product remains the same as the starting materials, up to 400 °C, although the relative intensities of all the zirconium oxide bands are increasingly reduced with higher temperature.

The reaction proceeds at 525 °C to form ZrF_4, as can clearly be seen from the dramatic changes in the relative intensities of the Raman bands in the region between 100 and 800 cm^{-1}, although some ZrO_2 left in the bulk material.

5.5.3 Comparison between the Raman spectra of the products from the reaction between ZrO_2 and F_2 at two different temperatures, with those of ZrO_2 and ZrF_4, in the spectral region 100 to 800 cm^{-1}

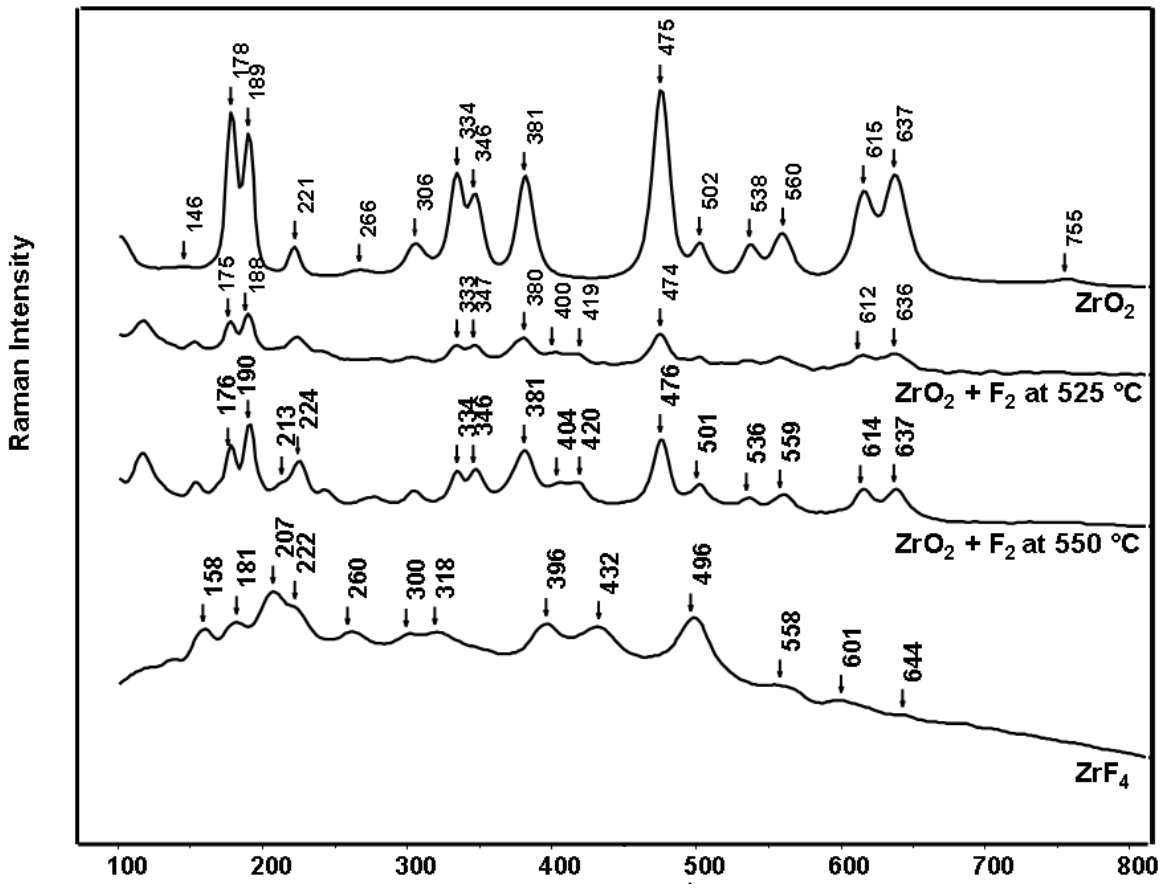

Figure 5.5: Raman spectra of ZrO_2, ZrF_4 and of the reaction products formed during the reaction between ZrO_2 and F_2 at 525 and 550 °C.

5.5.4 Raman spectra of the products from the reaction between zirconium oxide and F_2 at 525 and 550 °C, in the spectral region 100 to 3500 cm^{-1}

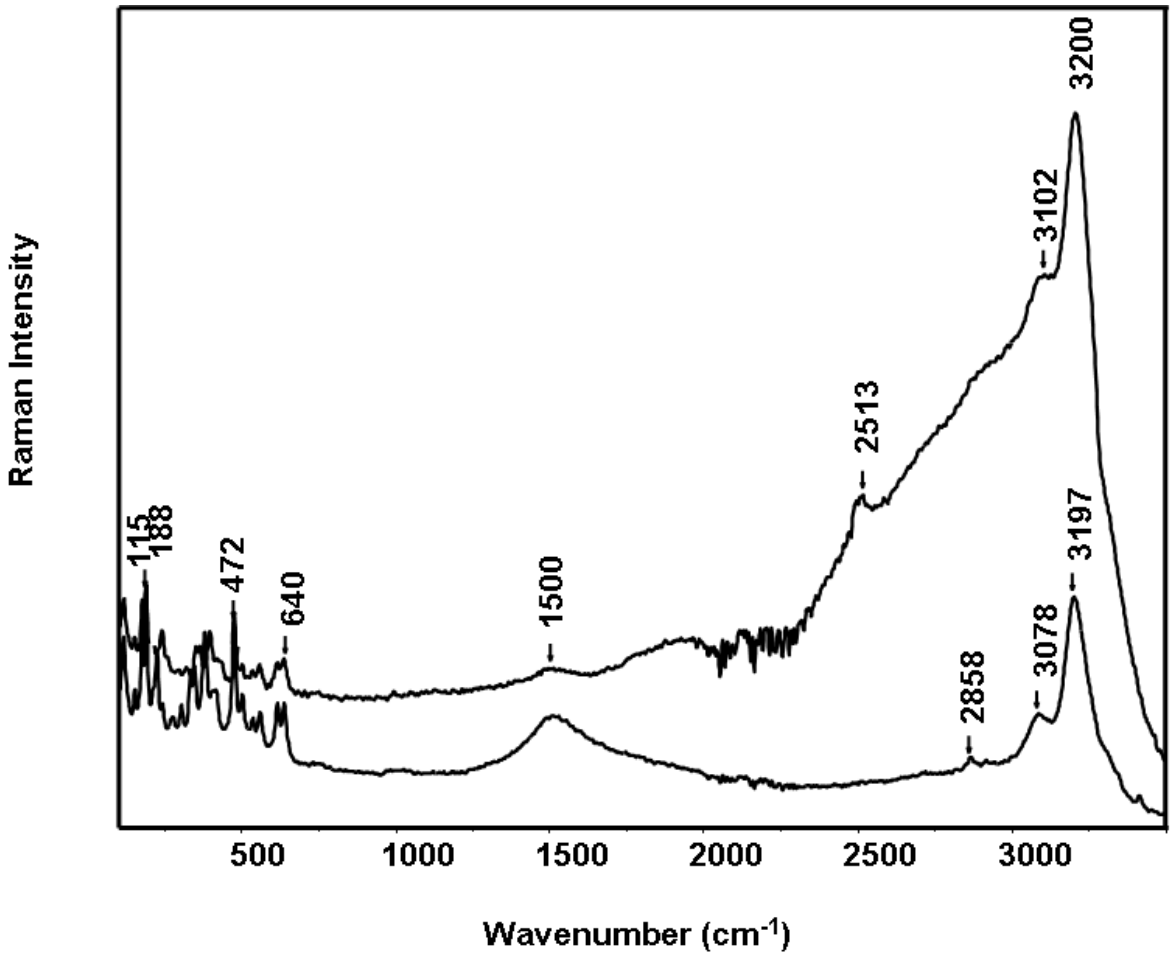

Figure 5.6: Raman spectra of the products of the between ZrO_2 and F_2 at 525 (top) and 550 °C (bottom) in the spectral region of 100 to 3500 cm^{-1}.

Fig. 5.5 depicts comparison spectra of the reaction products between ZrO_2 and F_2 at 525 and 550 °C, with the starting material ZrO_2 and the product ZrF_4. Since the Raman spectrum of ZrO_2 has higher intensity Raman bands than the reaction product, ZrF_4, even small amounts of the remaining starting material can be observed in the Raman spectra at 175, 188, 222, 241, 278, 306, 333, 347, 380, 420, 474, 612 and 636 cm^{-1}. In comparison characteristics Raman bands for ZrF_4 were observed at 153, 260, 400, 436 cm^{-1}. Raman bands of an unknown phase, possibly the $ZrO_{0.33}F_{3.33}$ identified from X-ray powder diffraction data, were observed at 213, 243 and 278 cm^{-1}. Raman spectra of this oxyfluoro compound were not yet available in the literature.

5.5.5 Comparative Raman study of the products from the reactions between ZrO_2 and F_2 and HF at different temperatures

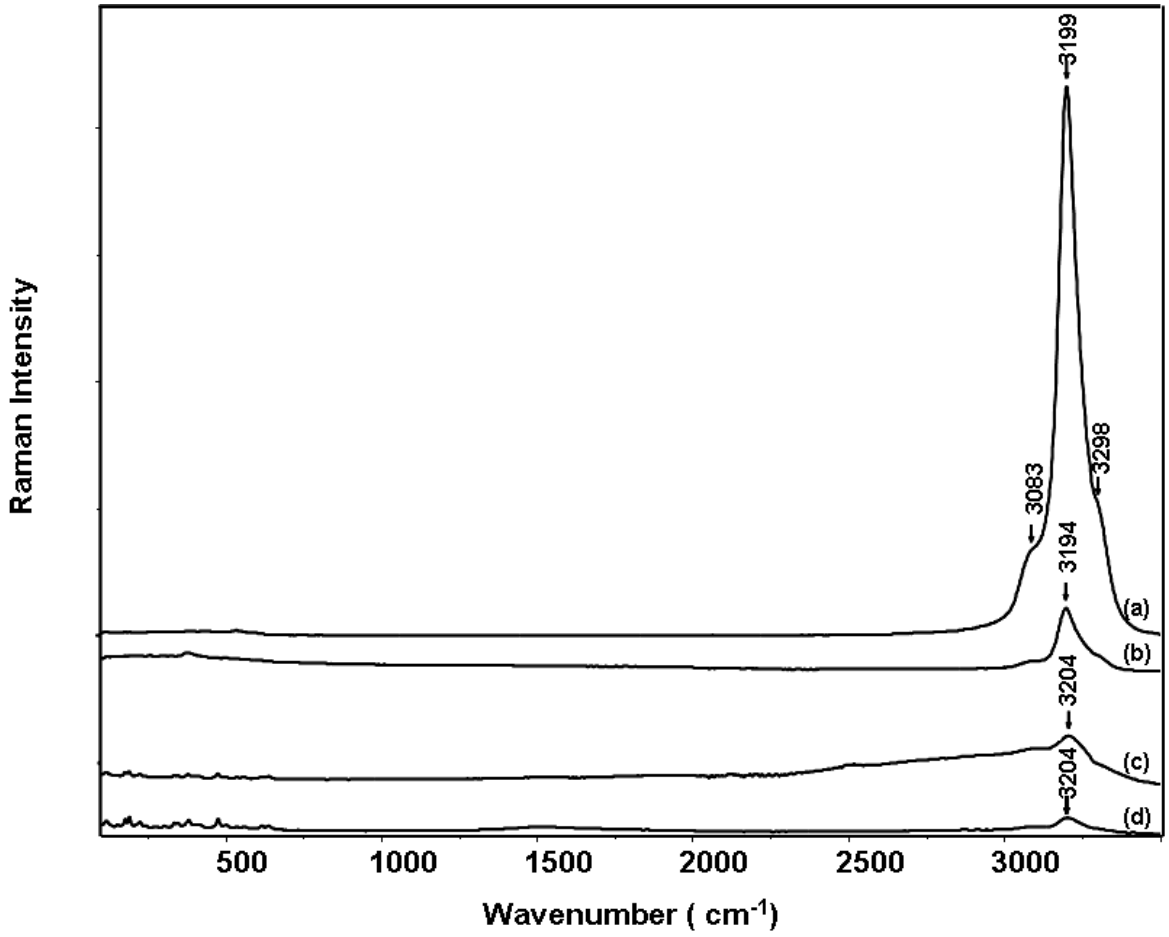

Figure 5.7: Comparison between the Raman spectra of the products from the reaction between ZrO_2 and HF at 600 (a) and 500 °C (b), with products from the reaction between ZrO_2 and F_2 at 525 (c) and 550 °C (d) in the region 100 to 3500 cm^{-1}.

Fig. 5.7 shows a comparison of the Raman spectra between the reaction products of ZrO_2/HF at 500 and 600 °C with the reaction products of ZrO_2/F_2 at 525 and 550 °C in the region 100 to 3500 cm^{-1}. Some HF adsorption appears to have occurred for the F_2 samples, as can be seen from the band on each sample appearing around 3200 cm^{-1}. The adsorption of HF on the sample surface increases with temperature (in the case of HF reaction) but the opposite is true for the F_2 reaction with ZrO_2, where the amount of HF adsorbed appears to decrease with temperature. This is probably as a result

of desorption of the gas product (HF formed between F_2 and H_2O in the atmosphere) from the oxide surface.

More detailed Raman spectra of the ZrO_2 and F_2 reaction products at 525 °C and 550 °C are shown in Fig. 5.6, where the Raman bands in the higher wavenumber region occur not only at 3200 cm^{-1}, the high intensity Raman band, but also at lower intensity bands at 2513, 2858, 3078 and 3102 cm^{-1} and even a broad band at 1500 cm^{-1}.

Infrared spectra will have to be recorded of the reactant, products and standards of the possible products for comparison with the Raman spectra and X-ray powder diffraction results. As Raman spectroscopy is more sensitive for a stronger Raman scatterer like ZrO_2, the Raman spectrum of this starting material may be of higher intensity than the product, e.g. ZrF_4 formed during the high-temperature reaction, masking some of the product Raman bands.

Table 5.2: Summary of Raman bands in wave numbers (cm^{-1}) observed for ZrO_2, ZrO_2 reacted with F_2 at 30, 300, 350, 400, 525 and 550 ˚C, and ZrF_4.

ZrO_2	ZrO_2 reacted with F_2 at 30˚C	ZrO_2 reacted with F_2 at 300 ˚C	ZrO_2 reacted with F_2 at 350 ˚C	ZrO_2 reacted with F_2 at 400 ˚C	ZrO_2 reacted with F_2 at 525 ˚C	ZrO_2 reacted with F_2 at 550 ˚C	ZrF_4 this work	ZrF_4[116]	Unknown phase
								80 s	
								90 s	
					118 m	118 m		**110**	
					153 w	**158 w**	**158 w**	**163 m**	
178 vs	178 vs	178 vs	178 s	178 s	175 m	176 m	**181w**	**178 w**	
189 vs	190 vs	190 vs	190 s	190 s	188 m	190 m		**198 w**	
						213 vw	**207 m**		**213 vw**
222 m	222 m	222 m	222 w	222 w	222 vw	224 w	**222m sh**	**222 w**	
					241 vvw	**243 vw**			**243 vw**
266 vw	267 vw	-	-	-	**260 vvw**		**260 w**	**260m**	
					278 vw	**277 vw**			**278 vw**
306 m	306 m	306 m	306 w	306 w	306 vw	306 vw	**300 w**		
							317 w		
334 s	334 s	334 s	334 m	334 m	333 w	334 w			
346 s	347 s	347 s	347 m	347 m	347 w	346 w		**345 w**	
381 s	381 s	381 s	381 m	381 m	380 m	381 m	**381 w**	**391 w**	
					400 vw	**404 vw**	**396 m**		
					419 vw	420 vw		**407 ms**	
					436 vvw		**432 m**	**425 w**	
475 vs	476 vs	476 vs	476 s	476 s	474 m	476 m		**484 w**	
502 m	502 m	502 m	502 w	502 w		501 vw	**496 m**	**505 w**	
538 m	538 m	538 m	538 w	538 w		535 vvw			
560 m	558 m	558 m	558 w	558 w		559 vw	**558 vw**		
							600 vw		
615 s	615 s	615 s	615 m	615 m	612 w	614 m			
637 s	638 s	638 s	638 m	638 m	636 w	637 w	**644 vw**	**655 w**	
755 w	755 w	755 w	755 vw	755 vw					

w = weak; m= medium; s = strong; v = very; sh = shoulder

5.6 CONCLUSIONS

The conversion of ZrO_2 to ZrF_4 was achieved with fluorine gas at 525 ˚C with respect to the theoretical mass increase of 35.7 %. It was concluded that the formation of ZrF_4 was via the oxyfluoride, therefore a pure ZrF_4 could not be identified. It is also suspected that the temperature where ZrF_4 forms could be the same temperature where it starts to sublime.

5.7 X-RAY DIFRACTOGRAMS

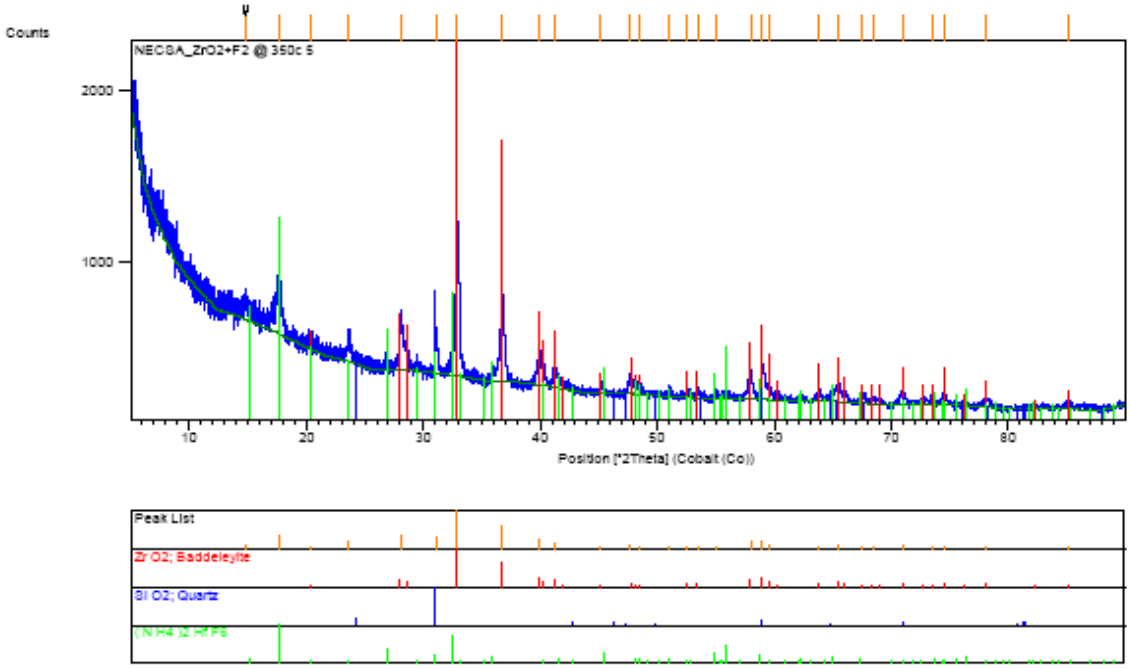

Figure 5.8: Diffraction pattern of the products from the ZrO_2/F_2 reaction at 350 °C.

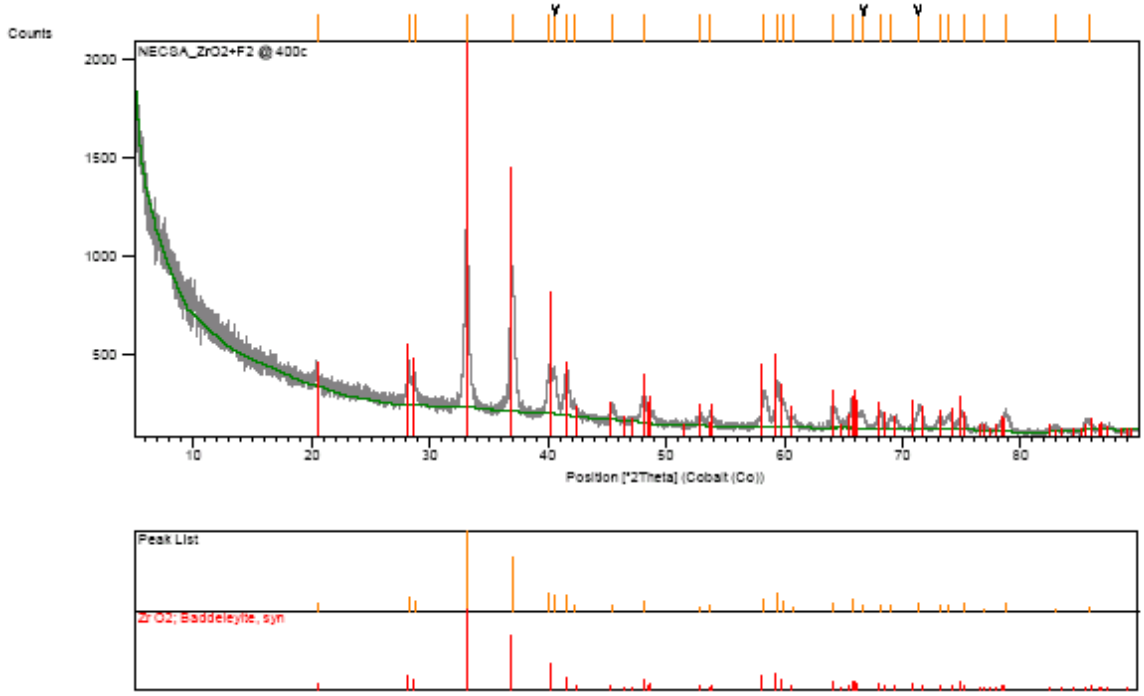

Figure 5.9: Diffraction pattern of the products from the ZrO_2/F_2 reaction at 400 °C.

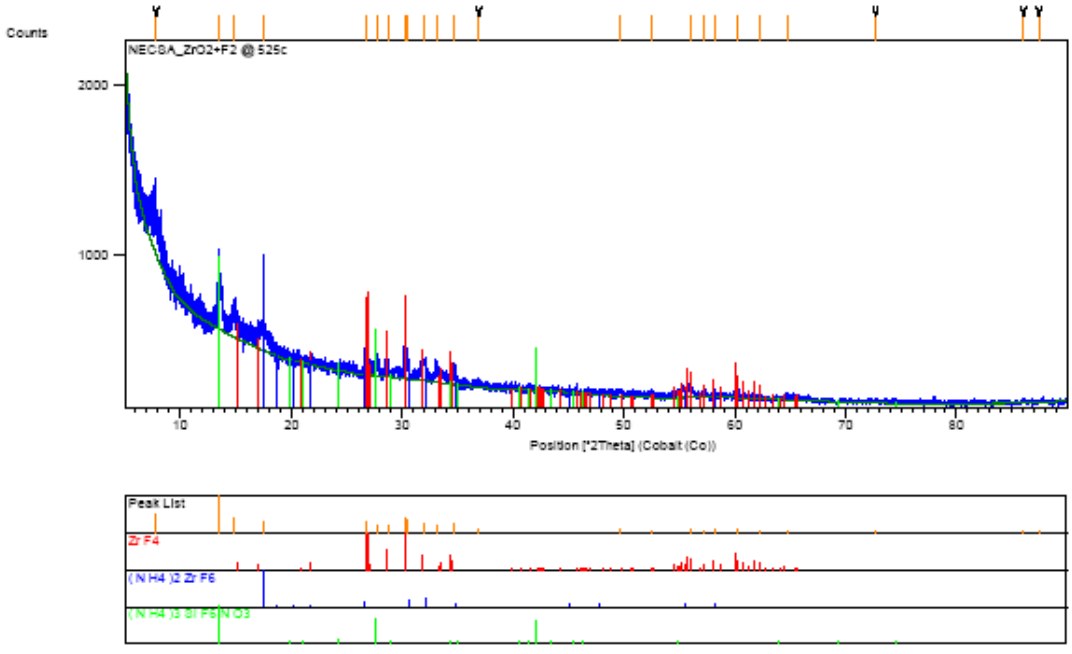

Figure 5.10: Diffraction pattern of the products from the ZrO_2/F_2 reaction at 525 °C.

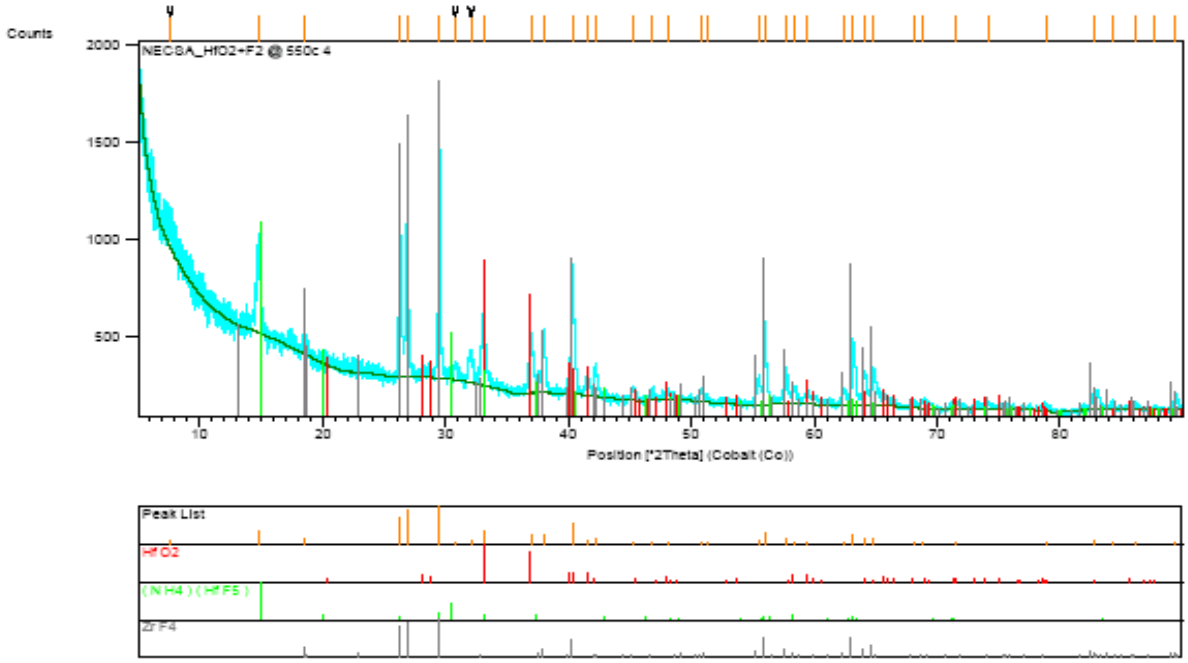

Figure 5.11: Diffraction pattern of the products from the ZrO_2/F_2 reaction at 550 °C.

CHAPTER 6

COMPARATIVE STUDY OF ZIRCONIUM AND HAFNIUM SPECIES

6.1 INTRODUCTION

The aim of this study was to investigate methods to purify zirconium (primarily from hafnium) by separating the fluorides produced by dry fluorination processing routes. The previous chapters detailed studies with respect to dry fluorination methods. This chapter deals with the fluorination of mixtures of zirconium and hafnium oxides, the evaluation thereof and the sublimation behaviour of zirconium and hafnium tetrafluorides. It also contains an overall evaluation of the study conducted. These studies were carried out to evaluate possible separation mechanisms for these two species using hydrogen fluoride or fluorine gas.

6.2 EXPERIMENTAL

Thermogravimetric studies were carried out according to the procedures as described in Chapter 4.

6.3 RESULTS AND DISCUSSION

Fluorination of ZrO_2/HfO_2 mixtures and sublimation of commercial zirconium and hafnium tetrafluoride samples were investigated by means of thermogravimetry.

Note: Unfortunately dynamic TG runs (up to 800 °C) for HfO_2 with HF and F_2 could not be completed due to these reactions destroying a stirrup in the instrument while fluorinating.

6.3.1 Thermogravimetric study of the fluorination of a 50:50 mixture of ZrO_2 and HfO_2 with F_2

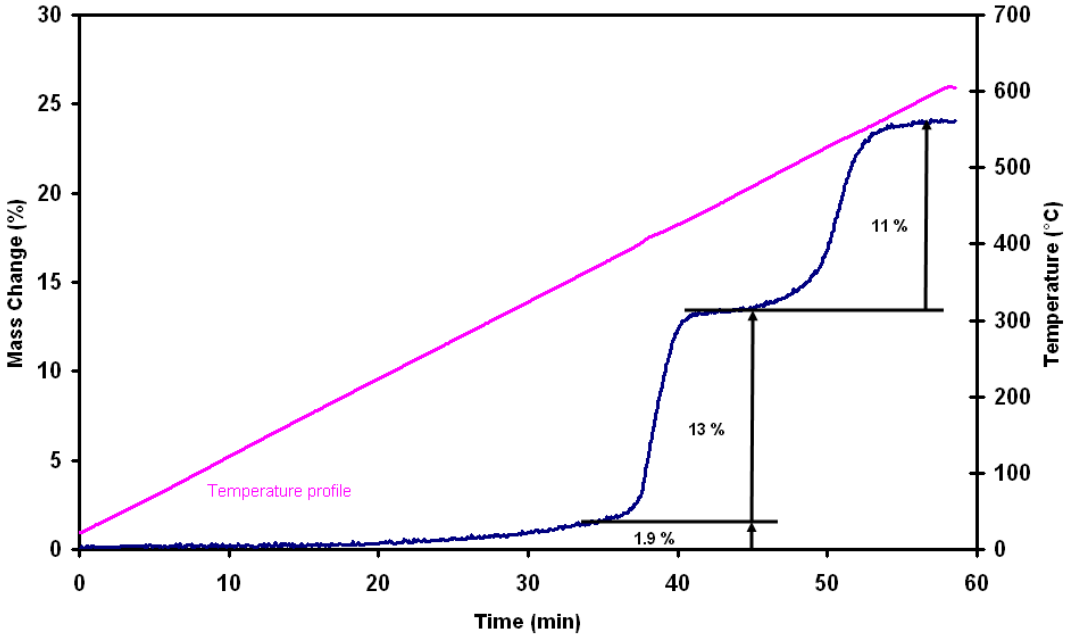

Figure 6.1: Thermogravimetric curve of the fluorination of a ZrO_2/HfO_2 (50:50) mixture with F_2.

Fig. 6.1 depicts the fluorination of a 50:50 (by mass) physical mixture of ZrO_2 and HfO_2 with fluorine gas. This sample was heated from room temperature to 600 °C at 10 °C/min. The reaction mixture fluorinated via a triple-step reaction curve, with a first, second and third mass increase of approximately 1.9, 13 and 11 % respectively.

6.3.2 Thermogravimetric study of the fluorination of a 50:50 mixture of ZrO_2 and HfO_2 with HF

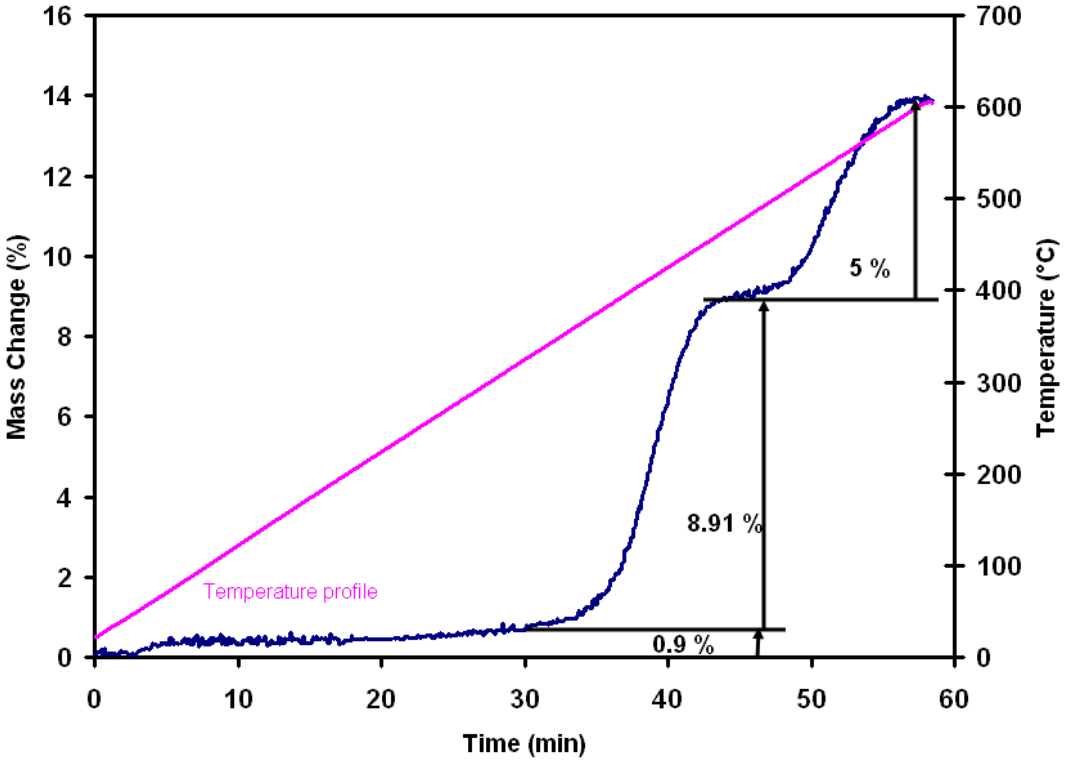

Figure 6.2: Thermogravimetric curve of the fluorination of a ZrO_2/HfO_2 (50:50) mixture with HF.

A sample of ZrO_2/HfO_2 (50:50 by mass) mixture was heated from 30 to 600 °C at a heating rate of 10 °C/min, whilst under 10 % HF/N_2 atmosphere. The result is depicted in Fig. 6.2. The reaction occurs via a three-step mechanism, with a first, second and third mass gain of 0.9, 8.91 and 5 % respectively. This reaction behaviour is similar to that depicted in Fig. 6.1 where fluorine gas was used as a fluorinating agent.

6.3.3 Thermogravimetric study of the fluorination of a 75:25 mixture of ZrO_2 and HfO_2 with HF

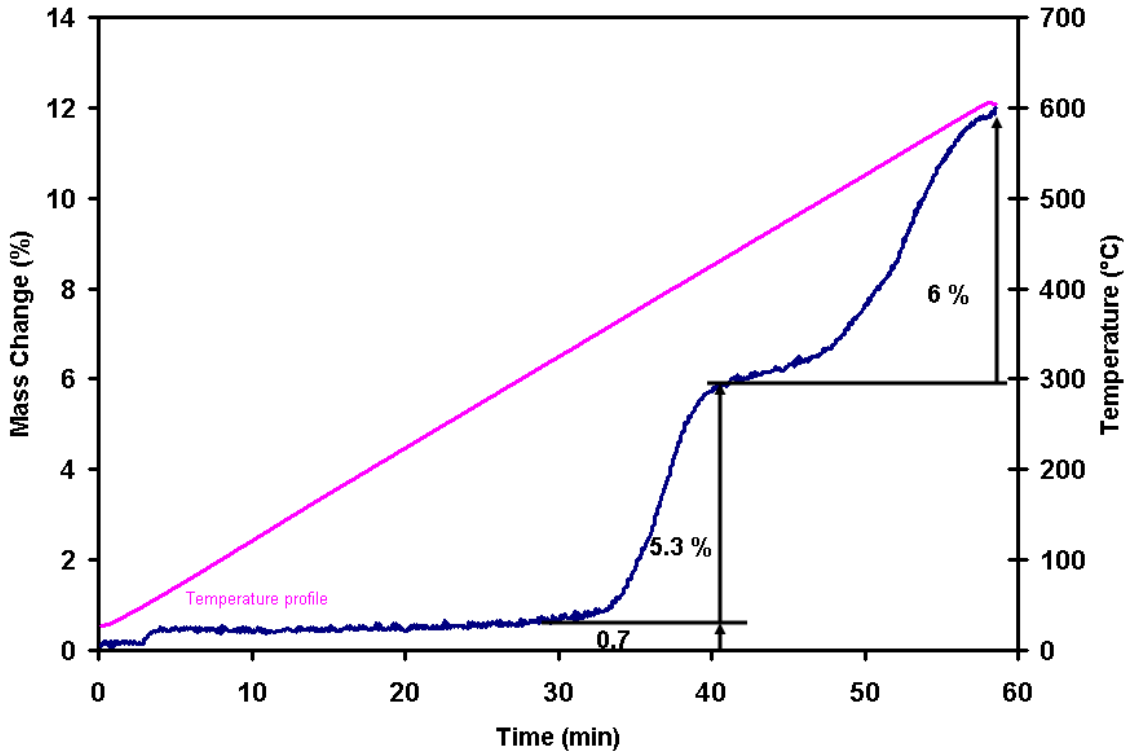

Figure 6.3: Thermogravimetric curve of the fluorination of a ZrO_2/HfO_2 (75:25) mixture with HF.

Fig. 6.3 depicts the fluorination of a 75:25 (by mass) physical mixture of ZrO_2 and HfO_2 with hydrogen fluoride. The reaction depicts almost similar results as for a 50:50 reaction mixture, with a total mass increase of ca. 12 %.

6.3.4 Comparative thermogravimetric study of the fluorination of a 50:50 mixture of ZrO_2 and HfO_2 with HF and F_2

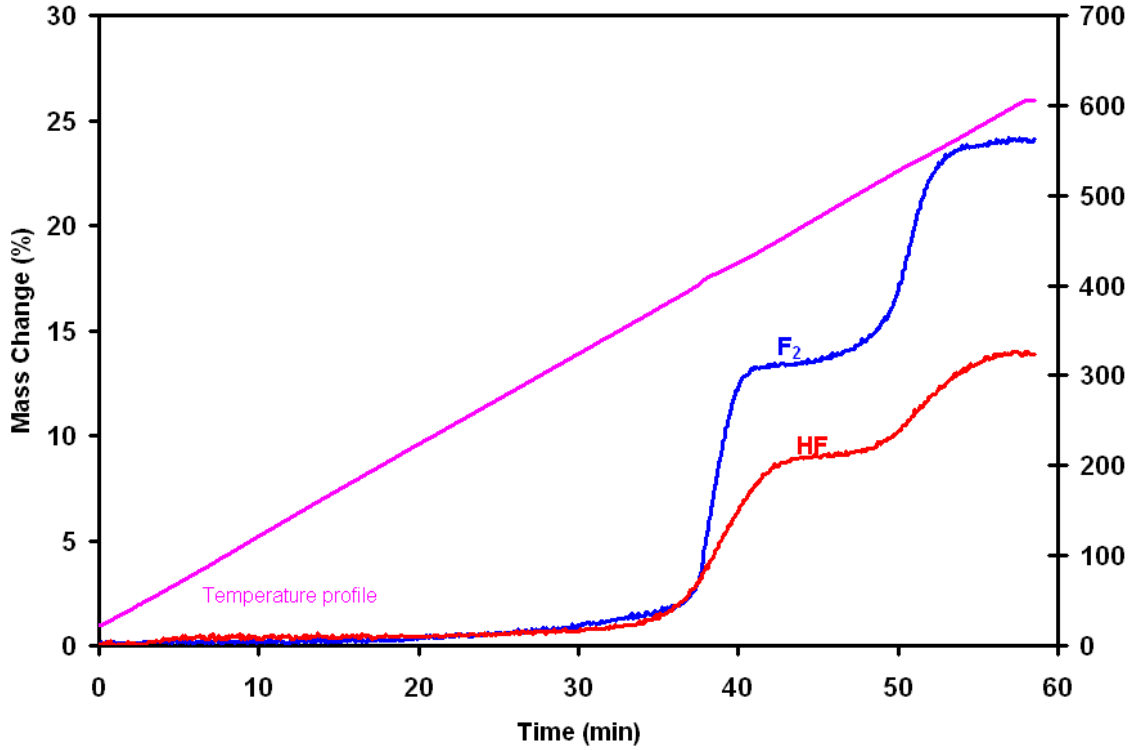

Figure 6.4: Comparative thermogravimetric study of the reaction between a 50:50 reaction mixture of ZrO_2 and HfO_2, with HF and F_2.

From Fig. 6.4, it is evident that the initial reaction rates of the two reactions are identical until approximately 30 min. After 30 min the F_2 graph shows a higher apparent reaction rate, with a total mass increase of ca. 24 %. It was established in Chapter 5 that the interaction of ZrO_2 with F_2 at 550 °C showed that sublimation was in progress but in this case at 600 °C, there was no indication of sublimation.

The HF graph depicts a slower apparent reaction rate with a total mass increase of approximately 14 %, which can be ascribed to two possible consecutive reactions taking place at the same time. These mixtures were prepared to establish which of the oxides will be fluorinated first. However, this technique did not show any differences that can be manipulated to effect separation.

It was established that when fluorinating with fluorine gas, a total mass increase of ca. 24 % was observed, which was more than the theoretical mass increase expected when converting HfO_2 to HfF_4 (20.9 %), and less than the theoretical mass increase expected when converting ZrO_2 to ZrF_4 (35.7 %). There is no evidence to assign a particular mass change to Zr or Hf individually.

6.3.5 Comparative isothermal thermogravimetric study of the reaction between ZrO_2 and HfO_2 and HF

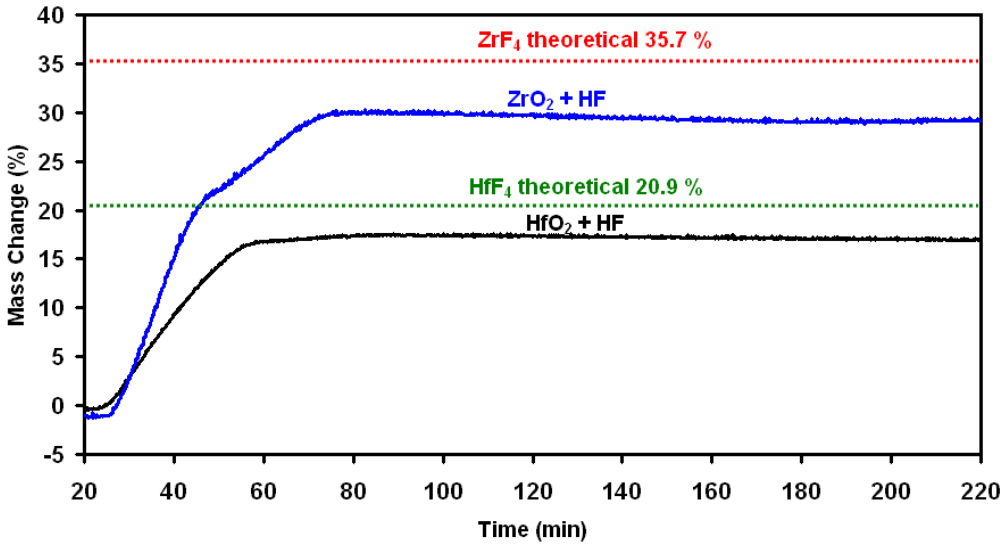

Figure 6.5: Isothermal reactions of ZrO_2 and HfO_2 with HF at 500 °C.

Fig. 6.5 outlines a comparative TG study of the isothermal fluorination of ZrO_2 and HfO_2 with HF at 500 °C. It can be seen that a slight degree of mass loss occurs at this temperature for the formed ZrF_4, while the mass increase for HfO_2 was approximately 17 %, without any indication of sublimation. None of the two species reached the expected theoretical mass increase, which are indicated by two horizontal lines (red line representing ZrF_4 (35.7 %) and the green line HfF_4 (20.9 %)). ZrO_2 has a higher apparent rate of reaction when compared to HfO_2 and the formation of zirconium tetrafluoride was via a

double-step reaction. This figure indicates that a selective fluorination could be possible at a suitable temperature (between 500 and 550 °C). However due to the small temperature margin it will be difficult to effect a one-step separation method.

6.3.6 Comparative isothermal thermogravimetric study of the reaction of ZrO_2 and HfO_2 with F_2

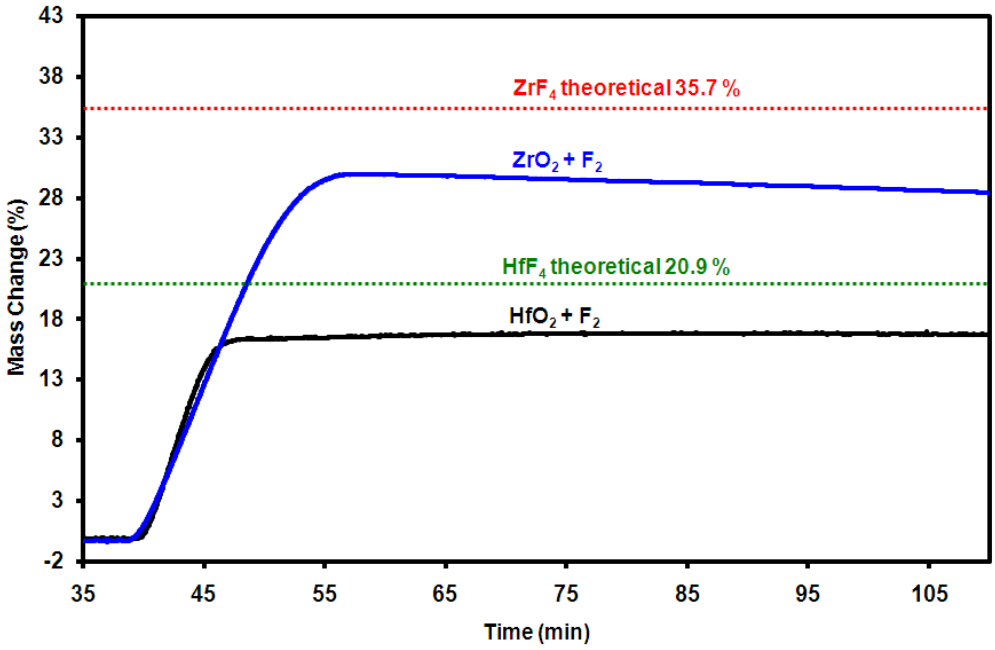

Figure 6.6: Isothermal reactions of ZrO_2 and HfO_2 with F_2 at 550 °C.

Fig. 6.6 outlines a comparative TG study of the isothermal fluorination of ZrO_2 and HfO_2 with F_2 at 550 °C. It has already been established in Chapter 5 that sublimation was in progress at this temperature for ZrF_4, while conversion of HfO_2 was stable with a mass increase of approximately 17 %. This finding can potentially be used to effect selective separation, whereby ZrF_4 is selectively sublimed from HfF_4. A problem was experienced when a stirrup in the instrument was destroyed while fluorinating these metal oxides at temperatures higher than 550 °C. Therefore sublimation for the hafnium species could not be determined with fluorine gas at higher temperatures.

6.3.7 TGA investigation of the sublimation behaviour of ZrF_4

Since zirconium and hafnium have very similar chemical and physical properties, these two elements are notoriously difficult to separate. One possible separation/purification technique is sublimation, which process relies on the difference in volatility between the two fluorides.

In order to interpret the possibility of hydration of the ZrF_4 sample, it is necessary to define the possible reactions that could have taken place.

- **Addition of one molecule of H_2O on ZrF_4**

$$ZrF_4 + H_2O \rightarrow ZrF_4.H_2O \quad \text{.....6.1}$$

The theoretical mass increase accompanying this reaction is ca. 11 %.

- **Removal of one molecule of H_2O from ZrF_4**

$$ZrF_4.H_2O \xrightarrow{\Delta} ZrF_4 + H_2O \quad \text{.....6.2}$$

The theoretical mass loss accompanying this reaction is ca 9.7 %.

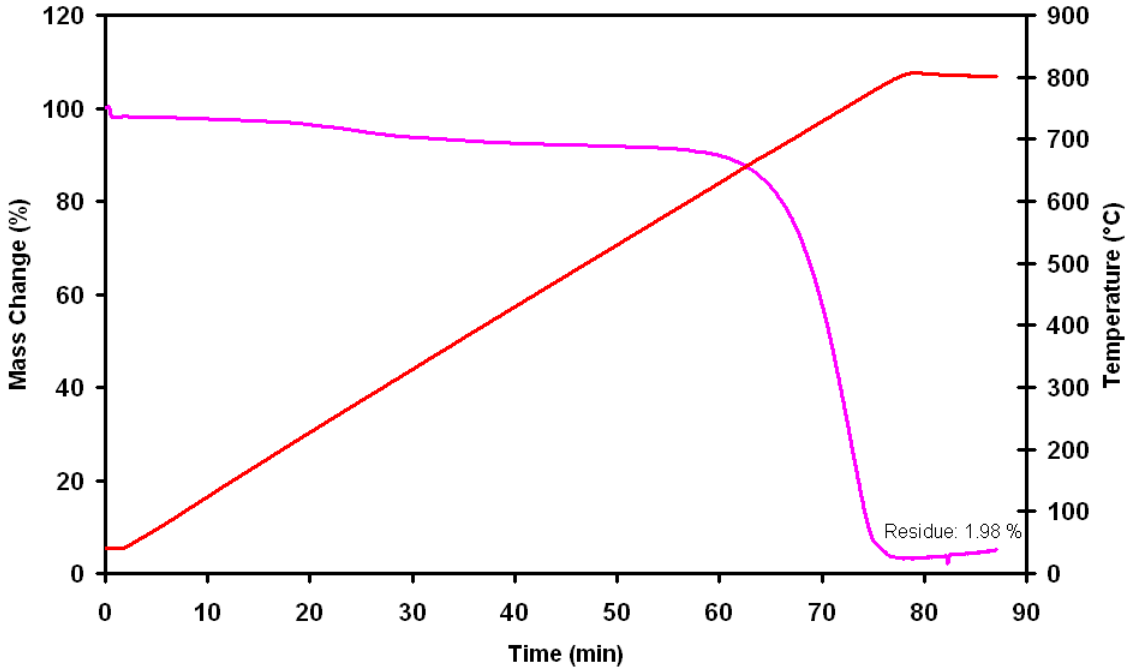

Figure 6.7: Sublimation curve of ZrF_4 in a nitrogen gas atmosphere.

This investigation was conducted with commercial ZrF_4 using nitrogen (N_2) purging gas and a heating rate of 10 °C/min. The resultant thermogravimetric curve is shown in Fig. 6.7. Since ZrF_4 is conventionally synthesized using zircon ($ZrSiO_4$) as precursor, it can be expected that the ZrF_4 will also contain the fluorides of the impurities present in zircon. Some impurities will sublime at low temperatures (below that of ZrF_4) while others however, sublime at relatively high temperatures, e.g. CaF_2 at 1418 °C. ZrF_4 is hygroscopic and the presence of adsorbed or crystal water can be expected. The initial continuous mass loss totaling approximately 8.5 % observed from initial heating can therefore be ascribed to desorption of one mole of H_2O molecules that could have been absorbed per mole of ZrF_4 during the course of sample transfer or storage. The remaining ZrF_4 (together with lower volatility impurity fluorides) started subliming at approximately 674 °C, with a resultant residue of 1.98 %, which most probably constitutes the less volatile impurity fluorides or the formed oxyfluorides. Further detailed investigations will focus on the purification of ZrF_4 of more volatile fluoride impurities in atmospheres like HF and F_2 at temperatures lower than 500 °C.

6.3.8 TGA investigation of the sublimation behaviour of HfF_4

In order to interpret the possibility of hydration of the HfF_4 sample, it is necessary to define the possible reactions that could have taken place.

- **Addition of one molecule of H_2O on HfF_4**

$$HfF_4 + H_2O \rightarrow HfF_4.H_2O \quad \text{.....6.3}$$

The theoretical mass increase accompanying this reaction is ca. 7 %.

- **Addition of two molecules of H_2O on HfF_4**

$$HfF_4 + 2H_2O \rightarrow HfF_4.2H_2O \quad \text{.....6.4}$$

The theoretical mass increase accompanying this reaction is ca. 14 %.

- **Removal of one molecule of H_2O from $HfF_4.H_2O$**

$$HfF_4.H_2O \xrightarrow{\Delta} HfF_4 + H_2O \quad \text{.....6.5}$$

The theoretical mass loss accompanying this reaction is ca. 7 %.

- **Removal of two molecules of H_2O from $HfF_4.2H_2O$**

$$HfF_4.2H_2O \xrightarrow{\Delta} HfF_4 + 2H_2O \quad \text{.....6.6}$$

The theoretical mass loss accompanying this reaction is ca. 12 %.

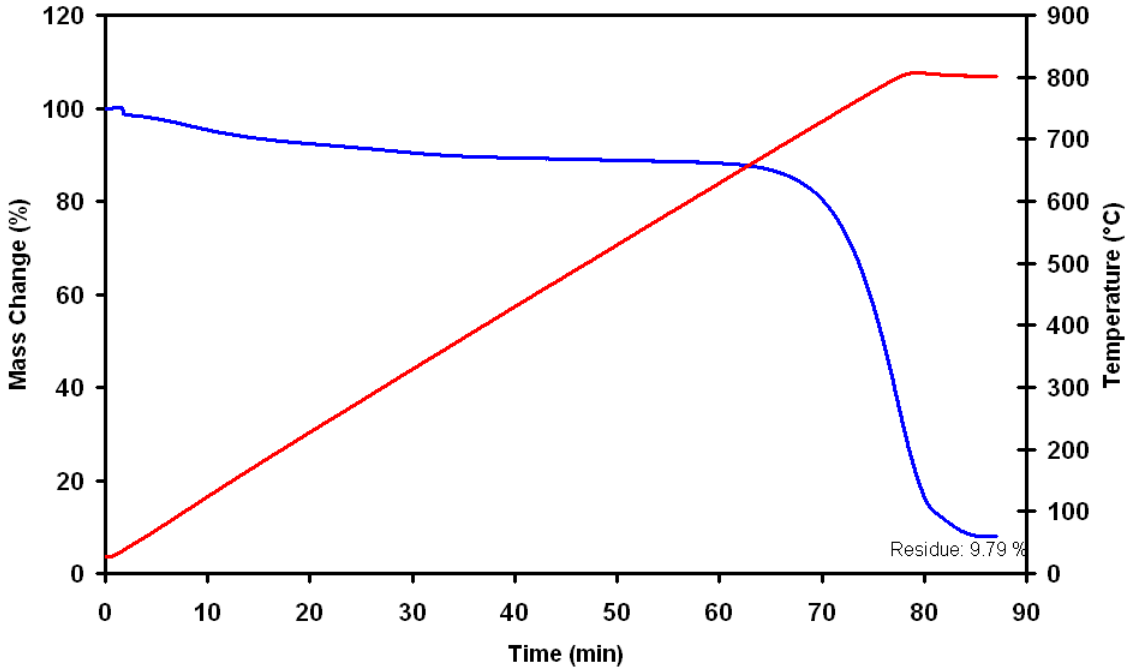

Figure 6.8: Sublimation curve of HfF_4 in a nitrogen gas atmosphere.

It has already been pointed out that published data regarding the sublimation temperature of HfF_4 was very scarce and conflicting, and therefore it was necessary to determine the sublimation temperature of HfF_4. To this effect a TGA experiment was carried out on HfF_4 in N_2 as purge gas and a heating rate of 10 °C/min. The results are shown in Fig. 6.8. Heating to 650 °C resulted in a mass loss of approximately 15 %, which was ascribed to desorption of approximately two moles of H_2O molecules that could have absorbed on the HfF_4. The HfF_4 sample only started to sublime at temperatures exceeding 650 °C, and the eventual residue was 7.97 %. When comparing the experimental results from Figs. 6.7 and 6.8, it is evident that ZrF_4, which starts subliming at approximately 674 °C, is more volatile than HfF_4, which only starts subliming at approximately 718 °C.

6.3.9 Comparative sublimation studies of ZrF_4 and HfF_4

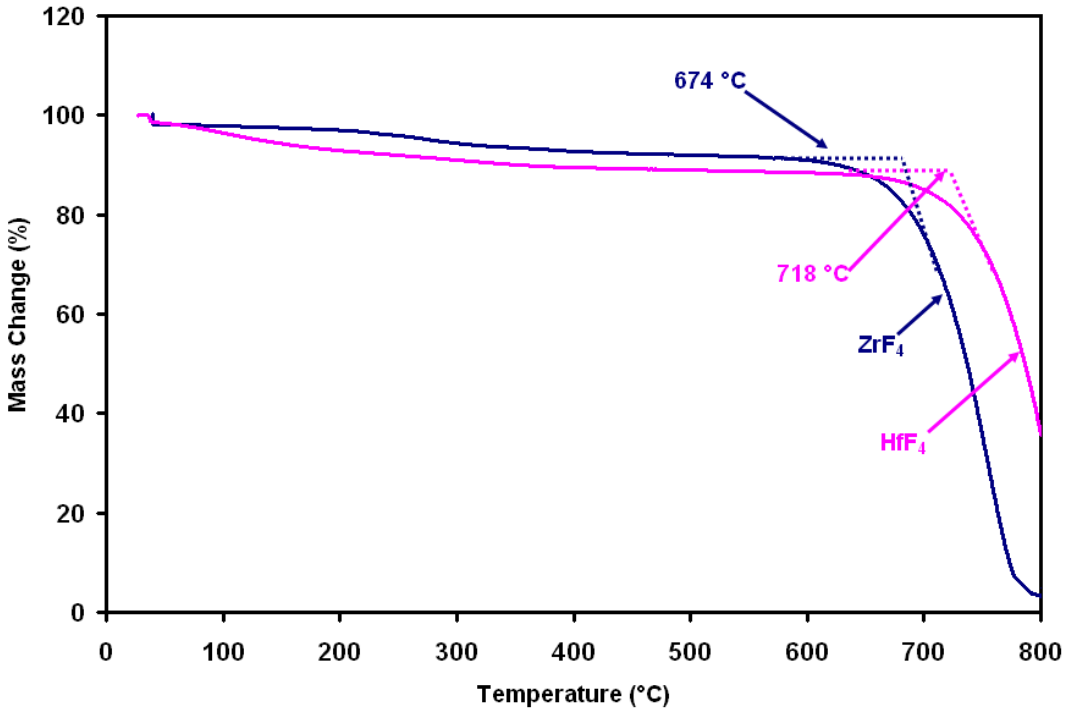

Figure 6.9: Sublimation curves of ZrF_4 and HfF_4.

For comparative purposes the sublimation thermogravimetric curves for HfF_4 and ZrF_4 are overlaid in Fig. 6.9. Considering the onset sublimation temperatures from Fig. 6.9, it is evident that ZrF_4, which starts subliming at ca. 674 °C, is more volatile than HfF_4, which only starts to sublime at approximately 718 °C. It is likely that an approximate 50 °C sublimation temperature difference is not sufficient to achieve complete separation in one separation cycle. For an ideal separation by sublimation in one step, a bigger sublimation temperature difference is required. For the purpose of this study, it would have been of great importance if HfF_4 could have sublimed prior to ZrF_4, as it would have been easy to remove the impurity (HfF_4) from the bulk (ZrF_4).

6.3.10 TGA investigation of the reaction between ZrF_4 and CH_4

An experimental thermogravimetric analysis was done on ZrF_4 with CH_4 gas and it was found that this reaction resulted in ZrF_4 being coated with carbon. Thus, even if this reaction is thermodynamically feasibly, the kinetic constraints (e.g. mass transfer) negatively contribute to the success of the reaction. It is recommended that further experiments be carried out in an attempt to overcome/exploit these kinetic constraints.

6.4 CONCLUSIONS

Fluorinations of ZrO_2/HfO_2 mixture were carried out with HF and F_2 to establish which species will be fluorinated first and therefore possibly to effect separation. It was concluded that experimentally there was no indication of selective fluorination or separation and it is recommended that more work be done to explore this possibility. It is also concluded that there is no evidence permitting the assignment of a particular mass increase to zirconium or hafnium individually.

Isothermal comparative studies were carried out at 500 °C with HF, and at 550 °C with F_2, to investigate the possibility of selective fluorination and/or separation. Another comparative study was carried out with commercial ZrF_4 and HfF_4, to explore separation/purification by selective sublimation. A sublimation temperature difference of ca. 50 °C was observed during these studies, and it was concluded that separation/purification will prove to be a challenging exercise and would have to be effected by a multi-step process.

CHAPTER 7

EVALUATION OF STUDY

7.1 SCIENTIFIC RELEVANCE OF THE STUDY

All the major global role-players in the nuclear industry utilize $ZrCl_4$ as precursor for manufacturing nuclear-grade Zr metal. However, the hygroscopicity of $ZrCl_4$ is a major problem, and very special precautions have to be taken to prevent the incorporation of O-species into the eventual Zr metal. The purification of $ZrCl_4$ of deleterious contaminants is a routine industrial process, but is very intricate and costly. The manufacturing of $ZrCl_4$ is also an established technology, but is very dependent on an established carbochlorination industry, which the RSA does not possess.

The alternative option is to establish a Zr metal industry based on ZrF_4 as precursor. This would entail the viable and economic development of the following processes:

- Manufacturing of anhydrous ZrF_4 from zircon;
- Purification of contaminants by preferably an anhydrous route like sublimation;
- Reduction of the purified ZrF_4 by a continuous plasma route, which includes firstly the conversion of ZrF_4 to $ZrCl_4$ before reduction.

The aim of this study was to investigate the viability of manufacturing routes based on zircon as starting material, and F_2 gas and anhydrous HF as fluorinating agents. Due to its very high chemical inertness, the majority of the experiments were carried out using ZrO_2 as starting material, and progressing to DPDZ (desilicated, plasma dissociated zircon). To achieve the purpose of the study the following investigations were carried out in fluorine and hydrogen fluoride atmospheres:

- Determining the optimum synthesis conditions for manufacturing of pure ZrF_4 from ZrO_2;

- Determining whether ZrF_4 formation proceeds via intermediate compounds;
- Determining whether selective fluorination can be utilized as a purification method for the synthesis of nuclear-grade ZrF_4.

The investigations were carried out using a thermogravimetric analyzer (TGA) under strictly anhydrous conditions. Each experiment was preceded by an evaluation of the thermodynamic viability of the particular reaction, using HSC. Analyses of the reaction products were carried out by means of XRD, Raman and SEM techniques.

This study has helped to clarify conflicting evidence from literature, e.g.:

- Can ZrO_2 be fluorinated at room temperature?
- What are the exact sublimation temperatures of ZrF_4 and HfF_4?
- Is the initial room temperature uptake of HF by ZrO_2 due to physio-sorption or chemi-sorptions?
- What is the role of water during the fluorination process?
- Can selective fluorination effect purification of ZrF_4 of HfF_4?
- Does the fluorination of ZrO_2 to ZrF_4 proceed via oxyfluoride intermediates?
- Can Raman spectroscopy contribute to a better understanding of ZrO_2/HfO_2 fluorination reactions?
- Can plasma dissociated zircon be used as source for ZrO_2 to be fluorinated to nuclear-grade ZrF_4?

7.2 FUTURE WORK FROM STUDY

To further expand the scientific value of this work and to address identified uncertainties, the following potential studies have been identified for further attention:

- The double-step reaction observed during fluorination of 50:50 mixtures of zirconium and hafnium oxides will have to be investigated by means of XRD;

- Obtaining ZrO_2 (DPDZ) from PDZ and using this material for all future absorption and fluorination studies;
- Exploring the chemical characteristics of natural ZrO_2 and that obtained from PDZ (DPDZ);
- Determining the enthalpy of interaction between ZrO_2 and DPDZ with HF at 30 °C with a Setaram C80 calorimeter. This calorimetric study will assist with further understanding on the adsorption studies;
- A reactor will be designed and constructed for laboratory-scale fluorination of ZrO_2 and DPDZ. The reactor will also incorporate a vacuum product collection vessel, for collection of sublimated product. The product collected from this vessel, will be transported to a specialized sublimation vessel, and purified to nuclear-grade ZrF_4;
- Infrared spectra will be used to assist Raman in characterizing the intermediates and the reaction products.

Appendix 1

HSC Chemistry 6.1

To start the HSC Chemistry 6.1 program, double clicking on its icon and a window similar to Fig. 1 will appear. Here one can select what thermodynamic data must be calculated. In this study the *Equilibrium Module* of HSC Chemistry 6.1 is primarily used. Many other functions are available but are not of interest to this study.

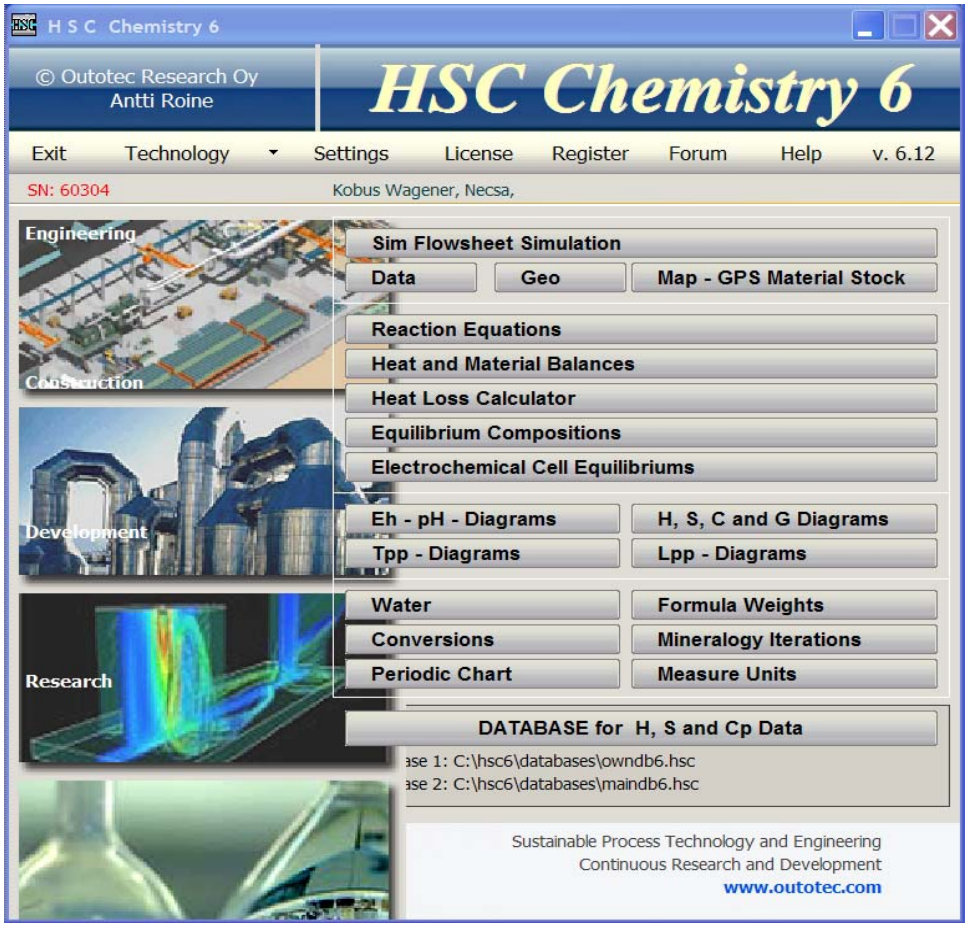

Figure 1.

Equilibrium Calculations

Equilibrium calculations for a mixture of species can be done by using the following procedure:

Choose the *Equilibrium Calculations* from the first window (Fig. 1) and the following window will appear (Fig.2). Click on the *Create New Input File* button.

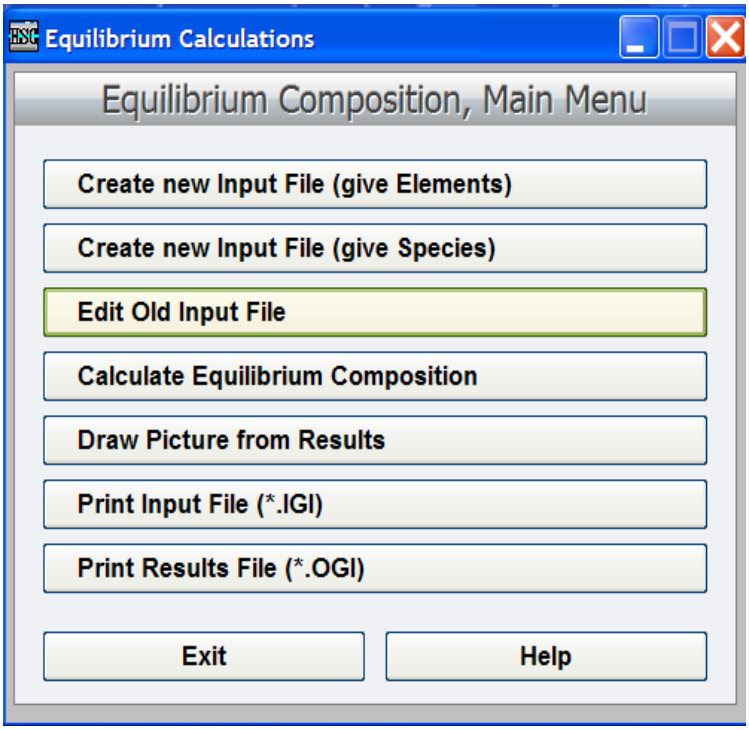

Figure 2.

When the window in Fig. 3 appears a selection of the elements must be made. These must include all the elements involved in the reactions. In this case Zr, O and F will be chosen.

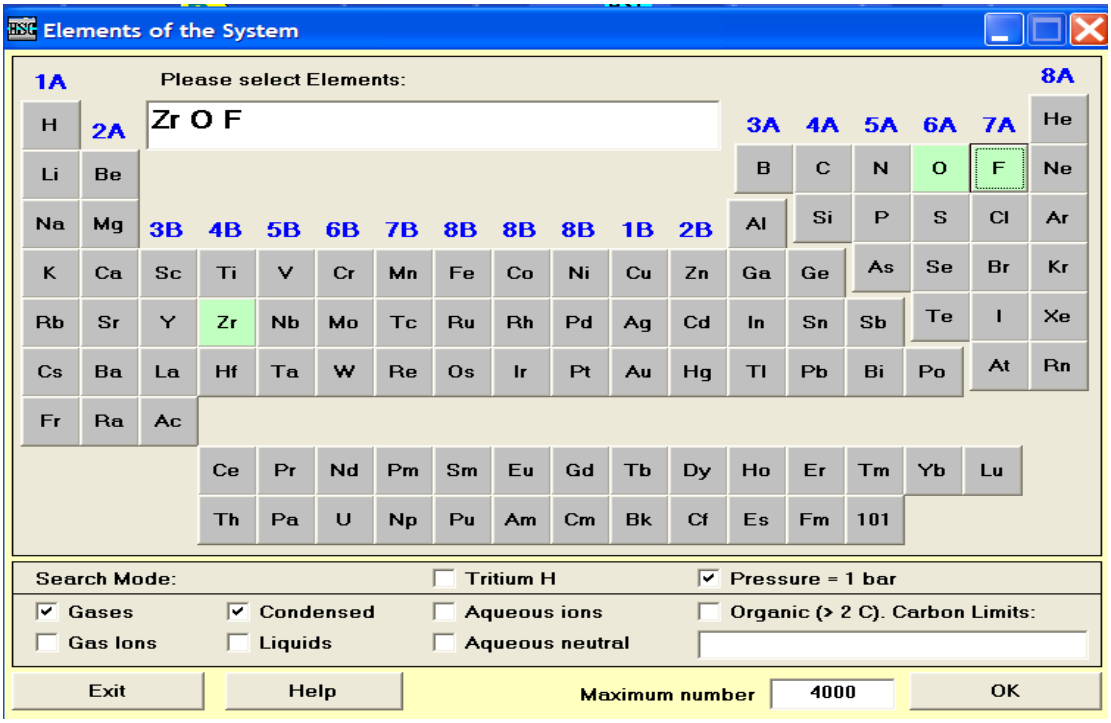

Figure 3.

When the *OK* button is selected the next window appears (Fig. 4). Here all the species with the particular chosen atoms are selected from the database and displayed. Now a selection can be made on the species involved in the equilibrium composition. After the unwanted species are deleted, the *Continue* button can be selected.

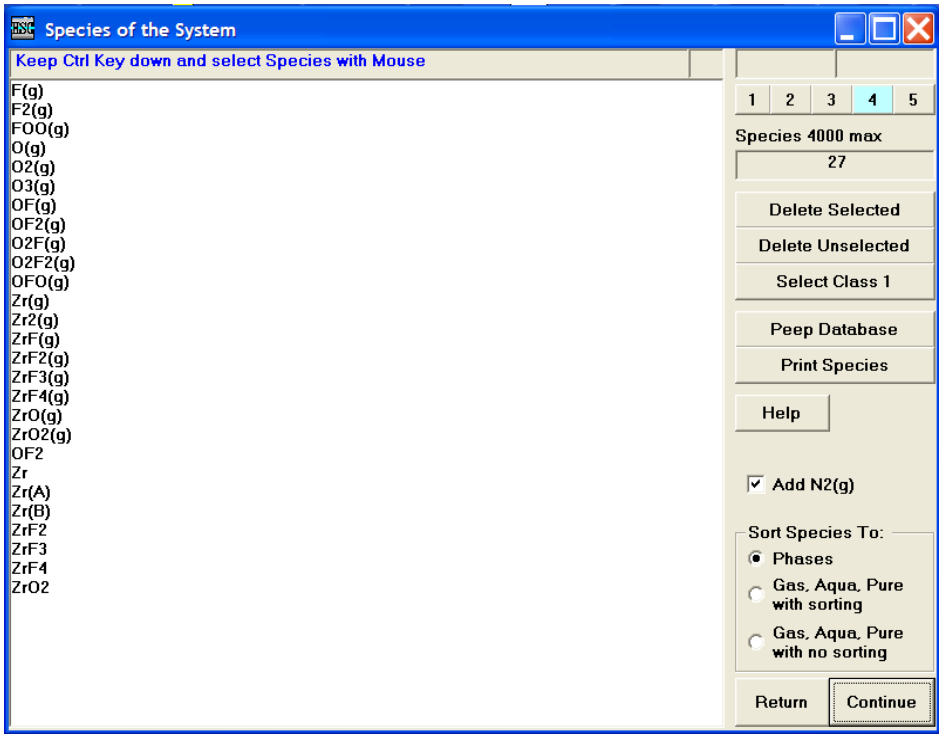

Figure 4.

The species can then be ordered in a spreadsheet format in alphabetical order, and the molecules and elements separated (Fig. 5). One or more species must be selected as starting species. These species must contain all the elements. Their molar ratio to one another must also be completed in the kmol column.

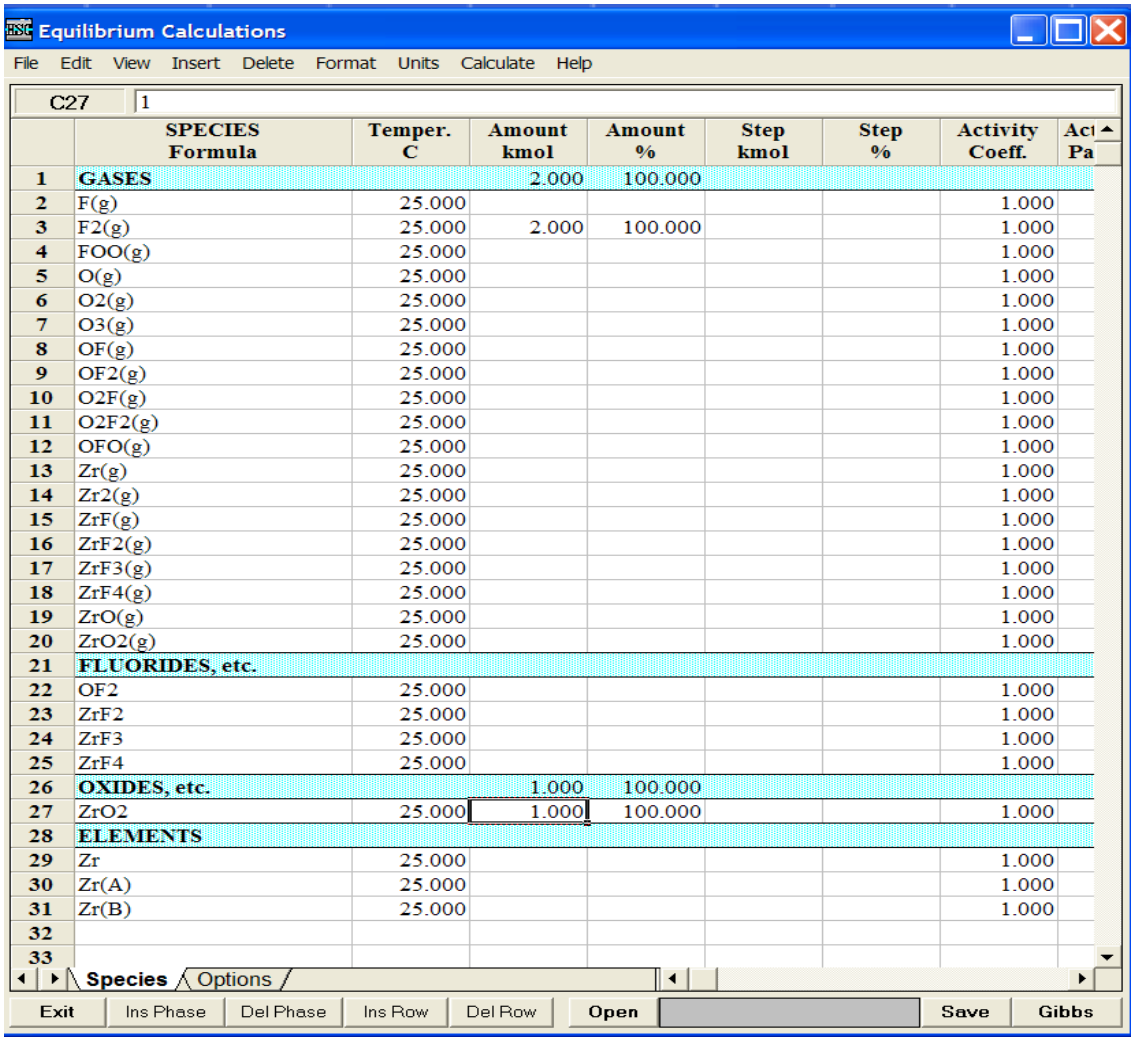

Figure 5.

By selecting the *Option* tab at the bottom of the window, the next window will appear (Fig. 6). Here the temperature or pressure can be varied in a predetermined number of steps. For our purpose the temperature will be varied from 0 to 1000 °C and the pressure be kept constant in 1 bar or varied in some instance. A tick must be made in the box next to *Increase Temperature*.

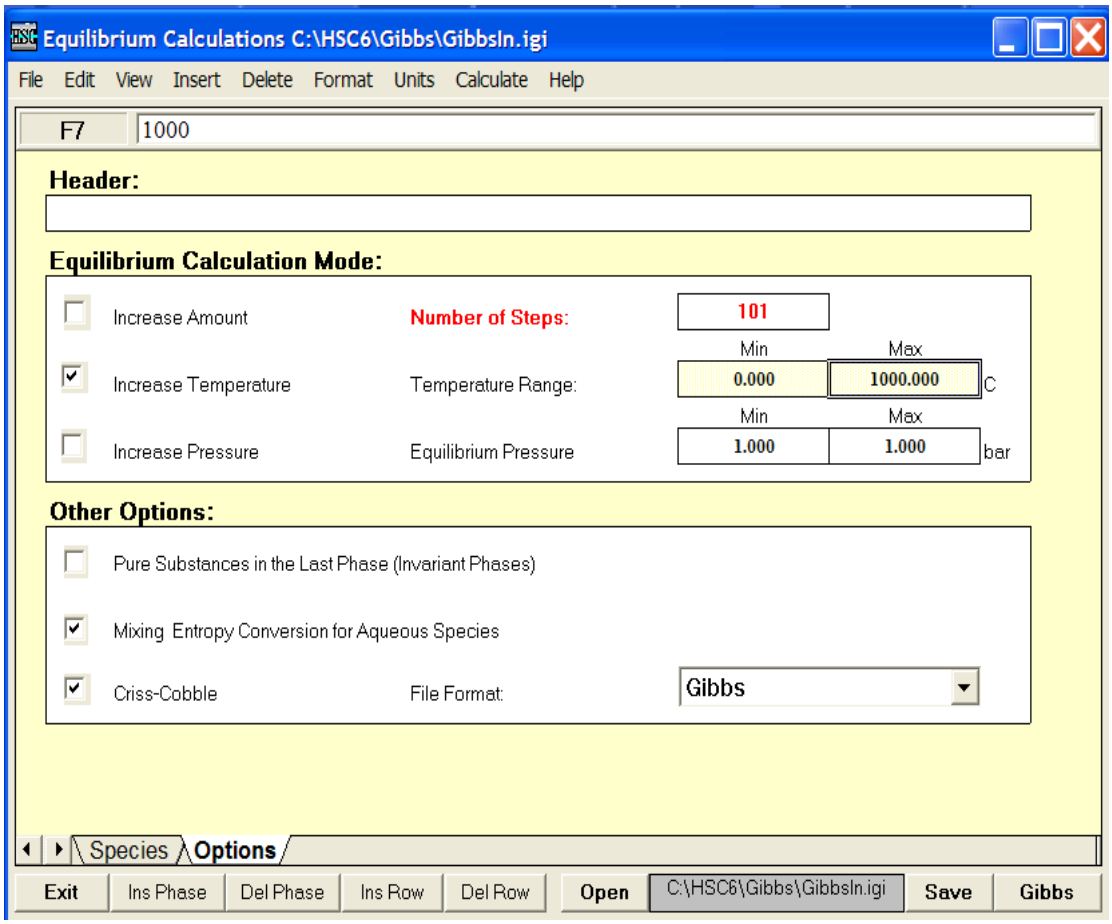

Figure 6.

After *Saving* and processing the *Gibbs* button, the next window appears (Fig. 7). Press *Calculate* button for the program to run the Gibbs energy minimization algorithm and then the *Draw Diagram* button to display the window shown in Fig. 8.

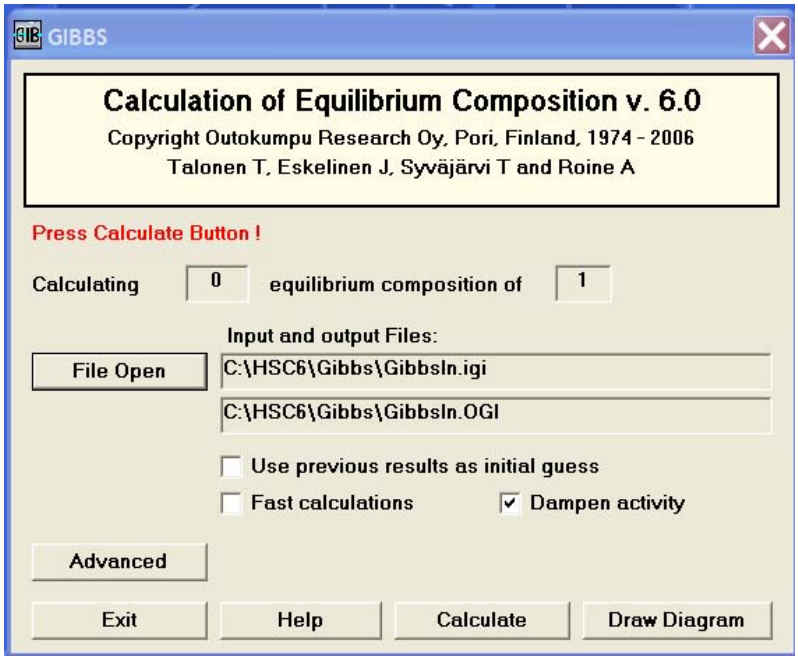

Figure 7.

In order to draw the diagram one must firstly choose the X-axis (Fig. 8). In this case it is the temperature. After selecting *OK*, one usually selects the whole series of species available and then selects *OK* again to proceed to the next window.

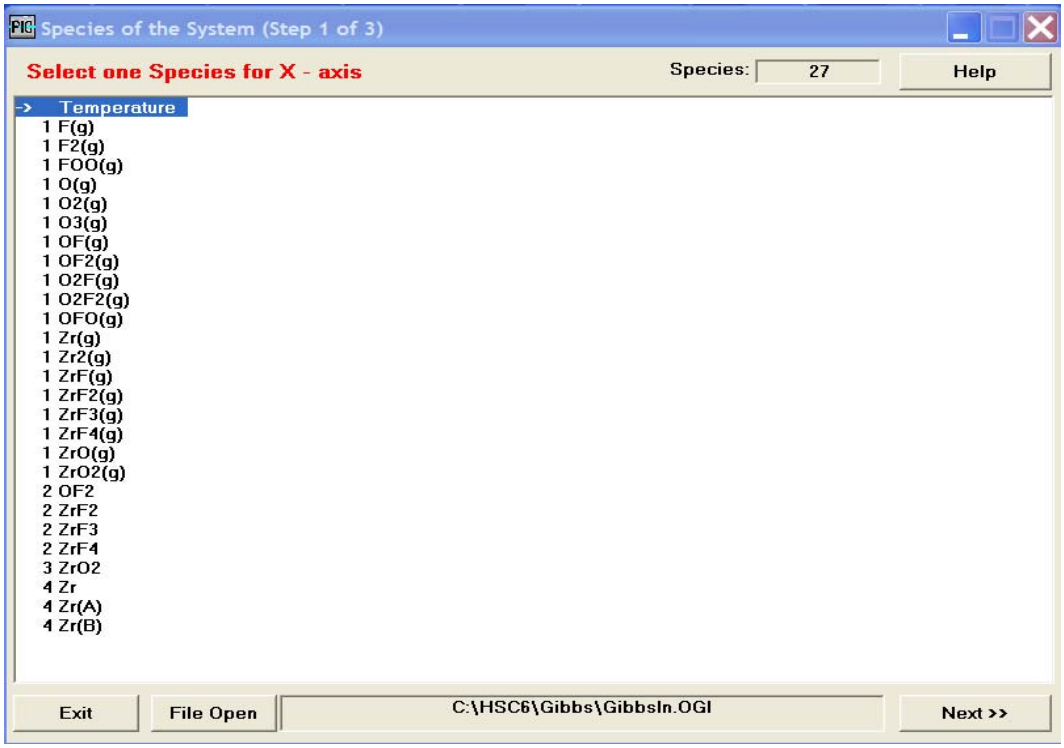

Figure 8.

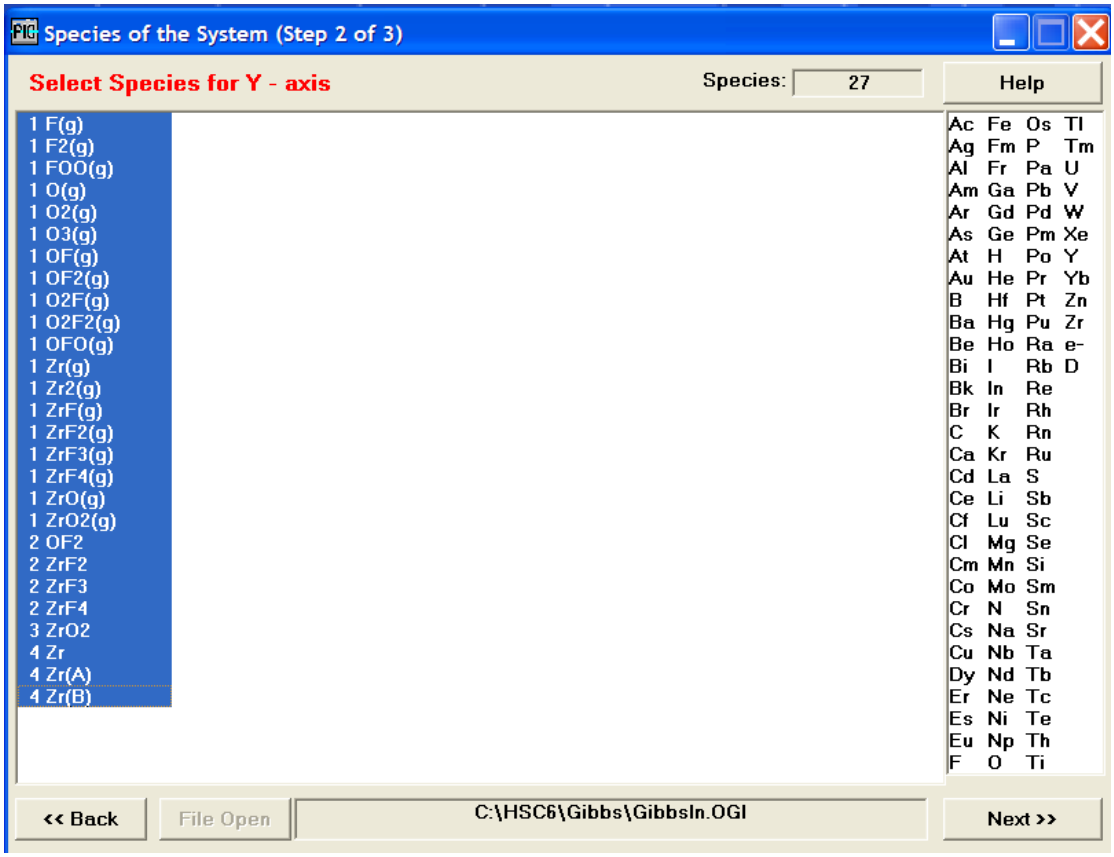

Figure 9.

In the window presented in Fig. 10, one can manipulate the x- and y-axis and the units. To draw a diagram, select the *Diagram* option.

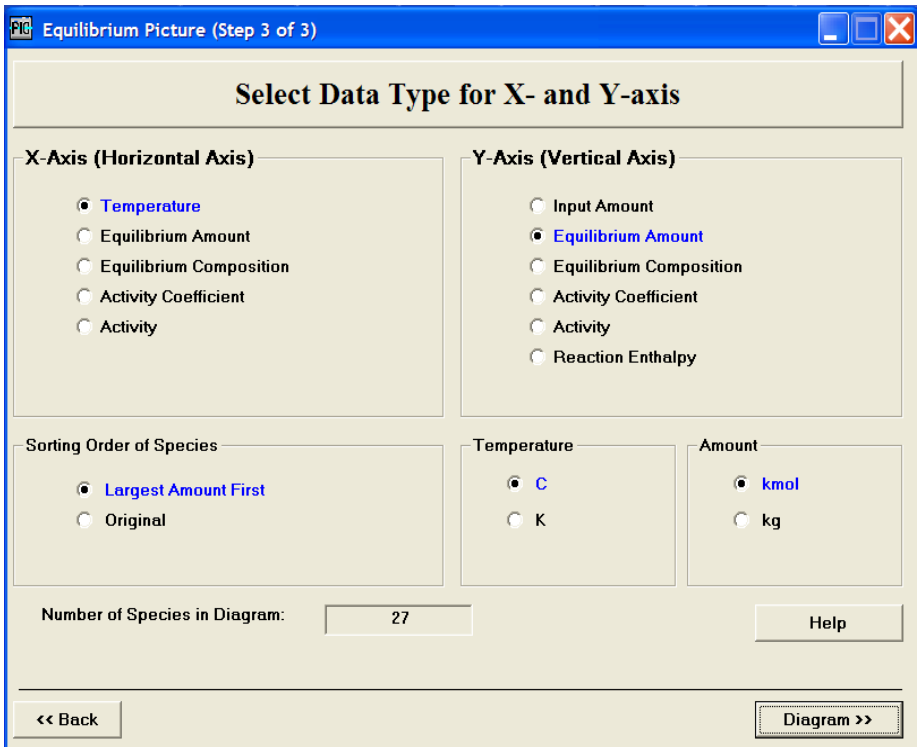

Figure 10.

The diagram (Fig. 11) may be *Copied* into a Word document or *Printed*. The axis of the diagram can be altered by selecting *Format* from the task bar and then selecting the axis to be changed.

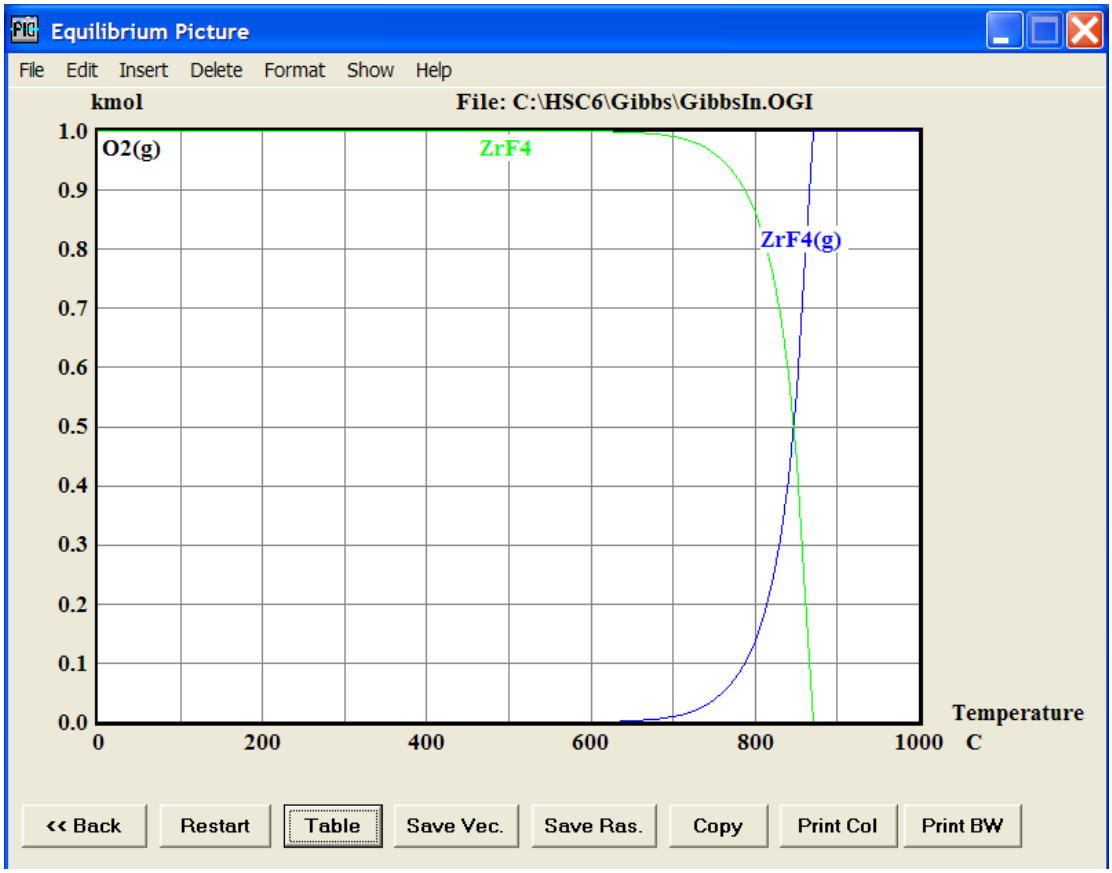
Equilibrium Picture
File Edit Insert Delete Format Show Help
kmol
File: C:\HSC6\Gibbs\GibbsIn.OGI
O2(g)
ZrF4
ZrF4(g)
1.0
0.9
0.8
0.7
0.6
0.5
0.4
0.3
0.2
0.1
0.0
0
200
400
600
800
1000
Temperature
C
<< Back
Restart
Table
Save Vec.
Save Ras.
Copy
Print Col
Print BW
Figure 11.

References

[1] W.B. Blumenthal, The Chemical Behavior of Zirconium, (1958).

[2] J.C. Bailar, H.J. Emeléus, Sir R. Nyholm, A.F. Trotman-Dickenson, Comprehensive Inorg. Chem., (1973) 419.

[3] Klaproth, Ann. Chim. Phys., **8** (1789).

[4] Klaproth, Chem. Ann. Crell., **1** (1789) 7.

[5] M. Eagleson, Concise Encyclopedia Chem., (1994) 1199.

[6] J.J. Berzelius, Ann. Chim. Phys., **20** (43) (1824).

[7] D. Lely Jr., L. Hamburger, Z. Anorg. Algem. Chem., **87** (1914) 209.

[8] A.E. van Arkel, J.H. de Boer, Z. Anorg. Allgem. Chem., **12** (1920) 651.

[9] W.J. Kroll, C.T. Anderson, H.P. Holmes, L.A. Yerkes, H.L. Gilbert, Trans. Electrochem. Soc., **94** (1948) 1.

[10] W.J. Kroll, A.W. Schlechten, L.A. Yerkes, Trans. Electrochem. Soc., **89** (1946) 263.

[11] W.J. Kroll, A.W. Schlechten, W.R. Carmody, L.A. Yerkes, H.P. Holmes, H.L. Gilbert, Trans. Electrochem. Soc., **92** (1947) 99.

[12] http://periodic.lanl.gov/elements/40.html. [4 August 2007]

[13] R. Stevens, Zirconia and Zirconia Ceramics, (1986) 8.

[14] G. von Hevesy, Chem. Rev., **2** (1925) 1.

[15] F.A. Cotton, G. Wilkinson, C.A. Murillo, M. Bochmann, Advanced Inorg. Chem., 6th Ed., (1999) 877.

[16] P. Besson, J. Guerin, P. Brun, M. Bakes, US Patent 4 021 531 (1977).

[17] O.D. Voit, Equilibrium Distribution Behavior of Zirconyl-Hafnyl Thiocyanates Between Methyl-Isobutyl-Ketone and Aqueous Phases, ISEC 80 Proceedings, (1980).

[18] J.A. Sommers, J.G. Perrine, US Patent 6 737 030 (2004).

[19] J. Huré, R. Saint-James, Proceedings of the International Conference on the Peaceful Uses of Atomic Energy, **8** (1956) 551.

[20] J. Huré, R. Saint-James, US Patent 2 757 081 (1956).

[21] V.A. Mayer, Annnual Book of ASTM Standards, (2006) 217.

[22] K. Minato, T. Ogawa, T. Koya, H. Sekino, T. Tomita, J. Nuclear Materials **279** (2-3) (2000) 181.

[23] http://www.energetic.com/ineri_client/pdfs/japan_06summary.pdf. [18 September 2007]

[24] G.L. Miller, Metallurgy of the Rarer Metals-2 2nd Ed., (1957) 13.

[25] http://en.wikipedia.org/wiki/zirconium. [4 August 2007]

[26] Kirk-Othmer Encyclopedia of Chemical Technology, **26** (2007) 621.

[27] Ullmann's Encyclopedia of Industrial Chemistry, **A28** (1996) 543.

[28] E. Snyders, DTech. Thesis, Tshwane University of Technology, RSA, (2007) 69.

[29] A.B.V. Da Silva, P.A. Distin, CIM Bulletin: Technical Paper, **91** (1998) 221.

[30] J. Huré, R. Saint-James, Proceedings of the International Conference on the Peaceful Uses of Atomic Energy, **8** (1956) 551.

[31] J.A. Sommers, J.G. Perrine, US Patent 6 737 030 (2004).

[32] L. Poriel, A. Favre-Réguillon, S. Pellet-Rostaing, M. Lemaire, Separation science and technology, **41** (2006) 1927.

[33] J.C. Sehra, R. Mallikarjunan, Bulletin of Material Science, **12** (3-4) (1989) 407.

[34] E.G. El-ammouri, P.A. Distin, Solvent Extraction and Ion Exchange, **14** (5) (1996) 871.

[35] R.C. Pastor, M. Robinson, US Patent 4 578 252 (1986).

[36] P.E.R. Nordquist Jr., A.H. Singer, US Patent 4 965 055 (1990).

[37] J. Jaganathan, K.J. Ewing, E.A. Buckley, L. Peitersen, I.D. Aggarwal, J. Microchemical, **41** (1990) 106.

[38] J. Lucas, J. Material Science, **24** (1989) 1.

[39] J.M. Parker Annu. Rev. Material Science, **19** (1989) 21.

[40] J.A. Sommers, US Patent 4 910 009 (1990).

[41] M. Robinson, R.C. Pastor, M. Branstein, US Patent 4 341 873 (1982).

[42] Z. Hubicki, Solvent Extraction and Ion Exchange, **6** (1988) 183.

[43] J.T. Nel, US Patent 5 958 355 (1999).

[44] C. Pin, S. Joannon, Talanta, **57** (2002) 393.

[45] R.J. Anderson, US Patent 2 639 218 (1953).

[46] I.E. Newnham, US Patent 2 961 293 (1960).

[47] H.A. Wilhelm, K.A. Walsh, US Patent 2 602 725 (1952).

[48] O.F. Spague, US Patent 2 789 882 (1957).

[49] C. Woolf, US Patent 2 805 121 (1957).

[50] H.A. Wilhelm, K.A. Walsh, US Patent 2 635 037 (1953).

[51] W.B. Blumenthal, The Chemical Behavior of Zirconium, (1958) 138.

[52] H.M. Haendler, S.F. Bartram, R.S. Becker, W.J. Bernard, W.W. Bukata, J. Am. Chem. Soc., **76** (1954) 2177.

[53] E. Wedekind, Ber., **44** (1911) 1753.

[54] H. St. C. Deville, Ann. Chim. Phys., **49** (3) (1857) 84.

[55] H. St. C. Deville, Ann. Chim. Phys., **5** (4) (1865) 109.

[56] K.A. Walsh, US Atomic Energy Comm. AECD-3640, **57** (1950).

[57] C.M. Stander, Beneficiation of zirconium metal: Thermodynamics of zirconium halides and oxides, Thermtron Plasma (Pty) Ltd, (2007).

[58] C.M. Stander, Thermochimica Acta, **209** (1992) 55.

[59] A.J. Megy, US Patent 4 072 506 (1978).

[60] J.H. Canterford, R. Colton, Halides of the Second and Third Row Transition Metals, (1991) 116.

[61] H. Becker, Basis for proposal concept designs on the production of nuclear-grade zirconium. Necsa Doc No. PTC-AMI-PRP-07001 R1, (2007).

[62] G.L. Miller, Metallurgy of the Rarer Metal-2 2nd Ed., (1957) 91.

[63] D.R. McFarlane, P.J. Mineely, P.J. Newnman, J. Non-crystalline Solids, **140** (1992) 335.

[64] G. von Hevesy, W. Dullenkopf, Zeitschrift fűr Anorganische und Algemeine Chemie, Band 221 (1934) 161.

[65] M. Bralia et al., Mat. Res. Bull., **24** (1989) 661.

[66] C. Marignac, Ann. Chem. Phys., **60** (1860) 257.

[67] W.B. Blumenthal, US Patent 2 626 203 (1952).

[68] H.A. Wilhelm, K.A. Walsh, US Patent 2 635 037 (1953).

[69] W.J.S. Craigen, E.G. Joe, G.M. Ritcey, Canadian Metallurgical Quarterly, **9** (1970) 485.

[70] P.C. Rivas, J.A. Martínez, A.M. Rodriques, A.R. Lopez Garcia, M. Dejneka, Hyperfine Interactions, **110** (1997) 195.

[71] P.C. Rivas, M.C. Caracoche, J.A. Martínez, M.T. Dova, A.R. Lopez Garcia, Hyperfine Interactions, **30** (1986) 49.

[72] M. Watanabe, S. Nishimura, EU Patent 0 134 643 (1984).

[73] A. Van Tets, Bereding van kerngraad sirkonium metaal; ń Literatuur oorsig. Interne verslag no. v068, Atoomenergiekorporasie van Suid-Afrika, (1991).

[74] D.R. Lide, CRC Handbook of Chemistry and Physics 83rd Ed., (2002-2003).

[75] N.Y. Tumanov (Co-author), Thermodynamic properties of polyatomic inorganic fluorides, (1972) 143.

[76] http://asia.matweb.com/search/specificMaterial.asp?bassnum=EINOR0299. [2007-11-01]

[77] S. Cantor, R.F. Newton, W.R. Grimes, F.F. Blankenship, J. Phys. Chem., **62** (1957) 96.

[78] K.A. Sense, M.J. Snyder, R.B. Filbert Jr., J. Phys. Chem., **58** (1954) 995.

[79] L.N. Sidorov, P.A. Akishin, V.B. Shol'ts, Yu.M. Korenev, Russ. J. Phys. Chem., **39** (1965) 1146.

[80] N.P. Galkin, Yu.N. Tumanov, V.I. Tarasov, Yu.D. Shishkov, Russ. J. Inorg. Chem., **8** (1963) 1054.

[81] C.A. Holden, H.S. Bryant, Separation Science, **4** (1) (1969) 1.

[82] H.P. Withers, A.J. Woytek, J.T. Lileck, US Patent 4 983 373 (1991).

[83] T. Tatsuno, Material Science Forum, **19-20** (1987) 181.

[84] H.W. Chandler, US Patent 3 276 862 (1966).

[85] I.E. Newnham, US Patent 2 916 350 (1959).

[86] A.I. Solov'ev, V.M. Malyutina, Russ. J. Non-Ferrous Metals, **43** (9) (2002) 14.

[87] J.G. Grasselli, B.J. Bulkin, Analytical Raman Spec., **114** (1991) 1.

[88] C. Carlone, J. Am. Phys. Soc., **45** (1992) 2097.

[89] M. Ishigame, T. Sakurai, J. Am. Ceram., **60** (7-8) (1977) 367.

[90] A. Jayaraman, S.Y. Wang, S.K. Sharma, L.C. Ming, J. Am. Phys. Soc., **48** (13) (1993) 9205.

[91] H. Arashi, T. Yagi. S. Akimoto, Y. Kudoh, Phys. Rev., B **41** (1990) 4309.

[92] M.A. Kerbs, R.A Condrate, Sr, Comm. Am. Ceram. Soc., (1982) 144.

[93] M. Goldstein, R.J. Hughes, W.D. Unsworth, Spectrochimica Acta., **31A** (1975) 621.

[94] W.H. Zachariasen, Acta Cryst., **2** (1949) 388.

[95] A. Roine, Antti, HSC Chemistry™ 6.1 User's Guide (2006).

[96] I.J. van der Walt, PhD Thesis, University of the North West, RSA (2007).

[97] L.P. Le Roux, Collaborative discussions and studies.

[98] M.L. Kotsar', V.B. Bateev, P.B. Baskov, V.V. Sakharov, V.D. Ferorov, V.V. Shatalov, Inorg. Mat., **37** (2001) 1085.

[99] W. Fischer, T. Petzel, S. Lauter, Z. Anorg. Chem., **333** (1964) 226.

[100] Yu.M. Koronev, I.D. Sorokin, N.A. Chirina, A.V. Novoselova, J. Inorg. Chem., **XVII** (5) (1972) 1195.

[101] R.A. Kent, K. Zmbov, J.D. McDonald, G. Besenbruch, T.C. Ehlert, R.G. Bautista, A.S. Kana'an, J.L. Margrave, Proc. Conf. Appl. Nonfissionable Ceram., (1966) 249.

[102] K. Nakarajan, M. Bhuphathy, R. Prasad, Z. Singh, V. Venugopal, D.D. Sood, J. Chem. Thermodynamics, **12** (1980) 329.

[103] B. Brunetti, V. Piacente, J. Alloys and Compounds, **236** (1996) 63.

[104] K.H. Lau, R.D. Brittain, D.L. Hildenbrand, J. Chem. Phys., **90** (2) (1989) 1158.

[105] B. Brunetti, V. Piacente, P. Scardala, J. Chem. Eng. Data, **54** (3) (2009) 940.

[106] Y.N. Tumanov, Feasible technological routes for processing zircon, Internal Necsa publication, (1993) 2.

[107] P. Rampersadh, PhD Thesis, University of Witwatersrand, RSA (2005).

[108] Analyses obtained from S. Verryn, Universtiy of Pretoria, RSA.

[109] Analyses obtained from S. Paul, Chemistry Department, UNISA, RSA.

[110] Analyses obtained from D. de Waal, NECSA, RSA.

[111] J. Nel, US Patent 5 688 477 (1997).

[112] M. Robinson, K.C. Fuller, Mat. Res., **22** (1987) 1725.

[113] R.H. Maybury, S. Gordon, J.J. Katz, J. Chem. Phys., **23** (1955) 1277.

[114] A. Anderson, B.H. Torrie, W.S. TSE, Chemical Physics Letters, **70** (2) (1980) 300.

[115] A. Anderson, B.H. Torrie, W.S. TSE, J. Raman Spectroscopy, **10** (1981) 148.

[116] M. Goldstein, R.J. Hughes, W.D. Unsworth, Spectrochimica Acta, **31** (1975) 621.

[117] H.M. Haendler, S.F. Becker, W.J. Bernard, W.W. Bukata, J. Am. Chem. Soc., **76** (1954) 2177.